Some computational explorations of matters related to neutrino oscillations.

A thesis presented in partial fulfillment of the requirements for the degree of

Doctor of Philosophy

in

Physics

at Massey University, Manawatū

New Zealand

William S. Marks

2020

Abstract

This thesis covers computational work on matters related to neutrino oscillations, with two main areas of focus. This first was the extraction of θ_{13}, the last neutrino oscillation parameter to be measured, from published reactor anti-neutrino data. The second covered the matter effect, where the presence of matter that couples to neutrinos modifies the oscillation patterns. The work on θ_{13} extraction sought to replicate the results of the Daya Bay and RENO collaborations from the published data; to determine the significance of pullfactors to the final result and, to address published concerns about the replicability of the Daya Bay results. The results were successfully replicated, the pullfactors were found to not be of much significance and a novel method of performing the extraction was developed. The work on the matter effect looked at the effects of varying matter distributions and the size of coherent effects from dark matter, which in turn looked at two different interaction types: weak-like interactions and scotogenic interactions. It was found that the standard formalism for treating matter effects is blind to matter inhomogeneities while the inclusion of coherence for the dark matter effect does not improve the range of detectability enough to justify efforts to resolve coherent effects. In addition to describing the work done, there is a short overview of the current state of the field of searches for neutrino-dark matter interactions.

Acknowledgements

I would like to thank my primary supervisor, Dr. Fu-Guang Cao, for his continual guidance and support throughout the course of my studies. I also thank him for allowing me to pursue the directions I thought were interesting, even if they deviated from the initial focus, and for taking point on the writing and submission of the first publication featuring my work.

I would also like to thank those who contributed to this thesis. These include Prof. Anthony Signal, whose feedback was crucial in the finishing of this thesis; Prof. S. T. Petcov, who enlightened me in regard to areas of theory that I was previously unaware of and revived my enthusiasm for the field, and the many anonymous journal referees whose criticism helped shape my work.

Last but not least, I would like to thank my family. Their love and support through the years can never be repaid and was absolutely essential for my success.

To these, I give many thanks.

List of Publications

- F. G. Cao and W. S. Marks. Extraction of neutrino mixing parameters from experiments with multiple identical detectors. International Journal of Modern Physics A, 33(22): 1–14, 2018.

- W. S. Marks. The effects of coherent neutrino mixing modulation by dark matter. Journal of Physics: Conference Series, 1468(1): 012198, 2020.

- W. S. Marks and F.-G. Cao. Meaningful Details: The value of adding baseline dependence to the Neutrino-Dark Matter Effect. International Journal of Theoretical Physics, 59(12): 3951–3966, 2020.

Contents

List of Figures

List of Tables

Chapter 1

Introduction

The work that will be described below, as the title suggests, involves exploring neutrino oscillations using computational methods. This followed two main themes: a search for evidence of neutrino-dark matter interactions and a focus on numerical calculations.

The investigation into potential connections between neutrinos and dark matter was initiated as a simple case of, "wouldn't it be interesting if...?" There wasn't much of a motivation to investigate this avenue other than simple curiosity and the main reason for suspecting that there might be some fruit from such a search was the observation that neutrinos and dark matter have a number of qualities in common[1]. In particular, there is the lack of participation in the electro-magnetic interaction, rendering neutrinos "dark". Indeed, this led to neutrinos at one point being a dark matter candidate, called Hot Dark Matter due to the relatively large kinetic energy of cosmogenic neutrinos [1].

The focus of this exploration was an attempt to identify novel signals of an interaction. Two areas in this field stood out, one theoretical and one phenomenological. The theoretical area was the Scotogenic models, which posit that neutrinos gain their mass through virtual couplings with dark matter candidates. These models were attractive as

[1]This is presumptive in the case of dark matter in as much as the actual properties of that substance are entirely speculative at this stage.

they can explain the smallness of the neutrino mass, as well as other features that depend on the model. The downside is that there are a very large number of models. Despite that being the case, there are features shared between the models so they were considered in all explorations.

The phenomenological area was a potential modulation of neutrino mixing patterns induced by interactions with dark matter. When this phenomenon occurs in normal matter, it is called (unsurprisingly) the matter effect. It is also called the Mikheyev-Smirnov-Wolfenstein (MSW) effect, after the original proposers [2]. Suggestions of the observability of such an effect on astrophysical neutrinos were quite new when this project was initiated and therefore there was a focus on this area. Additionally, the previous work focused solely on decoherent neutrinos, so this work focused on coherent effects as these are computationally straightforward.

The work on mixing modulation led to a side project that investigated the possibility of using neutrinos and mixing modulation to detect exoplanets (planets outside of our solar system). It was determined that it can't be done due to a combination of the sheer difficulty of isolating neutrinos from another star, which would be at the same energy as solar neutrinos with the same spectrum. It was also found that the problem of including inhomogeneities in calculations is decidedly non-trivial. That latter point is considered the main takeaway from this sub-project.

An additional investigation conducted was into the extraction of the mixing angle θ_{13}. In particular, it attempted to replicate the given value in the RENO and Daya Bay publications. It also explored the functions used to do so and the effects from changing the number of parameters used. Additionally, a novel method of performing the extraction was developed. The significance of this parameter is that it was the last mixing parameter to be measured, the determination of which is necessary for any other calculations involving neutrino oscillations to be performed.

In summary, the research consists of three components with two main thrusts. The

two thrusts are the θ_{13} extraction and mixing modulation, with the later being further divided into the work on exoplanets and the dark matter effect. This is accompanied by a short review of the literature on neutrino-dark matter interactions. The chapter order is as follows: Chapter 1 (this chapter) is the Introduction; Chapter 2 presents an overview of neutrinos; Chapter 3 presents an overview of dark matter; Chapter 4 is the θ_{13} analysis; Chapter 5 is the work on mixing modulation and, Chapter 6 is the conclusion/summary.

The following two sections (of this chapter) give a very brief overview of the Standard Model of both Particle Physics and Cosmology.

1.1 The Standard Model of Particle Physics

In the Standard Model of Particle Physics, fundamental particles are first divided into two categories: fermions and bosons, which are classified by their spin-values and therefore the statistics they obey.

Classically, the behaviour of ensembles of non-interacting particles (Ideal Gases) is described by the Maxwell-Boltzman distribution. This distribution gives the fractional number of particles at a particular energy, $f(E)$, at a given temperature, T, and is:

$$f(E) = g(T)e^{-\frac{E}{k_b T}}, \tag{1.1}$$

where $g(T)$ is the degrees of freedom and k_b is Boltzman's constant. In Quantum Mechanics, this distribution is changed by the introduction of spin, which is a fundamental property possessed by particles that functions as an intrinsic angular momentum and comes in either integer or half-integer multiples of a constant.

When spin is introduced, this requires corrections at low temperatures and/or high densities. The resulting distribution for integer-spin particles is called the Bose-Einstein distribution and the distribution for half-integer particles is called the Fermi-Dirac distri-

bution. The Bose-Einstein distribution is:

$$f(E) = \frac{g(T)}{e^{\frac{E}{k_b T}} - 1}, \tag{1.2}$$

while the Fermi-Dirac distribution is

$$f(E) = \frac{g(T)}{e^{\frac{E}{k_b T}} + 1}, \tag{1.3}$$

where the terms are as in the Maxwell-Boltzmann distribution. From these distributions, integer-spin particles are called bosons and half-integer spin particles are called fermions.

In terms of fundamental particles (which have no internal structure) the bosons are the mediators for interactions and the fermions make up matter. When bosons have mass, they are short-lived and mediate short range interactions. Low mass fermions are stable on cosmological timescales and thus comprise the (visible) matter of the universe. Most of the following discussion is taken from [3], in particular the equations.

There are four interactions in the standard model: gravity, the weak interaction, the electro-magnetic interaction and, the strong interaction. The gravitational force is described by General Relativity and does not have a (full) particle physics description[2]. The weak interaction is mediated by the neutral Z and charged W bosons. These interactions are called neutral-current and charged-current interactions, respectively. The electro-magnetic interaction is mediated by massless photons, which were the first bosons to be discovered and were the motivation for the Bose-Einstein distribution. The strong interaction is mediated by gluons, which are massless like photons but possess a colour charge[3] and are thus self interacting.

The fermions are divided into two categories: quarks and leptons. The primary distinction is that the quarks participate in the strong interaction and the leptons do not.

[2]A boson mediator for gravity, the graviton, has been proposed but has never been observed. However, gravitational waves have been observed which makes the existence of gravitons more than a mere possibility [4].

[3]Colour is the name given to the charge associated with the strong interaction. This is why the description of the strong interaction is called Quantum Chromodynamics.

Table 1.1: The Fermions

The Quarks			
Particle	u	c	t
Charge	$\frac{2}{3}e$	$\frac{2}{3}e$	$\frac{2}{3}e$
Mass	2.5MeV	1.27GeV	172GeV
	d	s	b
Charge	$-\frac{1}{3}e$	$-\frac{1}{3}e$	$-\frac{1}{3}e$
Mass	5MeV	101MeV	4.19GeV
The Leptons			
	e	μ	τ
Charge	$-1e$	$-1e$	$-1e$
Mass	0.511MeV	106MeV	1777MeV
	ν_e	ν_μ	ν_τ
Charge	0	0	0
Mass	N/A	N/A	N/A

Because of their participation in the strong interaction, quarks have never been observed in a free state[4]. The quarks are further divided into two classes, positively charged quarks (with a charge magnitude two-thirds that of the electron) and negatively charged quarks (with a charge magnitude one-third that of the electron). The leptons are also divided into two classes, the charged leptons (with the charge of the electron) and uncharged leptons (the neutrinos)[5].

As stated before, gravity is described by Einstein's General Relativity, where gravity

[4]Due to the fact that free quarks have never been observed, their masses are speculative and the values obtained are calculation method dependent.

[5]The listed neutrino flavour eigenstates, properly speaking, do not have mass values as each is a superposition of the three mass eigenstates. Simply put, a flavoured neutrino simultaneously has three different values for its mass. This is explained more fully in the chapter on neutrinos.

Table 1.2: The Bosons

Particle	γ	g	$W^{\pm}$	Z^0	H
Electric Charge	0	0*	$\pm 1e$	0	0
Mass	0	0*	80GeV	91GeV	127GeV

is a distortion of the geometry of space-time caused by the presence of mass-energy. The equation for this is:

$$R_{\mu\nu} - \frac{1}{2}Rg_{\mu\nu} + \Lambda g_{\mu\nu} = \frac{8\pi G}{c^4}T_{\mu\nu}, \tag{1.4}$$

where $R_{\mu\nu}$ is the Ricci tensor, $R = g^{\mu\nu}R_{\mu\nu}$ is the Ricci curvature, $g_{\mu\nu}$ is the metric tensor (which is defined as the Minkowski metric with a distortion caused by the presence of mass-energy), Λ is the cosmological constant, G is the gravitational constant, c is the speed of light and, $T_{\mu\nu}$ is the energy distribution tensor. The Ricci tensor is:

$$R_{\mu\nu}(g) = \partial_\alpha \Gamma^\alpha_{\mu\nu} - \partial_\nu \Gamma^\alpha_{\mu\alpha} + \Gamma^\beta_{\alpha\beta}\Gamma^\alpha_{\mu\nu} - \Gamma^\beta_{\alpha\nu}\Gamma^\alpha_{\mu\beta}, \tag{1.5}$$

where repeated indices have been summed over and

$$\Gamma^\lambda_{\mu\nu} = \frac{1}{2}g^{\lambda\sigma}(\partial_\mu g_{\nu\sigma} + \partial_\nu g_{\mu\sigma} - \partial_\sigma g_{\mu\nu}). \tag{1.6}$$

Solving equation 1.4 is extremely difficult and exact solutions are possible only under special circumstances.

The interactions of particle physics are described by Lagrangians, with the electromagnetic and weak interactions being combined into a single Lagrangian. The motivation for this is that there is a close relationship between the two interactions, particularly between photons and the neutral weak Z bosons. The Electro-Weak Lagrangian (which governs the evolution of a fermion field ψ_i, with left-handed component Ψ_i while ignoring

gravity and the strong interaction) is

$$\begin{aligned}\mathcal{L}_{EW} &= \textstyle\sum_i \overline{\psi}_i \left(i\not{\partial} - m_i - \frac{gm_iH}{2M_W}\right)\psi_i \\ &\quad -\tfrac{g}{2\sqrt{2}} \textstyle\sum_i \overline{\Psi}_i\gamma^\mu(1-\gamma^5)(T^+W_\mu^+ + T^-W_\mu^-)\Psi_i \\ &\quad -e\textstyle\sum_i q_i\overline{\psi}_i\gamma^\mu\psi_i A_\mu \\ &\quad -\tfrac{g}{2\cos\theta_W}\textstyle\sum_i \overline{\psi}_i\gamma^\mu(g_V^i - g_A^i\gamma^5)\psi_i Z_\mu,\end{aligned} \tag{1.7}$$

where the first line is the standard propagator (which includes the Higgs field, H); the second line is the flavour changing charged-current weak interaction (with the charged boson fields, $W^\pm$); the third line is the electro-magnetic interaction (with the photon field A and positron charge e) and, the fourth line is the flavour-conserving neutral-current Weak Interaction (with neutral boson field Z). The γ^μ, γ^5 terms are the Dirac γ matrices. Electro-Weak Theory posits that there exists gauge bosons B and $W^i, i = 1, 2, 3$ with gauge couplings g' and g such that:

$$\begin{aligned}\theta_W &= \tan^{-1}\tfrac{g'}{g}, \\ e &= g\sin\theta_W, \\ A &= B\cos\theta_W + W^3\sin\theta_W, \\ Z &= -B\sin\theta_W + W^3\cos\theta_W, \\ W^\pm &= \tfrac{W^1 \mp W^2}{\sqrt{2}}.\end{aligned} \tag{1.8}$$

The terms

$$\begin{aligned}g_V^i &= t_{3L}(i) - 2q_i\sin^2(\theta_W), \\ g_A^i &= t_{3L}(i)\end{aligned} \tag{1.9}$$

are the vector and axial-vector couplings, with $t_{3L}(i)$ being the weak isospin of fermion i and q_i being the electric charge.

The Lagrangian for QCD, which describes the strong interaction between coloured quark fields $\psi_{q,a}$ and coloured gluon fields $\mathcal{A}_\mu^X (X = A, B, C)$, is

$$\begin{aligned}\mathcal{L} &= \textstyle\sum_q \overline{\psi}_{q,a}(i\gamma^\mu\partial_\mu - g_s\gamma^\mu t_{ab}^C\mathcal{A}_\mu^C - m_q\delta_{ab})\psi_{q,b} \\ &\quad -\tfrac{1}{4}F_{\mu\nu}^A F^{A,\mu\nu},\end{aligned} \tag{1.10}$$

where the first part produces the quark-gluon interactions and the second encodes the gluon self-interactions, using the field tensor:

$$F^A_{\mu\nu} = \partial_\mu \mathcal{A}^A_\nu - \partial_\nu \mathcal{A}^A_\mu - g_s f_{ABC} \mathcal{A}^B_\mu \mathcal{A}^C_\nu. \tag{1.11}$$

The colour shifting matrices, t^X_{ab}, which generate the colour charge exchanges, are related to the symmetry group form factors by the commutation relation:

$$[t^A, t^B] = i f_{ABC} t^C. \tag{1.12}$$

The self interacting gluon term makes performing calculations extremely difficult.

1.2 The Standard Model of Cosmology

In the Standard Model of Cosmology, the universe begins with a singularity where space is condensed to a point (although the universe is still infinite) before undergoing an expansion [5]. The early universe (up to 300k years old) was filled with a plasma that cooled as it expanded (a classical adiabatic expansion). At certain points, this plasma would cool to the point where a particular species (of particle) would cease to interact with the rest of the plasma, effectively "dropping out" (a phenomena known as decoupling) [5]. This was because the average energy of the plasma was no longer sufficient to support the interaction. One of the first (known) species to decouple was neutrinos, as they only interact weakly. This resulted in a "sea" of freely moving neutrinos, referred to as the Cosmic Neutrino Background (CNB). Unfortunately, these neutrinos are today of fairly low energy, so detecting them would be extremely difficult, although there are efforts being made [6].

The plasma ceased to exist (as a plasma) when the universe was approximately 300k years old. This event is called Recombination and was marked by the decoupling of photons from baryons, the last major decoupling event [7]. It is called Recombination because temperatures (and densities) became low enough for electrons to bind to protons,

forming primordial hydrogen, along with a few other light elements. This produced a sea of photons (analogous to the CNB) called the Cosmic Microwave Background (CMB) due to the fact that today these photons are in the microwave range. Study of the CMB is a very important tool in cosmology [7]. Most of the utility comes from examination of the anisotropies (deviations from the mean) of the CMB.

After Recombination came a period known as the Dark Ages, where there was no photon production. This period ended with the formation of the first galaxies. These galaxies were seeded by gravitational fluctuations caused by Dark Matter, a name given to matter that does not couple to photons. Because this matter does not couple to photons, it decoupled prior to recombination. (When the Dark Matter species decoupled depends on what interactions they do participate in.) This gave it more time to develop anisotropies, which is why it seeded galaxy formation.

The scale of the Dark Matter structures depended on the kinetic energy of the Dark Matter particles, which in turn depended on a combination of the time of decoupling and the mass of the Dark Matter particles relative to baryonic matter. The earlier the decoupling and the heavier the particles, the lower the kinetic energy. Kinetic energy is, in turn, directly correlated to structure size: higher kinetic energy means larger Dark Matter structures, which in turn means that the formation of the current baryonic structures starts at large scales and goes downward. Conversely, lower kinetic energy means that structure formation is bottom up: starting at small scale and leading to larger scale structures.

Observations have found that smaller structures are older than larger ones, leading to the paradigm of Cold Dark Matter (CDM). As previously stated, this means that either Dark Matter particles are very heavy (e. g. WIMPs) or they decoupled very early (e. g. axions). This rules out neutrinos as comprising the bulk of the Dark Matter in the universe. Some of the possible candidates are discussed in Chapter 3.

Recent observations have also found that the rate of expansion of the universe is increasing, which suggests that there is a positive value for the cosmological constant (the

parameter Λ in eq. 1.4). The cause of this is given the name Dark Energy, the nature of which is entirely unknown. The name itself comes from the fact that a non-zero Λ (or the functional equivalent thereof) can be generated by including vacuum energy in the energy tensor.

In addition to CDM and a non-zero Λ, observations of the CMB have found that (in general) regions of the universe that should have never been in contact with each other (i. e. are outside of each other's light cones) are in thermal equilibrium with each other. The main hypothesis to explain this is that these regions were, at one point, in contact with each other and that there was a period of rapid inflation of the universe that has since ceased. This hypothesis is called (strangely enough) Inflation. Thus, the official title of the current Standard Model of Cosmology is ΛCDM with Inflation.

Chapter 2

Neutrinos

Neutrinos are a type of fundamental particle with no electric charge. They are fermions (with a spin of one-half) in the lepton family (meaning they participate in the Weak Interaction but not the Strong Interaction). They are the lightest known particle possessing a non-zero rest mass. Their mass is so small that it has yet to be measured, but it is presumed to be sub-eV. As it is, there are a number of properties of neutrinos that remain unknown due to the great difficulties in working with them.

2.1 History

Wolfgang Pauli first proposed the idea of the neutrino in a letter to the Tübingen conference in 1930 (in which he called it the neutron) [8]. The reason for the proposal was to solve two problems: the beta decay energy spectrum and atomic spin. The problem with the first was that the energy of electrons emitted in beta decay has a continuous energy spectrum, which conflicted with the quantization of atomic energy levels. Two explanations for the source of the spectrum were proposed, one was that the electrons were emitted with continuous energy; the other was that other factors caused a previously discrete spectrum to spread into a continuous one. The two theories were favored by Charles Ellis and Lise Meitner, respectively. In 1930, Meitner proved Ellis' hypothesis

[8]. Unfortunately, this created something of a problem: as part of Meitner's discovery it was found that the energy of the emitted electron and photon together were, in general, not sufficient to account for the energy of the decay. This raised the possibility that the conservation of energy is not valid at the subatomic level, a hypothesis favored by Niels Bohr. The problem with atomic spin was that certain atomic nuclei with an odd number of protons were found to obey Bose-Einstein statistics, which correspond to particles of integer spin, as opposed to the prediction that they would obey Fermi-Dirac statistics, which correspond to particles of half-integer spin. This raised the possibility that the interpretation of the applicability of the statistics was in fact wrong. Pauli found that both of these problems could be solved by the simple postulation of a neutrally charged particle [9]. He predicted that the new particle would be about the mass of an electron (or at most one tenth the mass of a proton), have a tiny magnetic moment, would have half-integer spin like an electron or proton and would be emitted in beta decay along with the electron.

As it turned out, Pauli was both right and wrong. He was right in that both of these problems were the result of undetected particles. He was wrong in that it was two different particles involved. In 1932, James Chadwick[1] discovered the neutron, a half-integer spin particle contained in the nucleus that solved the nuclear spin problem. However, Chadwick's neutron was found to have approximately the mass of a proton (the neutron is slightly more massive) and was thus disqualified as the other particle in beta decay. It was also found that neutrons are quite unstable, which was why no free neutrons had ever been discovered. (Indeed, beta decay is the decay of an unstable neutron into a proton and electron.) Unfortunately, this created yet another problem with beta decay. Since the neutron possessed half-integer spin it could not simply be a bound state of a proton and an electron (which was the original proposal by Ernest Rutherford [9]) as each of those particles have half-integer spin. Therefore, not only did it seem that energy was

[1]Interestingly, it was Chadwick who had discovered the curious behavior of beta emission [9].

not conserved, but angular momentum was apparently not conserved as well.

These developments encouraged Pauli to present his idea more formally at the Solvay conference in 1933 [8]. In that conference, Pauli rigorously defended his idea against Bohr, who favored violation of the conservation laws. Pauli argued that it was nonsensical for one conservation law to be obeyed (conservation of charge) but for two others to be broken [8]. One attendee who was quite impressed with Pauli's idea was Enrico Fermi, who decided to develop a full theory of beta decay, which was eventually called the weak interaction [9]. In 1934, Fermi proposed his theory, which included Pauli's neutron, dubbed by Fermi the neutrino (Italian for little neutron). In Fermi's theory, a neutron would decay into an electron, a proton and, a neutrino, now called the anti-neutrino [8]. Conservation of charge was due to the electron-proton pair and the neutrino allowed both energy and angular momentum to be conserved.

One of the first results after Fermi's theory was published was that, also in 1934, Bethe and Peierls used Fermi's theory to calculated the probability of inverse beta decay[2] occurring [10], which would raise the possibility of direct detection. They found that the probability was dismally small and concluded that neutrinos are, for all intents and purposes, undetectable [9, 10]. At the same time, researchers were beginning to probe the depths of the nucleus and were discovering a number of interesting phenomena, including artificial radioactivity. In particular, Fermi's team in Rome was working on the use of neutrons to induce radioactivity and accidentally discovered that slow neutrons are much more likely to interact with a nucleus and thus had the potential to release previously unheard-of amounts of energy[3]. All of this, combined with the global political situation at the time, meant that there was no progress in neutrino physics for twelve years.

[2]Inverse beta decay is where a neutrino or anti-neutrino is captured by a neutron or proton respectively, with the nucleon becoming a proton or neutron and emitting an electron or a positron, respectively. These reactions, in particular the neutron generating ones, require high-energy neutrinos.

[3]The fact that this discovery had major implications was not lost on Fermi's team as they patented the process of slowing neutrons almost immediately after discovering it [12].

The next development in neutrino physics came in 1946 when Bruno Pontecorvo[4] reassessed the probability of inverse beta decay and concluded that, even though the probability of a single neutrino interacting with a nucleon was very low, if one had a very large number of high energy neutrinos being fired at a very large number of targets over a long period of time, then it was possible that there would be some interactions which could be detected if the right target was used [10]. Pontecorvo recommended the use of chlorine as it was readily available in the form of cleaning fluid and the reaction $\nu + {}^{37}Cl \rightarrow {}^{37}Ar + e^{-}$ would produce an isotope of argon that has a half-life of about 35 days. He also recommended the use of nuclear reactors as they produced very large quantities of neutrinos. This method was adopted by Ray Davis, a chemist turned physicist, who at the time was looking for a field where no-one else was working [9]. Therefore, Davis in 1955 set up a large tank near the Brookhaven reactor but discovered that the background noise from cosmic radiation was so large that it obscured any possible signal from neutrinos. Because of that, Davis relocated to the Savannah River reactor, where he could place his detector sufficiently deep underground that cosmic radiation would be reduced to an acceptable level. Unfortunately, the neutrinos produced by nuclear reactors are anti-neutrinos, which meant that the setup used by Davis was incapable of actually demonstrating the existence of neutrinos [5].

Since this result was prior to the discovery of parity violation, it was taken as proof that neutrinos are Dirac particles [11]. Prior to this, there was debate as to whether neutrinos are Dirac fermions with distinct particle and anti-particle states or Majorana fermions where each particle is its own anti-particle, as happens with the uncharged bosons. Majorana developed his theory in 1938 with the motivation of eliminating the negative energy solutions of the Dirac equation and the applicability of his equation was considered for both neutrons and neutrinos [11].

[4]Pontecorvo had been part of Fermi's team in Rome and was one of the two members, the other being Edoardo Amaldi, who first noticed the effects of slow neutrons [12].

As it was, the detection of (anti)neutrinos was made by a team led by Cowan and Reines in 1953 which was also located at the Hanson reactor with the result being confirmed in 1956 (ironically at Savannah River) [5]. Cowan and Reines used the reaction $\bar{\nu_e}+p \rightarrow e^+ + n$ which they detected by looking for the signature of positron annihilation followed by that of neutron capture 5 microseconds later. Aside from being able to detect anti-neutrinos produced by reactors, this method had the advantage of providing real-time data, while in the method used by Davis data collection occurred on a monthly basis. The process used by Cowan and Reines, which earned them Nobel Prizes and a crate of champagne from Pauli [8], is used in today's reactor anti-neutrino oscillation experiments.

In 1956, T. D. Lee and C. S. Yang proposed that parity symmetry[5] is violated in weak interactions, meaning that weak interactions are not symmetric with respect to spatial reflection. This earned them the Nobel Prize in 1957 after it was confirmed by C. S. Wu [9, 10, 5]. In fact, parity was found to be maximally violated. In brief, this means that in beta decay, the (anti)neutrinos are always emitted with (right)left-handed parity, which is determined by measuring the parity of the corresponding beta particle. This implied that neutrinos are massless (see below) [8, 9, 10], which was consistent with the experimental data of the time and, indeed, had been the general view since the 1930s. An interesting speculation that resulted from this development was the proposal of "sterile" neutrinos which are non-interacting, hence sterile. In this theory, (anti)neutrinos with the parity that is never observed do exist, but are incapable of interaction, which is why they are never observed. Prior to this discovery, it was believed that parity was a fundamental symmetry of the universe. Afterwards, it was proposed that the preserved symmetry is the combination of charge conjugation with parity reversal[6]. However, it has been found through the decay of different neutral mesons such as kaons that this second symmetry is also violated in quarks, albeit to a small degree. Violation in neutrinos will be discussed

[5]This is also called P-symmetry. The violation is called P-violation.

[6]This is called CP-symmetry and its violation is CP-violation.

below.

In 1962, at Brookhaven, it was demonstrated that muon-neutrinos and electron neutrinos are different, which was accomplished by using a particle accelerator to produce large numbers of muons which were fired at a target to produce a large number of neutrinos [5]. The detector (which was shielded by 13.5 meters of steel) was set to detect both muon and electron neutrinos. This was accomplished by using the reaction $\nu_l + n \rightarrow p + l$ (where $l = e^-, \mu$) and recording the type of lepton produced. In the experiment, 29 muons were detected versus six electrons, which demonstrated that muon-neutrinos and electron-neutrinos are different [5]. (Experiments of this type are still conducted and are referred to as accelerator neutrino experiments.)

In 1958, Pontecorvo proposed the existence of neutrino oscillations [13, 14]. Pontecorvo's original theory involved oscillations between neutrino and anti-neutrino, which was inspired by a false positive recorded by Davis. Later versions included flavor mixing and even mixing between "active" and "sterile" neutrinos [13, 14, 15]. By the 70s, Pontecorvo had settled on mixing between flavors. However, since Pontecorvo had defected to the Soviet Union from Britain in 1950 [9, 12], his work largely went unnoticed in the West, where most of the neutrino experiments were being carried out. As it was, the theory of neutrino oscillations was independently developed by Maki, Nakagawa and, Sakata who first published their work in 1962 and were the first to publish results on flavor oscillations [15].

After Cowan and Reines beat him to the first detection of neutrinos, Davis modified his experiment to detect solar neutrinos. To do this he greatly increased the size of his apparatus and relocated it to a deep mine, where most noise would be eliminated. He also enlisted the aid of astrophysicist John Bahcall, who performed the calculations that predicted the expected neutrino flux and what the energies of those neutrinos would be, which in turned predicted the number of measurements Davis would make [9]. In 1968, Davis did indeed detect solar neutrinos. However, the measured number was only a

fraction of the number predicted by Bahcall. Over the next decade, Bahcall improved his calculations and Davis improved his detector but the result remained the same: there was a big discrepancy between the two. This was labeled "the solar neutrino problem" [16] and was a source of embarrassment for the physics community, partly due to the high-profile nature of Davis' experiment (Davis had gotten the funding for his experiment largely because his proposal had been featured by Time magazine in 1964) [9]. Initially, there was speculation that there was something wrong with Davis' apparatus or method. However, after a few years Davis demonstrated that his apparatus and method were not to blame[7] [9]. Many, such as Davis' immediate supervisor at Brookhaven, thought that the calculations were wrong. But every attempt to determine where proved unsuccessful. Finally, physicists concluded that the reason for the discrepancy was that certain fundamental assumptions were wrong [16].

Throughout the history of physics, there have been a number of theoretical propositions that have produced a certain level of excitement in the physics community. One such theory was proton decay, which was a hot topic in the seventies and eighties. To detect proton decay (the details of which are irrelevant here), two experiments were set up in the early 80s, one in the US called IMB (which stands for Irvine-Michigan-Brookhaven) [17] which was located in the Morton-Thiokol mine in Ohio and one in Japan called Kamiokande (Kamioka Nucleon Decay Experiment), which was located deep in the Kamioka mine approximately 300km west of Tokyo, outside the city of Toyama [18]. These experiments consisted of gigantic tanks (several hundred thousand liters) of ultra-pure water (zero contaminants), lined with thousands of photomultiplier tubes, located deep underground in order to reduce background radiation [17, 18]. As it was, they never detected proton decay. However, while they were able to eliminate most of the background, they still received noise in the form of neutrinos [17, 18]. In particular, the neutrino noise detected

[7]For example, after being challenged by another scientist over his ability to extract argon from the apparatus, Davis introduced 400 atoms of argon into his tank and recovered every single one.

was in the form of scattering.

When a neutrino encounters an electron, there is a chance that the neutrino will interact with the electron and transfer its energy to the electron [5]. If the neutrino is of sufficiently high energy, the electron will be accelerated to a speed greater than that of light in the medium in which the electron is located (provided the medium is not the vacuum). This will produce Cherenkov light, which is the optical equivalent of a sonic boom. This light will be in the form of a ring, with the center of the ring being the direction of travel for the electron. In addition, if the neutrino is a muon-neutrino and of sufficiently high energy, then the electron might be converted into a muon, which will produce a Cherenkov ring that is shaped differently from that of an electron (the ring for an electron is more diffuse than that of a muon). Thus, it is possible, with these interactions, to determine not only the total flux of neutrinos, but their flavor and direction of travel, with the latter giving the source. In order to detect these events, one would need a very large tank of ultra-pure water lined with photomultiplier tubes that is located deep underground. In other words, one would need precisely the same setup used to look for proton decay. As it was, since the proton-decay teams didn't have anything better to do, they studied the neutrino background.

The first important discovery came in 1987 when both teams recorded a 15 second spike in their data [19, 20]. This was the result of neutrinos produced by supernova SN1987A, which was a major milestone as it was the first time neutrinos had been detected from a source outside the Solar System. After that, the Kamiokande team optimized their apparatus for neutrino detection, a decision that was helped by improved calculations on the likelihood of proton decay that suggested that the probability of them making a detection of its occurrence incredibly small [9].

While the detection of extra-Solar neutrinos was a milestone, observations primarily consisted of more mundane solar and atmospheric neutrinos. (Atmospheric neutrinos are produced by cosmic ray collisions.) However, they found that the total number of

atmospheric neutrinos detected was less than predicted [21], a result that became known as the "Atmospheric neutrino anomaly" [9]. It was the combination of this result with the one for Solar neutrinos that caused the theory of neutrino oscillations to gain acceptance.

The first result in favor of neutrino oscillations that was not based on any theoretical calculations of production came in 1998 [22, 23]. That year, after months of data collection, it was found that there was a discrepancy between the flux measured by "Super-Kamiokande", an updated version of Kamiokande that included equipment and personnel from both the original Kamiokande and IMB [24], and the flux measured by the Sudbury Neutrino Observatory (SNO) located in Sudbury, Ontario, Canada [16], which used large quantities of heavy water in the detector and measured interactions of the form $\nu_e + d \rightarrow p + p + e^-$. The solar neutrino flux measured by SNO was found to be substantially less than the flux measured by Super-Kamiokande. This was because SNO was only detecting electron neutrinos while Super-Kamiokande was detecting all neutrino flavors. This meant that the total flux was comprised of substantial quantities of the other two flavors, which meant that neutrino oscillations were occurring, which was the first failure of the Standard Model of Physics, which was why the two collaborations were awarded the Nobel Prize [25].

2.2 Oscillations

Neutrinos are always created via weak processes, so far as we know. Hence, they are always produced as coherent flavour eigenstates. Each flavour eigenstate is a super-position of three mass eigenstates and it is as a super-position of the mass eigenstates that neutrinos propagate, as mass eigenstates are the eigenstates of propagation[8]. Since the mass eigenstates are not degenerate (i.e. there are different neutrino species with different masses), these eigenstates will propagate at different velocities. As long as the wavepackets associ-

[8]The mass eigenstates are the states with a temporal existence. Pontecorvo also called them the stationary states.

ated with the mass eigenstates overlap, there will be interference between the eigenstates, which will produce periodic fluctuations in the detection probability of each of the flavour states. These are called neutrino oscillations and the phenomenon as a whole is called neutrino mixing or flavour mixing [13].

As per usual, the mass and flavour eigenstates are related by a transformation matrix. This matrix is analogous to the quark mixing matrix, which served as the motivation for the suggestion of neutrino mixing. Given that there are three neutrino flavour eigenstates and (as far as is currently known) these mix with three mass eigenstates, the transformation matrix is a 3 by 3 matrix. Usually called the PMNS matrix (for Pontecorvo, Maki, Nakagawa and, Sakata) [12, 14], it is canonically parameterised as:

$$U = \begin{bmatrix} c_{12}c_{13} & s_{12}c_{13} & s_{13}\mathrm{e}^{-\mathrm{i}\delta} \\ -s_{12}c_{13} - c_{12}s_{23}s_{13}\mathrm{e}^{\mathrm{i}\delta} & c_{12}c_{23} - s_{12}s_{23}s_{13}\mathrm{e}^{\mathrm{i}\delta} & s_{23}c_{13} \\ s_{12}s_{23} - c_{12}c_{23}s_{13}\mathrm{e}^{\mathrm{i}\delta} & -c_{12}s_{23} - s_{12}c_{23}s_{13}\mathrm{e}^{\mathrm{i}\delta} & c_{23}c_{13} \end{bmatrix} \times diag(1, \mathrm{e}^{\mathrm{i}\frac{\alpha}{2}}, \mathrm{e}^{\mathrm{i}\frac{\beta}{2}}), \quad (2.1)$$

where $c_{ij} = \cos(\theta_{ij})$, $s_{ij} = \sin(\theta_{ij})$, $\theta_{ij}, i, j = \{1, 2, 3\}$ is a mixing angle, δ is the Dirac charge+parity violating term, and α and β are the two Majorana charge+parity violating terms which are guaranteed to be zero if neutrinos are actually Dirac particles.

The probability for neutrino flavour n being detected given an initial state, m, is then:

$$\begin{aligned} P_{surv.}(\nu_m \to \nu_n) &= \left| \sum_{j=1}^{3} U_{nj} U_{jm}^{\dagger} \mathrm{e}^{-\mathrm{i}E_j t} \right|^2 \\ &= \left| U_{n1} U_{1m}^{\dagger} \mathrm{e}^{-\mathrm{i}E_1 t} + U_{n2} U_{2m}^{\dagger} \mathrm{e}^{-\mathrm{i}E_2 t} + U_{n3} U_{3m}^{\dagger} \mathrm{e}^{-\mathrm{i}E_3 t} \right|^2 \\ &= U_{n1} U_{1m}^{\dagger} U_{n1} U_{1m}^{\dagger} + U_{n2} U_{2m}^{\dagger} U_{n2} U_{2m}^{\dagger} + U_{n3} U_{3m}^{\dagger} U_{n3} U_{3m}^{\dagger} + \dots \\ &\quad \cdots + 4 U_{n1} U_{1m}^{\dagger} U_{n2} U_{2m}^{\dagger} \cos(\Delta_{12} t) + 4 U_{n1} U_{1m}^{\dagger} U_{n3} U_{3m}^{\dagger} \cos(\Delta_{13} t) + \dots \\ &\quad \cdots + 4 U_{n2} U_{2m}^{\dagger} U_{n3} U_{3m}^{\dagger} \cos(\Delta_{23} t), \end{aligned} \quad (2.2)$$

where t is time since production and Δ_{ij} is the energy difference between mass eigenstates i and j, which is usually approximated as $\frac{\Delta m_{ij}^2}{2E}$, with Δm_{ij}^2 being the difference of the squared masses, i and j, and E being the production energy; this is the ultra-relativistic

approximation. The convention $\hbar = c = 1$ has been used. It is derived from:

$$E_i = \sqrt{p_i^2 + m_i^2} \approx p_i + \frac{m^2}{2p} \approx E + \frac{m^2}{2E}, \tag{2.3}$$

when $m_i << p_i \approx E$. Currently, there are two known mass-squared differences which come from observations of solar and atmospheric neutrinos respectively.

The three mixing angles, $\theta_{12}, \theta_{23}, \theta_{13}$, are measured by different types of experiments. The first two are measured by solar and atmospheric neutrino measurements and were measured soon after the confirmation of neutrino oscillations. The solar parameters are θ_{12} and δm_{12}^2 which were measured by the SNO and Super-Kamiokande collaborations around 2002 by analyzing the difference between Neutral Current and Charged Current interactions and by performing global fits across all solar neutrino measurements, comparing measured fluxes with prediction [26, 27, 28]. The atmospheric neutrino parameters θ_{23} and $|\delta m_{23}^2|$ were also measured at Super-Kamiokande, along with long baseline accelerator experiments like K2K, MINOS and, T2K[9]. These experiments looked at neutrinos (primarily muon neutrinos) with an energy on the order of 1 GeV and baselines of a few hundred km.

The smallest mixing angle, θ_{13}, was the last to be measured. The type of experiment for measuring that angle is a short-baseline reactor anti-neutrino experiment utilising multiple detectors. In the most basic setup, there is a reactor core and two identical detectors. One detector called the near detector is located at a distance of approximately 100m from the reactor while the second detector (called the far detector) is located approximately 1km from the reactor. The experiment then consists of measuring the deviation from the inverse-square law between the two detectors. Naturally, this experiment can be conducted with more detectors and reactors. The first experiment to measure this value was Daya Bay in 2012. The initial setup consisted of six detectors and six reactors (later expanded to eight each). It was soon followed up by RENO with six reactors and two detectors

[9]The K2K and T2K experiments both used the Super-Kamiokande detector as the target.

and Double Chooz with two reactors and two detectors. This was significant as θ_{13} was one of the last Standard Model parameters to be measured. (The details are expanded in Chapter 4.)

In the PMNS matrix, the only parameters left to be measured are the CP-violating phase factors. The Dirac factor δ_{CP} is currently being measured in the T2K experiment, which uses muon neutrinos (and anti-neutrinos) produced by the J-PARC accelerator in Tokyo with a dual detector setup combining near and far detectors, much like the reactor experiments. The near detector is located at a distance of 280m from the production target while the far detector is the Super-Kamiokande detector 295km away. The latest result has found the 3σ interval to be $[-3.41, -0.03]$ for the Normal Hierarchy (see below) and $[-2.54, -0.32]$ for the Inverted Hierarchy [29], with the fits favouring maximal violation of CP-symmetry at $-\frac{\pi}{2}$.

In addition, the ordering of the neutrino masses has yet to be determined. As it stands, there are two possibilities due to the fact that the sign of the atmospheric mass-squared difference is unknown. These are called the Normal Hierarchy (NH) where

$$m_1 < m_2 < m_3 \tag{2.4}$$

and the Inverted Hierarchy (IH) where

$$m_3 < m_1 < m_2. \tag{2.5}$$

The ordering can be determined by intermediate baseline ($\approx$ 60km) reactor anti-neutrino experiments. The main upcoming experiment of this type is the proposed Jiangmen Underground Neutrino Observatory (JUNO), located in Kaiping, Jiangmen, China, approximately 53 km from the Yangjiang and Taishan nuclear power plants [30]. It was expected to begin data taking in 2020 [31].

Finally, the neutrino absolute mass scale needs to be determined. The main laboratory method for doing this is precision measurements of the β-decay energy spectrum of

tritium [11, 5], with the most advanced experiment being the KArlsruhe TRItium Neutrino (KATRIN) experiment, located in Karlsruhe Germany, which is expected to have a constraint on the smallest neutrino mass of 0.2 eV. To date, the experiment has only had one run which has produced a constraint of 6 eV, which is still above the constraint of 2 eV produced by the Troitsk and Mainz experiments [32]. There are also constraints from cosmological observations [33], such as CMB anisotropy studies, which will be discussed further below. These produce a constraint on the sum of the neutrino masses to be $\Sigma m_\nu < 0.13$ eV [34].

2.2.1 Matter Effect

The matter effect, commonly known as the Mikheyev-Smirnov-Wolfenstein (MSW) effect [2], is a modulation of the neutrino mixing spectrum resulting from passage through a weakly interacting medium [35, 36]. In the case of normal matter, this is the result of coherent forward-scattering by charged-current interactions. If the medium discriminates between flavours (e.g. the medium contains electrons that couple to the electron neutrino state more strongly than the other two flavours), then the states will propagate differently from the vacuum propagation and this produces the shift.

The Hamiltonian for neutrinos propagating through regular matter (matter that par-

ticipates in the standard Weak Interaction) is

$$\begin{aligned}
\mathcal{H}_{tot} &= \mathcal{H}_{vac} + \mathcal{H}_{int} \\
&= \begin{bmatrix} E_1 & 0 & 0 \\ 0 & E_2 & 0 \\ 0 & 0 & E_3 \end{bmatrix} - \sqrt{2} g_e N_e \begin{bmatrix} U_{1e}^\dagger U_{e1} & U_{1e}^\dagger U_{e2} & U_{1e}^\dagger U_{e3} \\ U_{2e}^\dagger U_{e1} & U_{2e}^\dagger U_{e2} & U_{2e}^\dagger U_{e3} \\ U_{3e}^\dagger U_{e1} & U_{3e}^\dagger U_{e2} & U_{3e}^\dagger U_{e3} \end{bmatrix} - \dots \\
&\cdots - \sqrt{2} g_\mu N_\mu \begin{bmatrix} U_{1\mu}^\dagger U_{\mu 1} & U_{1\mu}^\dagger U_{\mu 2} & U_{1\mu}^\dagger U_{\mu 3} \\ U_{2\mu}^\dagger U_{\mu 1} & U_{2\mu}^\dagger U_{\mu 2} & U_{2\mu}^\dagger U_{\mu 3} \\ U_{3\mu}^\dagger U_{\mu 1} & U_{3\mu}^\dagger U_{\mu 2} & U_{3\mu}^\dagger U_{\mu 3} \end{bmatrix} - \dots \\
&\cdots - \sqrt{2} g_\tau N_\tau \begin{bmatrix} U_{1\tau}^\dagger U_{\tau 1} & U_{1\tau}^\dagger U_{\tau 2} & U_{1\tau}^\dagger U_{\tau 3} \\ U_{2\tau}^\dagger U_{\tau 1} & U_{2\tau}^\dagger U_{\tau 2} & U_{2\tau}^\dagger U_{\tau 3} \\ U_{3\tau}^\dagger U_{\tau 1} & U_{3\tau}^\dagger U_{\tau 2} & U_{3\tau}^\dagger U_{\tau 3} \end{bmatrix}.
\end{aligned} \tag{2.6}$$

where E_i is the energy of mass-eigenstate i, N_j is the number density of lepton species j with coupling $\sqrt{2}g_j$ and, U is the PMNS matrix. The modified form of the survival probabilities can be obtained by diagonalizing the Hamiltonian and using the eigenvalues as effective mass-squared differences, with the eigen conjugates serving as a new transformation matrix [36].

Finding the eigenvalues is a straightforward, but tedious, affair. The characteristic polynomial is:

$$\det(\mathcal{H}_{tot} - \lambda I_3) = \lambda^3 + a\lambda^2 + b\lambda + c, \tag{2.7}$$

where a, b, and c are given by:

$$\begin{aligned}
a = \sqrt{2} g_e N_e (U_{1e}^\dagger U_{e1} + U_{2e}^\dagger U_{e2} + U_{3e}^\dagger U_{e3}) + \sqrt{2} g_\mu N_\mu U_{1\mu}^\dagger U_{\mu 1} + U_{2\mu}^\dagger U_{\mu 2} + U_{3\mu}^\dagger U_{\mu 3}) + \dots \\
\cdots + \sqrt{2} g_\tau N_\tau (U_{1\tau}^\dagger U_{\tau 1} + U_{2\tau}^\dagger U_{\tau 2} + U_{3\tau}^\dagger U_{\tau 3}) - \tfrac{\delta m_{12}^2}{2E} - \tfrac{\delta m_{13}^2}{2E} - 3\tfrac{m_1^2}{2E},
\end{aligned}$$

$$b = 3\left(\frac{m_1^2}{2E}\right)^2 + \frac{m_1^2}{2E}(2\frac{\delta m_{12}^2}{2E} + 2\frac{\delta m_{13}^2}{2E} - 2\sqrt{2}g_e N_e(U_{1e}^\dagger U_{e1} + U_{2e}^\dagger U_{e2} + U_{3e}^\dagger U_{e3}) - \dots$$
$$\cdots - 2\sqrt{2}g_\mu N_\mu(U_{1\mu}^\dagger U_{\mu 1} + U_{2\mu}^\dagger U_{\mu 2} + U_{3\mu}^\dagger U_{\mu 3}) - 2\sqrt{2}g_\tau N_\tau(U_{1\tau}^\dagger U_{\tau 1} + U_{2\tau}^\dagger U_{\tau 2} + U_{3\tau}^\dagger U_{\tau 3})) + \dots$$
$$\cdots + \frac{\delta m_{12}^2}{2E}\frac{\delta m_{13}^2}{2E} - \sqrt{2}g_e N_e U_{1e}^\dagger U_{e1}\frac{\delta m_{12}^2}{2E} - \sqrt{2}g_\mu N_\mu U_{1\mu}^\dagger U_{\mu 1}\frac{\delta m_{12}^2}{2E} - \sqrt{2}g_\tau N_\tau U_{1\tau}^\dagger U_{\tau 1}\frac{\delta m_{12}^2}{2E} - \dots$$
$$\cdots - \sqrt{2}g_e N_e U_{3e}^\dagger U_{e3}\frac{\delta m_{12}^2}{2E} - \sqrt{2}g_\mu N_\mu U_{3\mu}^\dagger U_{\mu 3}\frac{\delta m_{12}^2}{2E} - \sqrt{2}g_\tau N_\tau U_{3\tau}^\dagger U_{\tau 3}\frac{\delta m_{12}^2}{2E} - \dots$$
$$\cdots - \sqrt{2}g_e N_e U_{1e}^\dagger U_{e1}\frac{\delta m_{13}^2}{2E} - \sqrt{2}g_\mu N_\mu U_{1\mu}^\dagger U_{\mu 1}\frac{\delta m_{13}^2}{2E} - \sqrt{2}g_\tau N_\tau U_{1\tau}^\dagger U_{\tau 1}\frac{\delta m_{13}^2}{2E} - \dots$$
$$\cdots - \sqrt{2}g_e N_e U_{2e}^\dagger U_{e2}\frac{\delta m_{13}^2}{2E} - \sqrt{2}g_\mu N_\mu U_{2\mu}^\dagger U_{\mu 2}\frac{\delta m_{13}^2}{2E} - \sqrt{2}g_\tau N_\tau U_{2\tau}^\dagger U_{\tau 2}\frac{\delta m_{13}^2}{2E} + \dots$$
$$\cdots + \left(\sqrt{2}g_e N_e\sqrt{2}g_\mu N_\mu\right) U_{1e}^\dagger U_{e1} U_{2\mu}^\dagger U_{\mu 2} + \left(\sqrt{2}g_e N_e\sqrt{2}g_\mu N_\mu\right) U_{1\mu}^\dagger U_{\mu 1} U_{2e}^\dagger U_{e2} - \dots$$
$$\cdots - \left(\sqrt{2}g_e N_e\sqrt{2}g_\mu N_\mu\right) U_{1e}^\dagger U_{e2} U_{2\mu}^\dagger U_{\mu 1} - \left(\sqrt{2}g_e N_e\sqrt{2}g_\mu N_\mu\right) U_{1\mu}^\dagger U_{\mu 2} U_{2e}^\dagger U_{e1} + \dots$$
$$\cdots + \left(\sqrt{2}g_e N_e\sqrt{2}g_\mu N_\mu\right) U_{1e}^\dagger U_{e1} U_{3\mu}^\dagger U_{\mu 3} + \left(\sqrt{2}g_e N_e\sqrt{2}g_\mu N_\mu\right) U_{1\mu}^\dagger U_{\mu 1} U_{3e}^\dagger U_{e3} - \dots$$
$$\cdots - \left(\sqrt{2}g_e N_e\sqrt{2}g_\mu N_\mu\right) U_{1e}^\dagger U_{e3} U_{3\mu}^\dagger U_{\mu 1} - \left(\sqrt{2}g_e N_e\sqrt{2}g_\mu N_\mu\right) U_{1\mu}^\dagger U_{\mu 3} U_{3e}^\dagger U_{e1} + \dots$$
$$\cdots + \left(\sqrt{2}g_e N_e\sqrt{2}g_\mu N_\mu\right) U_{2e}^\dagger U_{e2} U_{3\mu}^\dagger U_{\mu 3} + \left(\sqrt{2}g_e N_e\sqrt{2}g_\mu N_\mu\right) U_{2\mu}^\dagger U_{\mu 2} U_{3e}^\dagger U_{e3} - \dots$$
$$\cdots - \left(\sqrt{2}g_e N_e\sqrt{2}g_\mu N_\mu\right) U_{2e}^\dagger U_{e3} U_{3\mu}^\dagger U_{\mu 2} - \left(\sqrt{2}g_e N_e\sqrt{2}g_\mu N_\mu\right) U_{2\mu}^\dagger U_{\mu 3} U_{3e}^\dagger U_{e2} + \dots$$
$$\cdots + \sqrt{2}g_e N_e\sqrt{2}g_\tau N_\tau U_{1e}^\dagger U_{e1} U_{2\tau}^\dagger U_{\tau 2} + \sqrt{2}g_e N_e\sqrt{2}g_\tau N_\tau U_{1\tau}^\dagger U_{\tau 1} U_{2e}^\dagger U_{e2} - \dots$$
$$\cdots - \sqrt{2}g_e N_e\sqrt{2}g_\tau N_\tau U_{1e}^\dagger U_{e2} U_{2\tau}^\dagger U_{\tau 1} - \sqrt{2}g_e N_e\sqrt{2}g_\tau N_\tau U_{1\tau}^\dagger U_{\tau 2} U_{2e}^\dagger U_{e1} + \dots$$
$$\cdots + \sqrt{2}g_e N_e\sqrt{2}g_\tau N_\tau U_{1e}^\dagger U_{e1} U_{3\tau}^\dagger U_{\tau 3} + \sqrt{2}g_e N_e\sqrt{2}g_\tau N_\tau U_{1\tau}^\dagger U_{\tau 1} U_{3e}^\dagger U_{e3} - \dots$$
$$\cdots - \sqrt{2}g_e N_e\sqrt{2}g_\tau N_\tau U_{1e}^\dagger U_{e3} U_{3\tau}^\dagger U_{\tau 1} - \sqrt{2}g_e N_e\sqrt{2}g_\tau N_\tau U_{1\tau}^\dagger U_{\tau 3} U_{3e}^\dagger U_{e1} + \dots$$
$$\cdots + \sqrt{2}g_e N_e\sqrt{2}g_\tau N_\tau U_{2e}^\dagger U_{e2} U_{3\tau}^\dagger U_{\tau 3} + \sqrt{2}g_e N_e\sqrt{2}g_\tau N_\tau U_{2\tau}^\dagger U_{\tau 2} U_{3e}^\dagger U_{e3} - \dots$$
$$\cdots - \sqrt{2}g_e N_e\sqrt{2}g_\tau N_\tau U_{2e}^\dagger U_{e3} U_{3\tau}^\dagger U_{\tau 2} - \sqrt{2}g_e N_e\sqrt{2}g_\tau N_\tau U_{2\tau}^\dagger U_{\tau 3} U_{3e}^\dagger U_{e2} + \dots$$
$$\cdots + \sqrt{2}g_\mu N_\mu\sqrt{2}g_\tau N_\tau U_{1\mu}^\dagger U_{\mu 1} U_{2\tau}^\dagger U_{\tau 2} + \sqrt{2}g_\mu N_\mu\sqrt{2}g_\tau N_\tau U_{1\tau}^\dagger U_{\tau 1} U_{2\mu}^\dagger U_{\mu 2} - \dots$$
$$\cdots - \sqrt{2}g_\mu N_\mu\sqrt{2}g_\tau N_\tau U_{1\mu}^\dagger U_{\mu 2} U_{2\tau}^\dagger U_{\tau 1} - \sqrt{2}g_\mu N_\mu\sqrt{2}g_\tau N_\tau U_{1\tau}^\dagger U_{\tau 2} U_{2\mu}^\dagger U_{\mu 1} + \dots$$
$$\cdots + \sqrt{2}g_\mu N_\mu\sqrt{2}g_\tau N_\tau U_{1\mu}^\dagger U_{\mu 1} U_{3\tau}^\dagger U_{\tau 3} + \sqrt{2}g_\mu N_\mu\sqrt{2}g_\tau N_\tau U_{1\tau}^\dagger U_{\tau 1} U_{3\mu}^\dagger U_{\mu 3} - \dots$$
$$\cdots - \sqrt{2}g_\mu N_\mu\sqrt{2}g_\tau N_\tau U_{1\mu}^\dagger U_{\mu 3} U_{3\tau}^\dagger U_{\tau 1} - \sqrt{2}g_\mu N_\mu\sqrt{2}g_\tau N_\tau U_{1\tau}^\dagger U_{\tau 3} U_{3\mu}^\dagger U_{\mu 1} + \dots$$
$$\cdots + \sqrt{2}g_\mu N_\mu\sqrt{2}g_\tau N_\tau U_{2\mu}^\dagger U_{\mu 2} U_{3\tau}^\dagger U_{\tau 3} + \sqrt{2}g_\mu N_\mu\sqrt{2}g_\tau N_\tau U_{2\tau}^\dagger U_{\tau 2} U_{3\mu}^\dagger U_{\mu 3} - \dots$$
$$\cdots - \sqrt{2}g_\mu N_\mu\sqrt{2}g_\tau N_\tau U_{2\mu}^\dagger U_{\mu 3} U_{3\tau}^\dagger U_{\tau 2} - \sqrt{2}g_\mu N_\mu\sqrt{2}g_\tau N_\tau U_{2\tau}^\dagger U_{\tau 3} U_{3\mu}^\dagger U_{\mu 2}$$

$$c = (\sqrt{2}g_e N_e U^\dagger_{1e} U_{e1} + \sqrt{2}g_e N_e U^\dagger_{2e} U_{e2} + \sqrt{2}g_e N_e U^\dagger_{3e} U_{e3} + \sqrt{2}g_\mu N_\mu U^\dagger_{1\mu} U_{\mu 1} + \sqrt{2}g_\mu N_\mu U^\dagger_{2\mu} U_{\mu 2} + \dots$$
$$\cdots + \sqrt{2}g_\mu N_\mu U^\dagger_{3\mu} U_{\mu 3} + \sqrt{2}g_\tau N_\tau U^\dagger_{1\tau} U_{\tau 1} + \sqrt{2}g_\tau N_\tau U^\dagger_{2\tau} U_{\tau 2} + \sqrt{2}g_\tau N_\tau U^\dagger_{3\tau} U_{\tau 3} - \tfrac{\delta m^2_{13}}{2E} - \tfrac{\delta m^2_{12}}{2E}) \left(\tfrac{m^2_1}{2E}\right)^2 -$$
$$\cdots - \left(\tfrac{m^2_1}{2E}\right)^3 + [(\sqrt{2}g_e N_e)^2 U^\dagger_{1e} U_{e2} U^\dagger_{2e} U_{e1} - (\sqrt{2}g_e N_e)^2 U^\dagger_{1e} U_{e1} U^\dagger_{2e} U_{e2} - (\sqrt{2}g_e N_e)^2 U^\dagger_{2e} U_{e2} U^\dagger_{3e} U_{e3} - \dots$$
$$\cdots - (\sqrt{2}g_e N_e)^2 U^\dagger_{1e} U_{e1} U^\dagger_{3e} U_{e3} + (\sqrt{2}g_e N_e)^2 U^\dagger_{1e} U_{e3} U^\dagger_{3e} U_{e1} + (\sqrt{2}g_e N_e)^2 U^\dagger_{2e} U_{e3} U^\dagger_{3e} U_{e2} + \dots$$
$$\cdots - (\sqrt{2}g_\mu N_\mu)^2 U^\dagger_{1\mu} U_{\mu 1} U^\dagger_{2\mu} U_{\mu 2} - (\sqrt{2}g_\mu N_\mu)^2 U^\dagger_{1\mu} U_{\mu 1} U^\dagger_{3\mu} U_{\mu 3} + (\sqrt{2}g_\mu N_\mu)^2 U^\dagger_{1\mu} U_{\mu 2} U^\dagger_{2\mu} U_{\mu 1} - \dots$$
$$\cdots + (\sqrt{2}g_\mu N_\mu)^2 U^\dagger_{1\mu} U_{\mu 3} U^\dagger_{3\mu} U_{\mu 1} - (\sqrt{2}g_\mu N_\mu)^2 U^\dagger_{2\mu} U_{\mu 2} U^\dagger_{3\mu} U_{\mu 3} + (\sqrt{2}g_\mu N_\mu)^2 U^\dagger_{2\mu} U_{\mu 3} U^\dagger_{3\mu} U_{\mu 1} + \dots$$
$$\cdots + (\sqrt{2}g_\tau N_\tau)^2 U^\dagger_{1e} U_{e3} U^\dagger_{3\tau} U_{\tau 1} - (\sqrt{2}g_\tau N_\tau)^2 U^\dagger_{1\tau} U_{\tau 1} U^\dagger_{2\tau} U_{\tau 2} + (\sqrt{2}g_\tau N_\tau)^2 U^\dagger_{1\tau} U_{\tau 2} U^\dagger_{2\tau} U_{\tau 1} - \dots$$
$$\cdots - (\sqrt{2}g_\tau N_\tau)^2 U^\dagger_{2\tau} U_{\tau 2} U^\dagger_{3\tau} U_{\tau 3} + -(\sqrt{2}g_\tau N_\tau)^2 U^\dagger_{1\tau} U_{\tau 1} U^\dagger_{3\tau} U_{\tau 3} + (\sqrt{2}g_\tau N_\tau)^2 U^\dagger_{2\tau} U_{\tau 3} U^\dagger_{3\tau} U_{\tau 2} + \dots$$
$$\cdots + \sqrt{2}g_e N_e U^\dagger_{1e} U_{e1} \tfrac{\delta m^2_{12}}{2E} + \sqrt{2}g_e N_e U^\dagger_{1e} U_{e1} \tfrac{\delta m^2_{13}}{2E} + \sqrt{2}g_e N_e U^\dagger_{2e} U_{e2} \tfrac{\delta m^2_{13}}{2E} + \dots$$
$$\cdots + \sqrt{2}g_e N_e U^\dagger_{3e} U_{e3} \tfrac{\delta m^2_{12}}{2E} + \sqrt{2}g_\mu N_\mu U^\dagger_{1\mu} U_{\mu 1} \tfrac{\delta m^2_{12}}{2E} + \sqrt{2}g_\mu N_\mu U^\dagger_{1\mu} U_{\mu 1} \tfrac{\delta m^2_{13}}{2E} + \dots$$
$$\cdots + \sqrt{2}g_\mu N_\mu U^\dagger_{2\mu} U_{\mu 2} \tfrac{\delta m^2_{13}}{2E} + \sqrt{2}g_\mu N_\mu U^\dagger_{3\mu} U_{\mu 3} \tfrac{\delta m^2_{12}}{2E} + \sqrt{2}g_\tau N_\tau U^\dagger_{1\tau} U_{\tau 1} \tfrac{\delta m^2_{13}}{2E} + \dots$$
$$\cdots + \sqrt{2}g_\tau N_\tau U^\dagger_{1\tau} U_{\tau 1} \tfrac{\delta m^2_{12}}{2E} + \sqrt{2}g_\tau N_\tau U^\dagger_{2\tau} U_{\tau 2} \tfrac{\delta m^2_{13}}{2E} + \sqrt{2}g_\tau N_\tau U^\dagger_{3\tau} U_{\tau 3} \tfrac{\delta m^2_{12}}{2E} - \dots$$
$$\cdots - \sqrt{2}g_e N_e \sqrt{2}g_\mu N_\mu U^\dagger_{1e} U_{e1} U^\dagger_{2\mu} U_{\mu 2} - \sqrt{2}g_e N_e \sqrt{2}g_\mu N_\mu U^\dagger_{1\mu} U_{\mu 1} U^\dagger_{2e} U_{e2} + \dots$$
$$\cdots + \sqrt{2}g_e N_e \sqrt{2}g_\mu N_\mu U^\dagger_{1e} U_{e2} U^\dagger_{2\mu} U_{\mu 1} + \sqrt{2}g_e N_e \sqrt{2}g_\mu N_\mu U^\dagger_{1\mu} U_{\mu 2} U^\dagger_{2e} U_{e1} - \dots$$
$$\cdots - \sqrt{2}g_e N_e \sqrt{2}g_\mu N_\mu U^\dagger_{1e} U_{e1} U^\dagger_{3\mu} U_{\mu 3} - \sqrt{2}g_e N_e \sqrt{2}g_\mu N_\mu U^\dagger_{1\mu} U_{\mu 1} U^\dagger_{3e} U_{e3} + \dots$$
$$\cdots + \sqrt{2}g_e N_e \sqrt{2}g_\mu N_\mu U^\dagger_{1e} U_{e3} U^\dagger_{3\mu} U_{\mu 1} + \sqrt{2}g_e N_e \sqrt{2}g_\mu N_\mu U^\dagger_{1\mu} U_{\mu 3} U^\dagger_{3e} U_{e1} - \dots$$
$$\cdots - \sqrt{2}g_e N_e \sqrt{2}g_\mu N_\mu U^\dagger_{2e} U_{e2} U^\dagger_{3\mu} U_{\mu 3} - \sqrt{2}g_e N_e \sqrt{2}g_\mu N_\mu U^\dagger_{2\mu} U_{\mu 2} U^\dagger_{3e} U_{e3} + \dots$$
$$\cdots + \sqrt{2}g_e N_e \sqrt{2}g_\mu N_\mu U^\dagger_{2e} U_{e3} U^\dagger_{3\mu} U_{\mu 1} + \sqrt{2}g_e N_e \sqrt{2}g_\mu N_\mu U^\dagger_{2\mu} U_{\mu 3} U^\dagger_{3e} U_{e2} - \dots$$
$$\cdots - \sqrt{2}g_e N_e \sqrt{2}g_\tau N_\tau U^\dagger_{1e} U_{e1} U^\dagger_{2\tau} U_{\tau 2} - \sqrt{2}g_e N_e \sqrt{2}g_\tau N_\tau U^\dagger_{1\tau} U_{\tau 1} U^\dagger_{2e} U_{e2} + \dots$$
$$\cdots + \sqrt{2}g_e N_e \sqrt{2}g_\tau N_\tau U^\dagger_{1e} U_{e2} U^\dagger_{2\tau} U_{\tau 1} + \sqrt{2}g_e N_e \sqrt{2}g_\tau N_\tau U^\dagger_{1\tau} U_{\tau 2} U^\dagger_{2e} U_{e1} - \dots$$
$$\cdots - \sqrt{2}g_e N_e \sqrt{2}g_\tau N_\tau U^\dagger_{1e} U_{e1} U^\dagger_{3\tau} U_{\tau 3} - \sqrt{2}g_e N_e \sqrt{2}g_\tau N_\tau U^\dagger_{1\tau} U_{\tau 1} U^\dagger_{3e} U_{e3} + \dots$$
$$\cdots + \sqrt{2}g_e N_e \sqrt{2}g_\tau N_\tau U^\dagger_{1e} U_{e3} U^\dagger_{3\tau} U_{\tau 1} + \sqrt{2}g_e N_e \sqrt{2}g_\tau N_\tau U^\dagger_{1e} U_{e3} U^\dagger_{3e} U_{e1} - \dots$$
$$\cdots - \sqrt{2}g_e N_e \sqrt{2}g_\tau N_\tau U^\dagger_{2e} U_{e2} U^\dagger_{3\tau} U_{\tau 3} - \sqrt{2}g_e N_e \sqrt{2}g_\tau N_\tau U^\dagger_{2\tau} U_{\tau 2} U^\dagger_{3e} U_{e3} + \dots$$
$$\cdots + \sqrt{2}g_e N_e \sqrt{2}g_\tau N_\tau U^\dagger_{2e} U_{e3} U^\dagger_{3\tau} U_{\tau 2} + \sqrt{2}g_e N_e \sqrt{2}g_\tau N_\tau U^\dagger_{2\tau} U_{\tau 3} U^\dagger_{3e} U_{e2} - \dots$$
$$\cdots - \sqrt{2}g_\mu N_\mu \sqrt{2}g_\tau N_\tau U^\dagger_{1\mu} U_{\mu 1} U^\dagger_{2\tau} U_{\tau 2} - \sqrt{2}g_\mu N_\mu \sqrt{2}g_\tau N_\tau U^\dagger_{1\tau} U_{\tau 1} U^\dagger_{2\mu} U_{\mu 2} + \dots$$
$$\cdots + \sqrt{2}g_\mu N_\mu \sqrt{2}g_\tau N_\tau U^\dagger_{1\mu} U_{\mu 2} U^\dagger_{2\tau} U_{\tau 1} + \sqrt{2}g_\mu N_\mu \sqrt{2}g_\tau N_\tau U^\dagger_{1\tau} U_{\tau 2} U^\dagger_{2\mu} U_{\mu 1} - \dots$$
$$\cdots - \sqrt{2}g_\mu N_\mu \sqrt{2}g_\tau N_\tau U^\dagger_{1\mu} U_{\mu 1} U^\dagger_{3\tau} U_{\tau 3} - \sqrt{2}g_\mu N_\mu \sqrt{2}g_\tau N_\tau U^\dagger_{1\tau} U_{\tau 1} U^\dagger_{3\mu} U_{\mu 3} + \dots$$
$$\cdots + \sqrt{2}g_\mu N_\mu \sqrt{2}g_\tau N_\tau U^\dagger_{1\mu} U_{\mu 3} U^\dagger_{3\tau} U_{\tau 1} + \sqrt{2}g_\mu N_\mu \sqrt{2}g_\tau N_\tau U^\dagger_{1e} U_{e3} U^\dagger_{3\mu} U_{\mu 1} - \dots$$
$$\cdots - \sqrt{2}g_\mu N_\mu \sqrt{2}g_\tau N_\tau U^\dagger_{2\mu} U_{\mu 2} U^\dagger_{3\tau} U_{\tau 3} - \sqrt{2}g_\mu N_\mu \sqrt{2}g_\tau N_\tau U^\dagger_{2\tau} U_{\tau 2} U^\dagger_{3\mu} U_{\mu 3} + \dots$$
$$\cdots + \sqrt{2}g_\mu N_\mu \sqrt{2}g_\tau N_\tau U^\dagger_{2\mu} U_{\mu 3} U^\dagger_{3\tau} U_{\tau 2} + \sqrt{2}g_\mu N_\mu \sqrt{2}g_\tau N_\tau U^\dagger_{2\tau} U_{\tau 3} U^\dagger_{3\mu} U_{\mu 1} - \tfrac{\delta m^2_{12}}{2E} \tfrac{\delta m^2_{13}}{2E}] \tfrac{m^2_1}{2E} + \dots$$
$$\cdots + \textit{terms independent of absolute mass.}$$

This assumed the normal hierarchy is used; the inverted hierarchy will produce similar results.

The solution to the characteristic equation, which is found by converting to a depressed cubic and using the triganometric solution, is:

$$\lambda_k = 2\sqrt{-\tfrac{p}{3}}\cos\left(\tfrac{1}{3}\arccos\left(\tfrac{3q}{2p}\sqrt{-\tfrac{3}{p}}\right) - \tfrac{2\pi k}{3}\right) - \tfrac{a}{3}, \tag{2.8}$$

where

$$p = \tfrac{3b-a^2}{3},$$

$$q = \tfrac{2a^3-9ab+27c}{27},$$

and $k = 0, 1, 2$.

A computation of p and q will reveal that they are independent of absolute mass, meaning that λ_k can be written as:

$$\lambda_k = \frac{m_1^2}{2E} + \lambda_k^*, \tag{2.9}$$

where λ_k^* is independent of absolute mass.

Thus, each eigenvalue is an effective mass-squared term, meaning that the probability equation will have the same form as in vacuum oscillations (Eq. 2.2) but with the mass-squared differences replaced with effective mass-squared differences and the mixing matrix terms replaced by modified mixing terms, which are modified by the eigenvectors of the modified mass matrix. Fortunately, establishing the independence of the eigenvectors is simple once the eigenvalues have been calculated.

Let $\mathbf{v}$ be an eigenvector of $\mathcal{H}_{tot}$. Then, by definition:

$$\begin{aligned} \lambda\mathbf{v} &= \mathcal{H}_{tot}\mathbf{v} \\ &= \left(\mathcal{H}^* + \tfrac{m_1^2}{2E}I_3\right)\mathbf{v} \\ &= \mathcal{H}^*\mathbf{v} + \tfrac{m_1^2}{2E}\mathbf{v}, \end{aligned} \tag{2.10}$$

where $\mathcal{H}^*$ is independent of absolute mass. Combining (2.9) with (2.10) and rearranging gives:

$$\mathcal{H}^*\mathbf{v} = \lambda_k^*\mathbf{v}, \tag{2.11}$$

meaning that $\mathbf{v}$ is also an eigenvector of $\mathcal{H}^*$ with eigenvalue λ_k^*. Since $\mathcal{H}^*$ is independent of absolute mass and λ_k^* is independent of absolute mass, it follows that $\mathbf{v}$ is also independent of absolute mass. This means that calculations can be performed without regard for the absolute mass scale, as is true for vacuum oscillations. The resulting formula is:

$$f_\beta = \sum_{\alpha=e,\mu,\tau} \left| \sum_{i=1}^{3} U_{\beta i} U_{i\alpha}^\dagger \mathrm{e}^{-\mathrm{i}E_i t} \right|^2 f_\alpha, \tag{2.12}$$

where f_α is the emission flavour vector (i.e. a normalized vector containing the three flavour fractions), f_β is the flavour vector at the detector and U is the matrix translating between the flavour basis and the effective mass basis.

$$\begin{aligned} f_\beta &= f_\alpha \times ((U_{\beta,1}U_{1,\alpha}^\dagger)^2 + (U_{\beta,2}U_{2,\alpha}^\dagger)^2 + (U_{\beta,3}U_{3,\alpha}^\dagger)^2 \\ &\quad + 2U_{\beta,1}U_{1,\alpha}^\dagger U_{\beta,2}U_{2,\alpha}^\dagger \cos(\Delta E_{12}t) + \dots \\ &\quad + 2U_{\beta,1}U_{1,\alpha}^\dagger U_{\beta,3}U_{3,\alpha}^\dagger \cos(\Delta E_{13}t) + 2U_{\beta,2}U_{2,\alpha}^\dagger U_{\beta,3}U_{3,\alpha}^\dagger \cos(\Delta E_{23}t)), \end{aligned} \tag{2.13}$$

where ΔE_{ij} is the difference between energies i and j, t is the time since neutrino creation and $U_{l,k}$ is the (l,k) term in the PMNS matrix, Eq. 2.1. In the presence of a medium (some non-zero V_{ij}) and taking the ultra-relativistic limit ($E_i \approx \frac{m_i^2}{2E}$ and t is replaced with L, the baseline), this is modified to:

$$\begin{aligned} f_\beta &= f_\alpha \times ((W_{\beta,1}W_{1,\alpha}^\dagger)^2 + (W_{\beta,2}W_{2,\alpha}^\dagger)^2 + (W_{\beta,3}W_{3,\alpha}^\dagger)^2 + \dots \\ &\quad + 2W_{\beta,1}W_{1,\alpha}^\dagger W_{\beta,2}W_{2,\alpha}^\dagger \cos(\frac{\Delta M_{12}^2}{2E}L) + \dots \\ &\quad + 2W_{\beta,1}W_{1,\alpha}^\dagger W_{\beta,3}W_{3,\alpha}^\dagger \cos(\frac{\Delta M_{13}^2}{2E}L) + \dots \\ &\quad + 2W_{\beta,2}W_{2,\alpha}^\dagger W_{\beta,3}W_{3,\alpha}^\dagger \cos(\frac{\Delta M_{23}^2}{2E}L)), \end{aligned} \tag{2.14}$$

where ΔM^2_{ij} is the effective mass-squared difference (which is energy dependent) and $W_{l,k}$ is the (l,k) term in the effective mixing matrix, which is also energy dependent. These terms are derived from the diagonalization of $\mathcal{H}_{tot}$ to produce $\mathcal{H}_{eff} = W^{\dagger}\mathcal{H}_{tot}W$, the effective Hamiltonian, which was done numerically[10].

An important aspect to remember is that the distribution of the matter through which the neutrinos pass is irrelevant to these calculations and that the number densities cited are the average densities along the baseline. The size of the effect is determined by the total number of opportunities for interaction the neutrinos have had along their flight-path, but not when those opportunities occurred.

2.2.2 Coherence

The formulas given above are valid so long as the wavepackets associated with the different mass states overlap (a condition known as coherence). The separation of the wavepackets occurs due to small differences in the relative velocities. If the wave-packet separation exceeds the wavepacket size, then de-coherence (a loss of coherence) occurs. Another form of de-coherence occurs when an experiment is incapable of resolving coherent effects.

Since time is related to distance traveled, this translates to a requirement that the baseline (distance traveled), L, be much less than the coherence length (the length beyond which decoherence is guaranteed), L_{coh} [37], which is given by:

$$L \ll L_{coh} = \sigma_X \frac{V_G}{\Delta V} \approx \sigma_X \frac{2E^2}{\Delta m^2}, \tag{2.15}$$

where σ_X is the wavepacket size, V_G is the group velocity, ΔV is the difference in wavepacket velocities, and the ultra-relativistic approximations, $V_G \approx 1$ and $\Delta V \approx \frac{\Delta m^2}{2E^2}$,

[10]Since the diagonalization was done numerically, the actual computations replaced $\frac{\Delta M^2_{13}}{2E}$ with $\delta\lambda_{ij}$., the difference between diagonal terms λ_i and λ_j in $\mathcal{H}_{eff}$. Thus, Eq. 2.12 becomes

$$f_\beta = \sum_{\alpha=e,\mu,\tau} \left| \sum_{i=1}^{3} W_{\beta i} W^{\dagger}_{i\alpha} \mathrm{e}^{-\mathrm{i}\lambda_i t} \right|^2 f_\alpha.$$

have been used[11]. An important feature to remember is that the wavepacket size is an effective size. This is, in general, the larger of the source's physical size and the inverse of the detector's energy resolution (presuming that the two differ greatly). Practically speaking, it is whichever makes observations the most difficult.

The limitation on the wavepacket size is that it be smaller than the oscillation wavelength, i.e:

$$\sigma_X \ll l_{osc} \approx \frac{4\pi p}{\Delta m^2}, \tag{2.16}$$

where p is the momentum of the wavepacket, which is generally substituted for energy, due to the ultra-relativistic nature of the neutrinos. Since, the wavepacket size will at least be as large as the source object, this puts a limit on the maximum size of the source.

These two equations can be combined and rearranged to give

$$L \ll \frac{8\pi E^3}{(\Delta m^2)^2} \tag{2.17}$$

which for $E \geq 1$ TeV[12] is satisfied by all baselines within the observable universe by several orders of magnitude.

In order to determine the relationship with the energy resolution, it helps to employ the relationship between wavepacket size and energy uncertainty,

$$\sigma_X \approx \frac{V}{\sigma_E} \approx \frac{1}{\sigma_E}. \tag{2.18}$$

Combining this relationship with the inequality, Eq. 2.15, gives [38],

$$\frac{\Delta m^2}{2E^2} \ll \frac{\sigma_E}{E} \ll \frac{2E}{L\Delta m^2}. \tag{2.19}$$

This puts a significant limit on the energy uncertainty for large L. At 1 PeV and with a baseline of 1 kpc[13], the requirement on energy resolution is $\frac{\sigma_E}{E} \ll 10^{-6}$, which is much

[11] Δm^2 is the larger of the two mass-squared differences, as that is the dominant factor. Also, the convention $\hbar = c = 1$ has been used.

[12] This choice of energy is motivated by ultra-high astrophysical neutrino studies, as those were the motivation for considering coherence effects (see Chapter 5).

[13] These values are again motivated by ultra-high energy neutrinos, with the choice of baseline being the distance to the nearest known black hole, A0620-00.

smaller than currently available.

It should also be noted that there is a minimum limit on the wavepacket size. Essentially, the smaller the wave-packets the easier it is for them to separate. The most likely way this could occur is through magnetic squeezing (where magnetic fields constrain the parent particles, reducing the size of the wavepackets) which is predicted to occur in virtually all extra-galactic sources [39].

2.3 Mass Generation

There are two problems with massive neutrinos. One is the size of that mass; neutrinos are at least six orders of magnitude lighter than electrons (and are probably much lighter than that). Another is the fact that, as already stated, neutrinos have only ever been observed with one helicity state. Thus, they require a mass generation mechanism that can accommodate both features. The masses of other particles are generated via the Higgs mechanism, whereby they become massive after coupling to the Higgs field[14] [40]. This can work with the absolute neutrino mass scale, but only because the coupling constants in the Higgs interaction are undefined for anything other than the Weak bosons which leaves all other particle masses undefined. However, it requires the existence of four helicity states; this means that neutrinos would need some sort of right-handed state, in addition to the left-handed one, in order to work with the Higgs mechanism. One proposed solution is to have right-handed states which do not participate in the Weak interaction and are thus undetectable; these states are called "Sterile Neutrinos". Other solutions involve novel methods for neutrino mass generation. Some of these are discussed later.

A commonly proposed connection between neutrinos and DM is virtual mixing mass models, where the neutrino gains its very small mass through virtual mixing with DM. Virtual mixing models come in two basic varieties: the See-Saw models, which have mixing

[14]Technically, only the weak bosons gain mass via the Higgs mechanism; other particles gain their mass via Yukawa interactions which involve the Higgs field.

at tree-level, and the Radiative models, which occur at higher orders.

2.3.1 See-Saw Models

The see-saw model comes in three basic types: Type I, Type II, and Type III.

In the TI see-saw model, the "normal" neutrinos get their mass via the Higgs interaction, in which they alternate between left and right-handed states (with the right-handed states being newly added sterile states) [41, 42]. The right-handed states are presumed to be much more massive than the left-handed states. Additionally, the unique interactions of the right-handed states can involve new scalar fields, which themselves are capable of producing a dark matter candidate (a majoron), given global symmetry breaking induced by quantum-gravity [43]. In this model, the dominant neutrino mass term is the Majorana term.

In the TII see-saw model, the left-handed states couple to a triplet Higgs [44]. This induces both Dirac and Majorana mass terms in the left-handed state with the Dirac terms being the much more massive ones (making the TII see-saw structure the opposite of TI). TIII is a different type which does not produce a DM candidate as the heavy partners have zero hypercharge and are thus unstable [45].

2.3.2 Radiative Mass Generation

A Radiative Mass Generation (RMG) model involves the neutrino virtually splitting into a boson and fermion with the fermion coupling to the Higgs field before the particles reassemble into a neutrino [46, 47, 48]. There can also be any number of splittings after the first, with models being categorized by the number of such splittings (e.g. the basic version is called a one-loop model while a two-loop model has the fermion, after coupling to the Higgs, splitting into another boson-fermion pair with the second fermion also coupling to the Higgs and the second boson combining with the first to make a third, before the second fermion and third boson recombine into the neutrino). Such models can also involve

alternative Higgs models [48]. Additionally, most of the models studied in the literature have Majorana neutrinos/DM (e.g. [49, 50, 51, 52, 53, 54, 55, 56, 57]), although a few employ Dirac neutrinos (e.g. [58]). These models usually produce DM candidates in the form of the introduced fermions (occasionally the boson is the DM candidate), which are kept stable by some additional symmetry (usually Z_2 but can be higher order). The additional symmetry is usually added in explicitly [47, 59, 60, 61, 54], although some models called "minimal dark matter" models have the symmetry arise accidentally [62].

The advantage that RMG models have over basic see-saw models is that they can produce DM candidates at more reasonable masses and still have the neutrino masses remain sufficiently low [48]. The disadvantage, relative to the basic see-saw models, is that they introduce even more free-parameters and are more complex [63, 64].

The phenomenological implications of these theories tend to involve the properties of the DM candidates and the mediating bosons. Thus, the theoretically optimum way to distinguish between different theories would be to study the properties of DM particles. Unfortunately, this approach has a number of practical limitations, with the primary one being the fact that DM particles have never actually been observed [65]. Since DM particles have never been observed, distinguishing between different models needs to also be done using indirect observations (i.e. by looking for corollaries to the theories). That being said, the production of DM particles at particle accelerators should be possible [66, 67]. Most DM theories, particularly the RMG theories, have the DM gaining mass via the normal Higgs mechanism. This means that, assuming that there are no issues with quantum numbers, a Higgs boson produced with enough energy should be able to decay into a DM particle-antiparicle pair due to the fact that the DM couples to the Higgs field.

One indirect distinction that has been made is the one between Majorana and Dirac neutrinos. As noted above, most models assume Majorana neutrinos, partly because the implications of Majorana neutrinos were of greater interest [68]. However, the lack of any concrete evidence for Majorana neutrinos [69], despite years of searching (mostly in

the form of neutrinoless double beta decay searches), has spurred recent interest in Dirac neutrinos [70, 71]. Therefore, another potential avenue of research would be to try and identify the implications unique to Dirac theories.

Another way to glean information regarding interactions of this type would be to measure the absolute neutrinos mass scale which would give information regarding the strength of the interaction. This, naturally, carries with it all of the difficulties with making this measurement. At the moment, the most advanced laboratory experiments involve measuring the tail of the tritium beta-decay energy spectrum [72, 73, 74, 75, 76, 77]. This would reveal the mass of the lightest neutrino, which would reveal the masses of all the neutrinos as the mass-squared differences are known. The most sensitive measurements of the neutrino mass scale come from cosmological constraints [115], such as Cosmic Microwave Background anisotropy observations. However these contain a degree of model dependence and should be complimented by other types of measurement.

That being said, there are other ways to constrain models (e.g. [78, 79, 80, 81]), and all experimental avenues need to be pursued due to multiple free parameters (at least three for the simplest models) [63].

DRC 16

MASSEY UNIVERSITY
GRADUATE RESEARCH SCHOOL

STATEMENT OF CONTRIBUTION
DOCTORATE WITH PUBLICATIONS/MANUSCRIPTS

We, the candidate and the candidate's Primary Supervisor, certify that all co-authors have consented to their work being included in the thesis and they have accepted the candidate's contribution as indicated below in the *Statement of Originality*.

Name of candidate:	William S. Marks
Name/title of Primary Supervisor:	Dr. Fu-Guang Cao
Name of Research Output and full reference:	
W. S. Marks. The effects of coherent neutrino mixing modulation by dark matter. Journal of Physics: Conference Series, 1468(1): 012198, 2020.	
In which Chapter is the Manuscript /Published work:	Chapter 2 & 5
Please indicate:	
• The percentage of the manuscript/Published Work that was contributed by the candidate:	100%
and	
• Describe the contribution that the candidate has made to the Manuscript/Published Work:	
The work is a conference proceeding based on a presentation given by the Candidate at TAUP 2019.	
For manuscripts intended for publication please indicate target journal:	
Candidate's Signature:	William S Marks
Date:	19/01/21
Primary Supervisor's Signature:	Fu-Guang Cao
Date:	19/01/2021

(This form should appear at the end of each thesis chapter/section/appendix submitted as a manuscript/ publication or collected as an appendix at the end of the thesis)

GRS Version 4– January 2019

DRC 16

MASSEY UNIVERSITY
GRADUATE RESEARCH SCHOOL

STATEMENT OF CONTRIBUTION
DOCTORATE WITH PUBLICATIONS/MANUSCRIPTS

We, the candidate and the candidate's Primary Supervisor, certify that all co-authors have consented to their work being included in the thesis and they have accepted the candidate's contribution as indicated below in the *Statement of Originality*.

Name of candidate:	William S. Marks
Name/title of Primary Supervisor:	Dr. Fu-Guang Cao
Name of Research Output and full reference:	
W. S. Marks and F. B. Cao, Meaningful details: The value of adding baseline dependence to the neutrino-duck amplitude effect, International Journal of Theoretical Physics, 59(12): 3951-3966, 2020.	
In which Chapter is the Manuscript /Published work:	Chapters 2 and #5.2
Please indicate:	
• The percentage of the manuscript/Published Work that was contributed by the candidate:	90%
and	
• Describe the contribution that the candidate has made to the Manuscript/Published Work:	
The Candidate performed the research described in the publication. The candidate also wrote the publication in its entirety and handled the submission process. The Co-Author provided direction and feedback.	
For manuscripts intended for publication please indicate target journal:	
Candidate's Signature:	William S. Marks
Date:	19/01/21
Primary Supervisor's Signature:	Fu-Guang Cao
Date:	19/01/2021

(This form should appear at the end of each thesis chapter/section/appendix submitted as a manuscript/ publication or collected as an appendix at the end of the thesis)

GRS Version 4– January 2019

Chapter 3

Dark Matter

Dark matter is the historical name for any form of matter that is not luminous. In the past the term was generally applied to non-stellar baryonic matter such as gases and debris. In the past few decades, the term has come to describe a currently unknown form of non-baryonic matter that is presumed to comprise most of the matter in the universe. Dark matter is relevant because at one point neutrinos were the leading candidate and because dark matter is related to some of the work.

3.1 History

Searches for non-luminous matter that can only be detected gravitationally date back to the 19th century [1]. The early searches were too imprecise to measure any deviations, in part because they only investigated the near vicinity of the solar system (where effects due to dark matter are minimal) and also because galaxies (the scale at which dark matter effects become apparent) had yet to be discovered. That changed in the 1930s with measurements of galactic cluster velocity dispersions [1].

These measurements were bolstered by galactic rotation curve observations in the 1950s, which consistently found that the matter in the outer regions of most galaxies was moving too fast for the gravitational pull of the luminous matter in the galaxies to hold

it in, indicating some form of non-luminous matter [1]. In particular, it indicated some form of non-luminous matter in the outer reaches of galaxies. Further measurements over the ensuing decades showed that this non-luminous matter contributed the majority of the mass in most galaxies [1].

It was eventually determined that the only way this matter could be non-luminous (and undetected) but baryonic was if it consisted of MAssive Compact Halo Objects, (MACHOS) [1]. These are presumed to be objects such as rogue planets or small black holes floating around the outer reaches of galaxies. The reason baryonic matter would need to take this form is simply that if it was diffuse and there was enough of it to explain the rotation curves, then it would absorb some of the light emitted by the host galaxy and we would see it. This naturally leads to a solution where the matter is clumped into dense objects that do not block or diffuse light, hence MACHOS.

The method developed for detecting MACHOS was gravitational micro-lensing searches [82, 83]. These search for fluctuations in the light emitted by distant objects caused by gravitational distortion. While some fluctuations were detected, the event rate was far too low to provide the missing matter [84, 85]. That meant that the missing matter must be non-baryonic.

The first candidate for this non-baryonic form of matter was neutrinos, as neutrinos were (and are) the only known stable particle with the property of not coupling to photons [86, 1]. This has since been ruled out. Cosmological models have consistently shown that a neutrino dominated universe will have what is known as top-down structure formation, where the largest structures (galactic super-clusters) form first, followed by smaller structures such as galaxies [86, 1]. However, the structure of the observable universe is most consistent with bottom-up structure formation, where smaller structures form first. This has led to the current paradigm of Cold Dark Matter [86, 1].

Cold Dark Matter (CDM) is non-baryonic matter that decoupled from the rest of the universe at an early stage and is presumed to have very low kinetic energy [1]. Most CDM

proposals are of rather massive particles (GeV and above), although lower masses have also been suggested. These lower mass proposals are restricted in their possible coupling strengths.

An additional historical motivation for dark matter proposals was closure of the universe. Simply put, the general curvature of the universe is determined by the total energy content of the universe and there isn't enough luminous matter in the universe to make it flat, i.e. keep geometry Euclidian. (In fact, even at the largest scales our universe seems to be perfectly Euclidian, a feature that very much requires explanation.) Naturally, dark matter was at one time the prime candidate for providing closure [1].

3.2 Candidates

The lower limit on the size of the dark matter particle comes from the requirement that the De Broglie wavelength be (roughly) smaller than the size of a galaxy. The upper limit was established by a requirement that it was once in thermal equilibrium. In between these two limits there is a very large range for which a large number of suggestions. The ones discussed here are the ones most relevant to this research (i.e. neutrinos). This list is far from exhaustive.

It should also be mentioned that most of the discussion so far has presumed a single species of dark matter. Technically, is is possible the dark matter is actually multi-partite [87], which could potentially manifest itself as discrepancies between interaction specific searches (if not all species participate in a particular interaction) and the gravitational measurements.

3.2.1 Unparticle Dark Matter

Most discussions of dark matter generally assumed that dark matter comes in the form of particles, like all other known matter. However, there exists the possibility that DM is

something else entirely. One such possibility is Unparticle Dark Matter.

The distinguishing feature of Unparticle Matter is that it consists of scale invariant fields (in the Quantum Field Theory sense) with non-zero mass [88, 89]. By contrast, all scale invariant particle fields have zero mass. It has been suggested that these fields would appear to be collections of a non-integer number of particles [88]; variable mass particles [90] and/or, continuous mass distributions [91]. These fields have never been observed, which indicates that these particles cannot interact with the vast majority of SM particles. However, the possibility exists that these fields can interact with neutrinos. These interactions may be of any Type, but they cannot be used in RMG models, and defining number density (as is explicitly required in Types B & C) is quite difficult. The main implication of neutrino-unparticle interactions is that, since unparticle fields can take on an arbitrarily small mass (i.e. less than the mass of neutrinos), neutrinos can experience decay [92]; specifically, the heavier neutrino states will decay to the lightest one. This means (observationally speaking) that neutrinos with a sufficiently long baseline will be observed with a fixed flavour spectrum corresponding to the flavour composition of the lightest neutrino state, which, given current knowledge, can be one of two states. Calculations were performed to see if neutrino decay could explain the postulated ICE-CUBE anomaly. It cannot as the postulated ICECUBE anomaly consists of a flavour ratio of $(f_e, f_\mu, f_\tau) \approx (0, 0.2, 0.8)$[1], while both neutrino decay scenarios predict larger electron components and smaller tauon components [93]. That does not exclude the existence of unparticle-neutrino interactions; testing for that will require observations of very long base-line neutrinos produced with a known flavour spectrum.

Determining whether neutrino decay (if found) is due to the existence of unparticles is a potential subject of research. Of course, the confirmation of the Higgs mechanism have caused unparticle fields to fall out of favor as the mechanism does not allow for arbitrary mass, although there is still some consideration [94, 95]. That does not mean that the

[1]It is important to note that this anomaly has not been confirmed as the

existence of unparticle matter is impossible, just highly improbable.

3.2.2 WIMPs

WIMPs (Weakly Interacting Massive Particles) are presumed to be massive particles (several GeV or more) that only participate in the Weak Interaction [96] or in an interaction that has the same energy dependency as the Weak Interaction. This essentially makes them like neutrinos, only much more massive. The main motivation for suggesting these particles is Super Symmetry, a theory originating in string theory that postulates that every SM particle as a partner that is a boson/fermion if the SM particle is a fermion/boson. These new particles are protected by at least one unbroken symmetry and so there is at least one new, stable neutral particle. The heaviness is invoked to (at least in part) explain why no such particles have been found at particle accelerators. (There are also certain masses which are preferred from a cosmological standpoint.)

WIMPs are considered because, if they existed, they would be guaranteed to interact with neutrinos. The downside to WIMPs is their high mass, which results in a very low number density. Given how small the Weak Interaction cross-section is, that means that actually observing neutrino-WIMP interactions would be rather difficult. The Weak Interaction has been used as a model for how interactions can occur, specifically interactions that scale in the same way as the Weak Interaction. Mainly, that means the cross-section scales with the square of the energy at low energies, with the degree decreasing as energy increases [97].

3.2.3 Axions

Axions are a proposed type of particle most notable for its extremely low mass (less than 10^{-5} eV). The proposal for their existence comes from the Strong CP problem, where CP is violated in the Strong interaction without (arbitrary) fine tuning or unless a new global symmetry is introduced which is spontaneously broken, producing a new particle [98].

Due to their very light mass, axions would be plentiful in number. Thus, they are considered a sort of "best-case scenario" for interactions with neutrinos. The downside is that it is unknown whether they would interact with neutrinos if they existed. As it is, there is no compelling reason to believe that they would. It is also unknown whether such an interaction would be strong enough, as axions are expected to participate in interactions with smaller cross-sections than the Weak-Interaction. Thus, the axions considered in this research are not particularly realistic.

3.2.4 Scotons

Other types of dark matter with more "neutrino-centric" motivations have been considered. The most notable of these is the "Scoton", which is motivated by the radiative mass generation models that were discussed in the chapter on neutrinos. As stated before, some of the predicted new particles are potentially stable across cosmological timescales, making them dark matter candidates [99].

These particles are generally presumed to have masses ranging from keV to MeV. This is theoretically attractive as this, potentially, fills the mass gap between electrons and neutrinos, which is by far the largest in the Standard Model. Moreover, it is phenomenologically attractive as there are additional ways to search for interactions if the mass is in this range which will be discussed later.

Another characteristic of these interactions is how the interaction strength scales with energy, namely that it doesn't. A constant interaction cross-section gives interactions of this type certain distinctive signatures differing from the other proposed interaction types which are energy dependent. This is particularly relevant to the anisotropy measures which will be mentioned below as those are most sensitive to constant cross-sections.

3.3 Previously Proposed ways to Detect Interactions with Neutrinos

An area of focus in this research was neutrino-dark matter interactions and the likely observational signatures of those. This primarily consisted of calculations involving a possible matter effect involving dark matter. The other proposed ways to detect a neutrino dark matter interaction which did not receive any new work are briefly discussed here.

A common way of parameterising interaction strengths is the potential, which is a product of the interaction cross-section and the number density [100]. That is because most observables are dependent on both quantities. This work has continued the practice of using potentials, although the dark matter and interaction types implied by the potentials will, of course, be stated for clarity.

3.3.1 Dark Matter Anihilation and Decay

Dark matter annihilation is, as the name suggests, the annihilation of scoton, anti-scoton pairs. Most searches for dark matter annihilation have focused on photon production [101, 102, 103, 104]; some have looked at neutrinos [105]. Additionally, there are searches for dark matter decay, which, naturally enough, is the conjectured decay of dark matter particles. Such events could manifest as spikes in energy spectra [106].

The main spectra considered for such searches are high energy astrophysical neutrinos as dark matter particles are generally presumed to have high mass [105, 107]. Also investigated is the solar neutrino spectra, as dark matter is presumed to collect in areas of high gravitational potential [108, 109].

The main utility in searching for such occurrences is that it doesn't require any dedicated equipment, only standard neutrino observatories. Thus, these experiments are cost effective.

The disadvantage is that this experiments are very much dependent on the cooperation of the universe. The discovery of annihilations of course depends on dark matter

consisting of scotons and anti-scotons, with the mix being sufficiently even so that there is a detectable event rate. It also depends on the scotons being massive enough that the produced neutrinos are at detectable energies.

3.3.2 Cosmological Anisotropies

As stated before, in the Standard Model of Cosmology, the universe begins with a singularity where space is condensed to a point (although the universe is still infinite) before undergoing an expansion [5]. The early universe (up to 300k years old) was filled with a plasma that cooled as it expanded (a classical adiabatic expansion). At certain points, this plasma would cool to the point where a particular species (of particle) would cease to interact with the rest of the plasma, effectively "dropping out" (a phenomena known as decoupling) [5]. This was because the average energy of the plasma was no longer sufficient to support the interaction. One of the first (known) species to decouple was neutrinos, as they only interact weakly. This resulted in a "sea" of freely moving neutrinos, referred to as the Cosmic Neutrino Background (CNB). Unfortunately, these neutrinos are today of fairly low energy, so detecting them would be extremely difficult, although there are efforts being made [6].

The plasma ceased to exist (as a plasma) when the universe was approximately 300k years old. This event is called Recombination and was marked by the decoupling of photons from baryons, the last major decoupling event [7]. This produced a sea of photons (analogous to the CNB) called the Cosmic Microwave Background (CMB) due to the fact that today these photons are in the microwave range. Study of the CMB is a very important tool in cosmology [7]. Most of the utility comes from examination of the anisotropies (deviations from the mean) of the CMB.

When the photons decoupled to produce the CMB, the spectrum should have been a classic black-body spectrum [7]. Indeed, the CMB is the most perfect example of a black-body spectrum currently known. In addition, the CMB should be (and is) very

homogeneous [7]. However, it is not perfectly homogeneous; there are some variations in it. This is interesting because the variations in the CMB are due to inhomogeneities in the universe. Once the effects of the Earth's motion and gravitatonal lensing are accounted for, the inhomogeneities are primarily due to inhomogeneities in the primordial plasma. This is of interest as these inhomogeneities were the seeds of the structure of the universe and, their nature can provide some insight into that structure. Thus, CMB anisotropies are important in the development of cosmological models [110].

If there was a coupling between neutrinos and dark matter, then there would be a delay in the decoupling of dark matter. This would result in Dark Matter becoming more diffuse which would suppress smaller scale fluctuations [111]. This in turn would manifest in the CMB with a suppression of smaller scale anisotropies [112, 113, 114]. Thus, measuring CMB anisotropies constrains the effective strength of interactions between neutrinos and dark matter[2].

Similar to the CMB anisotropy measurements are measurements of the Lyman-α forest [114]. The Lyman-α forest is named, appropriately enough, from the Lyman-α line in the hydrogen spectrum. By searching for this line and its red-shifted incarnations throughout the universe, it is possible to map the distribution of hydrogen throughout the universe and thus matter in general. Since the matter distribution of the universe was seeded by dark matter, this potentially provides a map of the distribution of dark matter in the universe. Thus, the Lyman-α forest provides another way to constrain neutrino-dark matter interactions, which is actually more sensitive than CMB spectral measurements. The downside is the enhanced model dependency of the Lyman-α forest, which renders results more controversial.

Overall, anisotropy measurements are fairly inexpensive to conduct as they utilise public data. Additionally, they are relatively sensitive to the strength of the neutrino dark matter interactions, compared to other measures. On the other hand, they are

[2]These results were used in the chapter on mixing modulation as a comparison point.

not particularly sensitive to energy dependent interactions; their sensitivity is to energy independent interactions [114].

The CMB anisotropies together with Large-Scale Structure observations are also used to provide constraints on the net mass of neutrinos and the effective number of neutrino species [115]. As stated before, these produce a constraint on the sum of the neutrino masses to be $\Sigma m_\nu < 0.13$ [34]. The effective number of neutrino species is the relativistic degrees of freedom in the early universe and includes exotic phenomena such as axions [116]. The expected value from the three SM neutrinos is $N_{eff} = 3.046$.

3.3.3 Resonant Absorption

One of the older proposals for detecting neutrino-dark matter interactions is Resonant Absorption [118]. The first work on the topic came in 1982 and proposed resonant absorption of high energy neutrinos by relic neutrinos [118]. Essentially, when the energy of the incident neutrinos matches that of a possible interaction product (namely, Z bosons), the probability of inelastic scattering is maximised and the neutrinos are selected out.

The original proposal focused on high energy neutrinos and the Weak Interaction as that is still the only interaction (other than gravity) that neutrinos are known to participate in and the high energy regime is where resonant absorption will occur with those interactions. The development of scotogenic models prompted proposals at lower energies. Specifically, this has prompted proposals for resonant absorption in supernova neutrino energy spectra, which has been done for both the diffuse supernova background [119] and galactic supernovae [31].

Performing such calculations includes a certain degree of model dependence (though certain parameters are constrained by the anisotropy data fits mentioned above). Since there are a very large number of models, this means that there is room to perform additional research in this field.

Chapter 4

Analysis of θ_{13} Determination Methods.

As stated in the chapter on neutrinos, the last parameter in the PMNS matrix angle is the smallest mixing angle, θ_{13}. While the previous two mixing angles (θ_{12} and θ_{23}) were primarily measured using naturally occuring neutrinos (solar and atmospheric, respectively), measuring θ_{13} used artificially sourced neutrinos.

The first experiment to produce a non-zero measurement of this parameter was the Daya Bay experiment (located at Daya Bay in Guangdong province, China) which reported a value in 2012. This was soon followed by RENO in South Korea, that same year. Both were short-baseline (less than 1km) reactor anti-neutrino experiments that used multiple, identical detectors situated at different distances from the source reactors. The goal was to measure the difference between detectors close to the reactors (the "near" detectors) and detectors farther away (the "far" detectors). Deviations from the inverse-square law were presumed to be due to oscillations and since the θ_{13} term is significant at these baselines, this enabled measurements.

Work was conducted to refine prior research into the data analysis of the 2013 Daya Bay results [120]. In brief, the research addressed claims that the Daya Bay result could not be replicated using the information provided [121]. It also addressed claims that the result was overly sensitive to un-physical parameters. The data analysis performed

by the collaborations used the χ^2 with pulls method. The method is a variation of the χ^2 goodness-of-fit test with the general idea being to find the range of values of some parameter of interest that produce a hypothesis which passes the test. Potential extraneous factors are included in the form of "pull-factors", which are associated with each source of uncertainty. These allow fine-tuning of the hypothesis, with spurious results avoided by having increases in the pull-factors result in increases in the value of χ^2, hence "pull". This method is related to the covariant approach, which deals with uncertainties using a covariant matrix. (It is worth noting that Daya Bay used the covariant method in later publications due to issues regarding the anti-neutrino energy spectrum [122, 123].) The source of the complaint was the pull-factors, the acquired values of which were not published.

It was found that the information provided, including papers cited, was sufficient to replicate the result and that the primary contribution was the parameter of interest. Portions of this were published in [124].

4.1 The Goodness-of-Fit.

The goodness-of-fit test uses a parameter, χ^2, to measure the agreement between a prediction and a measurement. Traditionally, first a prediction is made and then there is an experiment, with the goodness-of-fit being used afterwards to determine if the result of the experiment agrees (or not) with the prediction. An alternative (and very common) use involves first conducting the experiment and then using the goodness-of-fit to determine which theory (or which region of the parameter space under consideration) agrees with the result. However, in order to use a goodness-of-fit in the later way, the various potential sources of error and the various uncertainties need to be accounted for. The covariant and pull methods are two different ways to do that [125].

The covariant χ^2 is

$$\chi^2_{\text{cov}} = \sum_{m,n=1}^{N} \left(R_m^{\text{exp}} - R_m^{\text{the}}\right) \left[\sigma^2_{mn}\right]^{-1} \left(R_n^{\text{exp}} - R_n^{\text{the}}\right), \tag{4.1}$$

where N is the number of observations, R_i^{exp} is the ith observation, R_i^{the} is the corresponding "prediction" and, σ^2_{mn} is a covariant matrix containing the squares of all of the uncertainties [125]. The size of the matrix is $N \times N$ and is given by

$$\sigma^2_{mn} = \delta_{mn} u_m u_n + \sum_{k=1}^{K} c_m^k c_n^k, \tag{4.2}$$

where K is the number of sources of uncertainties, u_i is the uncorrelated uncertainty vector and, c_j^i is the correlated uncertainty matrix.

The χ^2 with pulls is

$$\begin{aligned} \chi^2_{\text{pull}} &= \sum_{n=1}^{N} \left(\frac{R_n^{\text{exp}} - R_n^{\text{the}} - \sum_{k=1}^{K} \xi_k c_n^k}{u_n}\right)^2 + \sum_{k=1}^{K} \xi_k^2 \\ &\equiv \chi^2_{\text{obs}} + \chi^2_{\text{sys}}, \end{aligned} \tag{4.3}$$

where each ξ_i is a pull-factor associated with uncertainty i and all other parameters are as before [125]. Traditionally, the minimizations are performed separately for χ^2_{obs} and χ^2_{sys}, with the later being performed first.

The two approaches are equivalent, with the covariant approach being better suited to cases where $N < K$ (as computation time scales with N) while the pull approach is better suited to cases where $N > K$ (as the computation time scales with K). Additionally, the pull approach allows for the easy identification of problematic components as they will have over-sized pulls associated with them.

4.2 The Daya Bay Experiment

The Daya Bay experiment, located in Guangdong province, China, consisted of (at the time) six identical detectors with 20t (tonnes) Gd doped liquid scintillator targets [120] (it has since been increased to 8 [123]). Detectors of this design work by coincidental observation of positron annihilation immediately followed by neutron capture by the gadolinium.

The target was surrounded by 20t of un-doped liquid scintillator that detected the gamma rays produced by the neutron capture. Both the target and the gamma catcher were contained in acrylic vessels with the outer vessel having reflectors on the top and bottom. This assembly was submersed in 37t of mineral oil, which served as a radiation shield. The total assembly was contained in a stainless steel cylinder that had 192 photo-multiplier tubes placed around the circumference [126].

The antineutrinos came from six reactors rated at a maximum thermal output of 2.9 GWth each that were divided into three pairs. The detectors were distributed among three underground experimental halls, two near, one far. The data acquisition time was 127.546 days for experimental hall 1 (the near hall with two detectors), 127.379 days for experimental hall 2 (the near hall with one detector) and, 126.271 for experimental hall 3 (the far hall), with data acquisition starting in December 2011 and ending in May 2012 [120].

4.2.1 The Data Analysis

The function used by Daya Bay [120] was:

$$\chi^2_{\mathrm{DB}} = \sum_{d=1}^{6} \frac{\left[M_d - T_d\left(1+\epsilon+\sum_{r=1}^{6}\omega_r^d\alpha_r+\rho_d\right)+\eta_d\right]^2}{M_d+B_d} + \sum_{r=1}^{6}\frac{\alpha_r^2}{\sigma_r^2} + \sum_{d=1}^{6}\left(\frac{\rho_d^2}{\sigma_d^2}+\frac{\eta_d^2}{\sigma_{db}^2}\right) \quad (4.4)$$

where M_d is the number of anti-neutrinos detected by detector d, T_d is the predicted number, B_d is the background, ϵ is a normalization factor, α_r is the pull factor associated with reactor r, ρ_d is the pull factor associated with detector d, η_d is the pullfactor associated with the background of detector d, σ_r is the uncertainty from reactor r, σ_d is the uncertainty from with detector d, and σ_{db} is the uncertainty from the background of detector d.

The prediction, T_d, is the estimated value for oscillationless anti-neutrino detection multiplied by the survival probability and integrated over the effective energy distribution (which is the product of the emission energy spectrum [127] and the absorption energy

spectrum [128]). The version of 2.2 relevant to reactor anti-neutrino experiments is:

$$\begin{aligned} P_{surv.}(\bar{\nu}_e \to \bar{\nu}_e) = 1 - \sin^2(2\theta_{12})\cos^4(\theta_{13})\sin^2\left(\tfrac{\Delta_{12}}{2}t\right) - \ldots \\ \cdots - \sin^2(2\theta_{13})\left(\cos^2(\theta_{12})\sin^2\left(\tfrac{\Delta_{13}}{2}t\right) + \sin^2(\theta_{12})\sin^2\left(\tfrac{\Delta_{23}}{2}t\right)\right) \end{aligned} \tag{4.5}$$

where the terms are as previously defined. Since the experiment had a short-baseline, $\approx$ 1km, Daya Bay used a simplified version [120]:

$$P_{surv.} = 1 - \sin^2(2\theta_{12})\cos^4(\theta_{13})\sin^2\left(\frac{\Delta m^2_{small}}{4E}L\right) - \sin^2(2\theta_{13})\sin^2\left(\frac{\Delta m^2_{big}}{4E}L\right) \tag{4.6}$$

which removes the mass hierarchy dependency. The two mass-squared differences are the experimentally measured mass-squared differences.

The term integrated over energy is

$$\frac{\int \sin^2 \frac{1.267\Delta m^2 L}{E} n_\nu(E)dE}{\int n_\nu(E)dE} \tag{4.7}$$

where

$$n_\nu(E) = S_\nu(E)\sigma_{IBD}(E) \tag{4.8}$$

i. e. the product of the emission and absorption energy spectra. These spectra are

$$S_\nu(E) = \Sigma_k \alpha_k S_k(E) \tag{4.9}$$

$$\sigma_{IBD}(E) = \sigma_1 + \sigma_2 \tag{4.10}$$

$$\sigma_1 = \sigma_0 \alpha_1 E_e p_e \tag{4.11}$$

$$\sigma_2 = \sigma_0(\alpha_1 + \beta_1\frac{\Delta}{M} + \gamma_1\frac{E_e}{M})E_e^2 \tag{4.12}$$

where $k = U_{235}, U_{238}, P_{239}$ &, P_{241}, each α_k is the contribution to the total from isotope k and:

$$S_k(E) = exp(\Sigma_{p=1}^6 \beta_{pk} E^{p-1}) \tag{4.13}$$

$$\sigma_0 = \frac{G_F^2\cos^2(\theta_C)}{\pi}(1 + \Delta^R_{inner}) \tag{4.14}$$

$$\alpha_1 = f^2 + 3g^2 \tag{4.15}$$

$$\beta_1 = -2(f + f_2)g - 2f^2 - 8g^2 \tag{4.16}$$

$$\gamma_1 = -4(f + f_2)g - 2f^2 - 10g^2 \tag{4.17}$$

$$\Delta = M_n - M_p \tag{4.18}$$

$$M = \frac{M_n + M_p}{2} \tag{4.19}$$

$$E_e = E - \Delta \tag{4.20}$$

$$p_e = \sqrt{E_e^2 - m_e^2} \tag{4.21}$$

where the β_{pk}'s are coefficients determined experimentally, G_F is the Fermi constant, θ_C is the Cabibbo angle, M_n is the neutron rest mass, M_p is the proton rest mass, m_e is the electron rest mass and, Δ^R_{inner}, f, g &, f_2 are additional parameters.

The actual data analysis was performed using two methods: one method involved creating a grid on the θ_{13} - ϵ plane and minimizing χ^2 with respect to the 18 pull factors, using the expected value (zero) as the starting point for each. This then created a contour which was scanned to find the absolute minimum. The process also made the measurement of the uncertainty of θ_{13} and ϵ fairly straight-forward.

The second method treated all 20 unknown parameters on an equal footing: it minimized all parameters simultaneously using inputs produced by a pseudo-random number generator in a range determined to be conducive to the production of reasonable results with the results then filtered according to theoretical and practical criteria. Namely, only results with a χ^2 within one theoretical standard deviation of the expected value and with a positive value for θ_{13} were allowed. This would be done multiple times with the results then averaged.

A consideration of the two methods will reveal that they are equivalent, in as much as each attempts to find the global minimum. The random input method is more efficient in the sense that it doesn't waste time producing data points in regions that do not contain the minimum. Another advantage the random input method has over the more

traditional contour scan method is that it provides more information about all of the parameters whereas the contour scan method only provides detailed information about the parameters of the contour. Since multiple minimizations are performed using random inputs, statistics can be calculated for each of the parameters which provides information about the importance of the parameter in the fit. Specifically, a large variance in the set of values of the parameter (relative to the magnitude of the parameter) which provide a valid fit indicates that it is unimportant to the fit.

4.2.2 Random Fit Details

The program used to perform the minimization was a purpose written program in MATLAB that consisted of six layers for each function. The first layer constructed 4.7 and the second implemented the energy portion of 4.6 as a function of E, L and, δm^2_{MINOS} (the mass-squared difference measured by the MINOS experiment) so that the same energy spectrum could be used by all four functions. The third layer constructed the actual function, using the parameters contained in the respective papers, while the fourth layer converted the function into a form that could be used by the minimization process. (The reason the function was not constructed explicitly for the minimization process was to preserve generality.)

The fifth layer consisted of a function that actually performed the minimization. The minimization method was the MATLAB command "fminsearch" which performs a minimization using the Nelder-Mead algorithm. (See [129] for details on this algorithm.) Since the algorithm requires a set of initial conditions and no estimates of values for the pull-factors could be found in either research paper, psuedo-random numbers were used. These numbers were produced using the MATLAB command "rand" which generates psuedo-random numbers using a Mersenne Twister (see [130] for details on this algorithm). This is an algorithm that uniformly generates numbers across the interval [0,1] given some initial seed value, with the seed in this instance being system time. These numbers were

then scaled by a factor called "q". Since the initial conditions for the minimization were "random", multiple minimizations would be performed and then averaged in order to counteract any instability in the algorithm, as there are, in general, fluctuations (mostly slight, sometimes severe) in the minimum produced from different initial conditions. In order to reduce outliers (the severe fluctuations), a selection criterion was implemented whereby only results where the χ value was below a certain point (the accuracy level, or "acc") would be included in the average (although outliers were not completely eliminated, see Discussion). The results produced would be the average values of all the parameters, the average χ value, the value of $\sin^2(2\theta_{13})$ and, the standard deviations of all of the above.

The sixth and final layer contained the input parameters that would be used in the minimization: the dm13, the number of iterations to be averaged, the "q" value and, the accuracy level. It also recorded the time for the program to run. This was an important feature as runtime was the primary measure of efficiency. The programs for all fitting functions followed this structure with the only differences being in the program that constructed the χ functions and in the size of the parameter vectors used in the layers above the function layer.

4.2.3 Reduced Functions

In addition to trying to reproduce the Daya Bay result, fits were performed for a simplified version of equation 4.4 which treated the detectors as identical and combined the pull factors for the detectors into a single parameter. This was motivated by a claim that there were too many pull factors [121] which lead to a desire to see if the same result could be obtained with fewer pull factors. The decision to reduce the detector pull factors was because the entire experiment was based on the detectors being identical.

Additional reductions assuming degeneracy between reactors were made. These were less justified given the uniqueness of individual nuclear reactors, but were performed to further analyse the relationship between the pullfactors and the final result. The first

of these (referred to as the second reduced function) assumed degeneracy within reactor pairs, as the reactors utilised by the Daya Bay experiment were constructed and operated in pairs. This reduced the total number of fitted parameters to 12. The third reduced function assumed total degeneracy between the reactors, reducing the parameter total to 10. This is not a very good approximation and was only implemented to investigate the relationship between the pullfactors and the parameters of interest.

The first reduced χ^2 function is:

$$\chi^2_{\mathrm{DB}} = \sum_{d=1}^{6} \frac{\left[M_d - T_d\left(1+\epsilon+\sum_{r=1}^{6}\omega_r^d\alpha_r+\rho\right)+\eta_d\right]^2}{M_d+B_d} + \sum_{r=1}^{6}\frac{\alpha_r^2}{\sigma_r^2} + \rho\frac{6}{\sigma_d^2} + \sum_{d=1}^{6}\frac{\eta_d^2}{\sigma_{db}^2}. \quad (4.22)$$

where ρ is the reduced detector pull factor and all of the other terms are the same. This function was manipulated in the same ways as the full function.

The second reduced function is given by:

$$\chi^2_{\mathrm{DB}} = \sum_{d=1}^{6} \frac{\left[M_d - T_d\left(1+\epsilon+\sum_{r=1}^{3}\left(\omega_{2r}^d+\omega_{2r-1}^d\right)\beta_r+\rho\right)+\eta_d\right]^2}{M_d+B_d} + \sum_{r=1}^{3}2\frac{\beta_r^2}{\sigma_r^2} + \rho\frac{6}{\sigma_d^2} + \sum_{d=1}^{6}\frac{\eta_d^2}{\sigma_{db}^2}. \quad (4.23)$$

where β_r is a new pullfactor corresponding to the reactor pairs to replace α_r. All other parameters have remained unchanged from 4.22. This function was only manipulated using the random input method.

The third reduced function is:

$$\chi^2_{\mathrm{DB}} = \sum_{d=1}^{6} \frac{\left[M_d - T_d\left(1+\epsilon+\alpha+\rho\right)+\eta_d\right]^2}{M_d+B_d} + \frac{\alpha^2}{\sigma_r^2} + \rho\frac{6}{\sigma_d^2} + \sum_{d=1}^{6}\frac{\eta_d^2}{\sigma_{db}^2}. \quad (4.24)$$

where α is the fully reduced reactor pullfactor. All of the other parameters remain the same as in the previous reduced functions and the evaluation was conducted by the random input method only.

4.2.4 Results

The results of the random input fits are given in tables 4.1 to 4.4 while the results of the contour scan fits are given in figures 4.1 and 4.2. The confidence intervals quoted

Table 4.1: Results of a random input fit for Eq. (4.4).

Parameter	χ^2		$\sin^2(2\theta_{13})$		$\epsilon(\times 10^{-4})$	
Mean	3.9		0.088		-2.3	
90%CI	0.073		0.00025		2.7	
Parameter	ρ_1	ρ_2	ρ_3	ρ_4	ρ_5	ρ_6
Mean ($\times 10^{-4}$)	4.9	-6.4	1.4	4.6	-0.24	-4.3
90%CI ($\times 10^{-4}$)	0.35	0.07	0.42	0.039	0.14	0.031
Parameter	α_1	α_2	α_3	α_4	α_5	α_6
Mean ($\times 10^{-4}$)	-6.7	-8.0	7.8	4.0	8.4	4.7
90%CI ($\times 10^{-4}$)	4.9	0.54	4.6	0.88	5.5	0.73
Parameter	η_1	η_2	η_3	η_4	η_5	η_6
Mean ($\times 10^{-1}$)	2.0	-1.2	1.8	4.2	1.5	4.5
90%CI ($\times 10^{-1}$)	1.5	2.4	2.6	1.6	3.8	2.1

refer to the uncertainty from having multiple results and are not related to the total uncertainty. The full and reduced function contour scans gave values for $\sin^2(\theta_{13})$ of $0.088^{+0.009}_{-0.008}$ and$0.089^{+0.008}_{-0.009}$ respectively, compared to 0.089 ± 0.010 obtained by Daya Bay [120]. As can be seen by a comparison with the two tables, the contour results agree with the random input results.

The results obtained here are in agreement with the result obtained by Daya Bay. Since these results were obtained using information from Daya Bay's publication and sources quoted therein, it contradicts the claim that Daya Bay's result is not reproducible; it clearly is. Also, the pull factors are not entirely unphysical and do not have an undue influence on the result. Indeed, if the χ^2 function is broken into two parts, χ^2_{obs} which contains terms in the summation with the parameter of interest and χ^2_{sys} which contains the other terms, then for both the full and reduced functions, $\chi^2_{\text{obs}} >> \chi^2_{\text{sys}}$, specifically,

Table 4.2: Results of a random input fit for Eq. (4.22).

Parameter	χ^2	$\sin^2(2\theta_{13})(\times 10^{-2})$		$\epsilon(\times 10^{-5})$	$\rho(\times 10^{-7})$
Mean	4.1	8.9		-1.9	1.3
90%CI	0.0086	0.0013		0.61	2.5
Parameter	α_1	α_2	α_3	α_4	α_5	α_6
Mean ($\times 10^{-4}$)	-10	-9.5	5.5	4.5	4.2	5.4
90%CI ($\times 10^{-4}$)	0.12	0.078	0.041	0.048	0.061	0.04
Parameter	η_1	η_2	η_3	η_4	η_5	η_6
Mean ($\times 10^{-1}$)	1.8	2.6	2.8	4.1	0.1	2.3
90%CI ($\times 10^{-1}$)	1.1	1.5	3.9	2.7	2.1	1.4

Table 4.3: Results of a random input fit for Eq. (4.23).

Parameter	χ^2	$\sin^2(2\theta_{13})(\times 10^{-2})$		$\epsilon(\times 10^{-5})$	$\rho(\times 10^{-7})$
Mean	4.1	8.9		-3.3	4.1
90%CI	0.014	0.0058		1.8	3.9
Parameter	η_1	η_2	η_3	η_4	η_5	η_6
Mean ($\times 10^{-1}$)	0.57	-0.63	1.4	3.0	0.97	5.6
90%CI ($\times 10^{-1}$)	1.9	3.1	0.86	1.8	5.4	6.4
Parameter	β_1		β_2		β_3	
Mean ($\times 10^{-4}$)	-9.7		5.0		5.0	
90%CI ($\times 10^{-4}$)	0.12		0.023		0.39	

Table 4.4: Results of a random input fit for Eq. (4.24).

Parameter	χ^2	$\sin^2(2\theta_{13})(\times 10^{-2})$	$\epsilon(\times 10^{-4})$	$\rho(\times 10^{-7})$	$\alpha(\times 10^{-6})$
Mean	4.2	8.8	-4.9	-1.3	0.64
90%CI	0.0031	0.0011	0.030	6.9	2.3

Parameter	η_1	η_2	η_3	η_4	η_5	η_6
Mean $(\times 10^{-1})$	1.2	0.94	1.9	0.89	2.0	1.8
90%CI $(\times 10^{-1})$	0.91	0.39	0.84	0.58	0.80	1.0

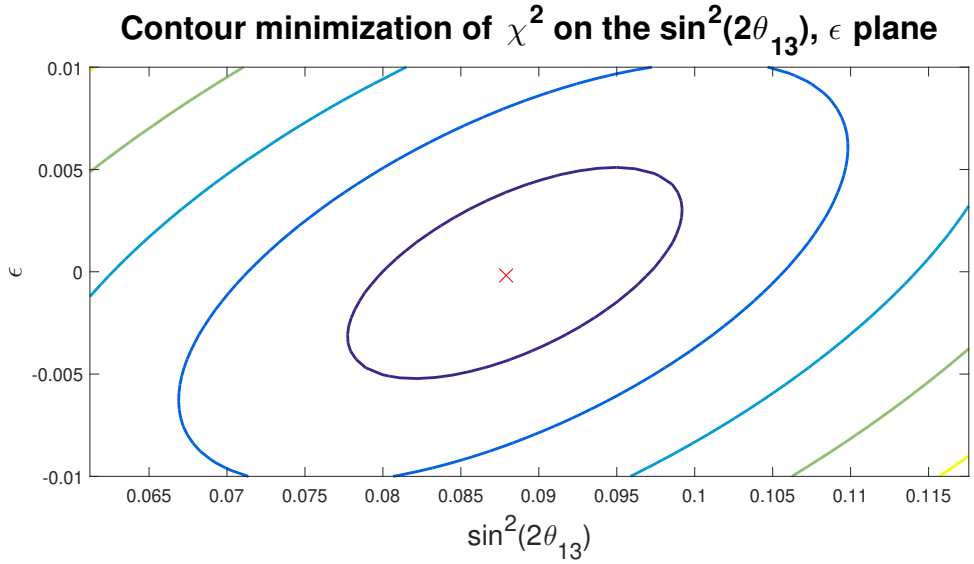

Figure 4.1: Contour plot of the $\sin^2(2\theta_{13})$, ϵ plane for Eq. (4.4). Each contour line represents 1σ. The red x is the minimum.

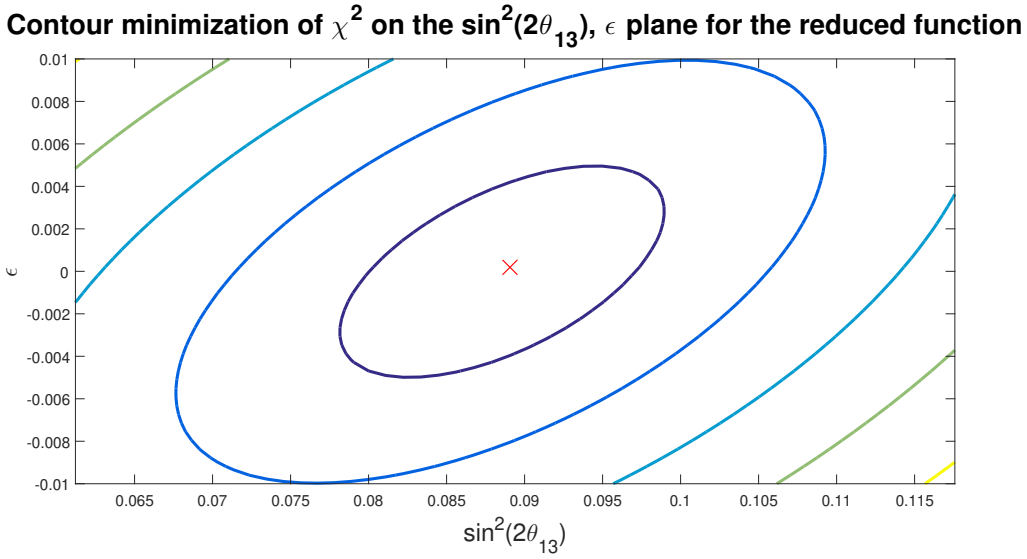

Figure 4.2: Contour plot of the $\sin^2(2\theta_{13})$, ϵ plane for Eq. (4.22). Each contour line represents 1σ. The red x is the minimum.

$\chi^2_{\text{obs}} = 3.47 > \chi^2_{\text{sys}} = 0.31$ for the full function and $\chi^2_{\text{obs}} = 4.06 >> \chi^2_{\text{sys}} = 0.05$ for the reduced function. Also, the pull factors themselves are fairly small and have large uncertainties, which shows that a great deal of variation for each pull factor is allowed. Together, these results show that the influence of the pull factors is quite small. This is in keeping with the probable purpose of the pull factors, to show if there is an issue with part of the experimental setup.

4.3 RENO

RENO (Reactor Experiment for Neutrino Oscillation), located in Yonggwang, South Korea, consisted of two identical 16t Gd doped liquid scintillator detectors, one near and one far, detecting anti-neutrinos from six reactors [131]. The six reactors consisted of two Combustion Engineering System 80 type reactors and four Korean Standard Nuclear Power Plant type reactors, rated at a maximum thermal output of 2.66 and 2.8 GWth respectively. The data acquisition time was 192.42 days for the near detector and 222.06

days for the far detector, starting in 2011 and ending in 2012. (For more details see [132] and [131].)

The data was analysed using the same χ^2 with pulls method used by Daya Bay. The χ^2 function used was:

$$\chi^2_{\text{RENO}} = \sum_{d=1}^{2} \frac{\left[N^d_{obs} + b_d - (1 + a + \epsilon_d) \sum_{r=1}^{6} (1 + f_r) N^{d,r}_{exp}\right]^2}{N^d_{obs}} + \sum_{r=1}^{6} \frac{f_r^2}{\sigma_r^2} + \sum_{d=1}^{2} \left(\frac{\epsilon_d^2}{\sigma_d^2} + \frac{b_d^2}{\sigma_{db}^2}\right) \tag{4.25}$$

where N^d_{obs} is the number of observed antineutrinos, b_d is the pull factor associated with the background of detector d, a is the normalization factor, ϵ_d is the pull factor associated with detector d, f_r is the pull factor associated with reactor r, $N^{d,r}_{exp}$ is the expected number of antineutrinos from reactor r detected by detector d, σ_r is the uncorrelated uncertainty associated with reactor$r$, σ_d is the uncorrelated uncertainty of detector d and, σ_{db} is the uncorrelated uncertainty of the background of detector d.

An additional reduced function was produced for RENO. This function assumed degeneracy between the detectors and between the reactors. It is given by:

$$\chi^2_{\text{RENO}} = \sum_{d=1}^{2} \frac{\left[N^d_{obs} + b_d - (1 + a + \epsilon) (1 + f) N^{d,r}_{exp}\right]^2}{N^d_{obs}} + \frac{f^2}{\sigma_r^2} + \frac{\epsilon^2}{\sigma_d^2} + \sum_{d=1}^{2} \left(\frac{b_d^2}{\sigma_{db}^2}\right) \tag{4.26}$$

where ϵ and f are the new, reduced pull-factors for the detectors and reactors respectively and all other parameters remain unchanged. The fitting for both functions was performed by the random input method described above only.

4.3.1 Results

The overall patterns in the parameters are largely the same as the ones for Daya Bay. The uncertainties in the pull-factors are of the same order as for the means and there is little difference between the full and reduced functions in terms of the final outcome.

Table 4.5: Results of a random input fit for Eq. (4.25).

Parameter	$\chi^2(\times 10^{-3})$		$\sin^2(2\theta_{13})$		$a(\times 10^{-4})$	
Mean	2.5		0.11		5.1	
90%CI	4.1		0.00017		0.10	
Parameter	f_1	f_2	f_3	f_4	f_5	f_6
Mean ($\times 10^{-5}$)	1.1	1.7	-2.6	5.8	3.0	2.6
90%CI ($\times 10^{-5}$)	1.7	3.1	4.1	9.9	5.7	4.7
Parameter	b_1		b_2	$\epsilon_1(\times 10^{-6})$	$\epsilon_2(\times 10^{-6})$	
Mean	0.34		0.92	-3.8	0.35	
90%CI	0.32		0.51	5.1	2.4	

Table 4.6: Results of a random input fit for Eq. (4.26).

Parameter	$\chi^2(\times 10^{-5})$	$\sin^2(2\theta_{13})$	$a(\times 10^{-4})$	$f(\times 10^{-6})$
Mean	2.5	0.11	5.1	3.4
90%CI	0.66	0.000014	0.046	4.0
Parameter	$\epsilon(\times 10^{-8})$	b_1	b_2	
Mean	6.8	0.11	0.15	
90%CI	109	0.060	0.15	

4.4 Discussion

Overall, the issues raised regarding the Daya Bay data analysis by Khan et. al. were not problems after all. The result was reproducible and was not dependent on unphysical parameters. However, this does not completely exonerate the Daya Bay collaboration. In particular, there were certain features of the method (primarily related to the pull factors) that were not properly explained in the Daya Bay publications and lacked references to sources that did explain. As it is, the collaboration eventually found that there were discrepancies in the energy spectrum [122], so they switched to the covariant matrix method [123].

A slightly more interesting result came from the use of different methods for handling the minimization. The random fit method proved to be much quicker than the region search method and possibly a little more precise. While it was only explicitly demonstrated for the Daya Bay results, the RENO results showed similar behaviour and would presumably show similar effects if it was given the same treatment.

If an analysis of this nature were to be conducted again, it would utilise the random fit method with an evolutionary algorithm to set the fitting parameters. More explicitly, it would perform series of random fit sets where the results from the previous fit would be used to optimise the next set.

DRC 16

MASSEY UNIVERSITY
GRADUATE RESEARCH SCHOOL

STATEMENT OF CONTRIBUTION
DOCTORATE WITH PUBLICATIONS/MANUSCRIPTS

We, the candidate and the candidate's Primary Supervisor, certify that all co-authors have consented to their work being included in the thesis and they have accepted the candidate's contribution as indicated below in the *Statement of Originality*.

Name of candidate:	William S. Marks
Name/title of Primary Supervisor:	Dr. Fu-Guang Cao
Name of Research Output and full reference:	
F.G. Cao and W.S. Marks, Extraction of neutrino mixing parameters from experiments with multiple identical detectors. International Journal of Modern Physics A, 33(22): 1-14, 2018	
In which Chapter is the Manuscript /Published work:	Chapter 4
Please indicate:	
• The percentage of the manuscript/Published Work that was contributed by the candidate:	75%
and	
• Describe the contribution that the candidate has made to the Manuscript/Published Work:	
The candidate performed the research under the direction of the Co-Author and wrote the results section of the publication. The Co-Author wrote the Introduction and handled submission. The parts written by the Co-Author are not in the Thesis.	
For manuscripts intended for publication please indicate target journal:	
Candidate's Signature:	William S. Marks
Date:	19/01/21
Primary Supervisor's Signature:	Fu-Guang Cao
Date:	19/01/2021

(This form should appear at the end of each thesis chapter/section/appendix submitted as a manuscript/ publication or collected as an appendix at the end of the thesis)

GRS Version 4– January 2019

Chapter 5

Mixing Modulation

A significant area of computational investigation was on the effect of matter on the neutrino mixing pattern (i.e. the matter effect). The primary focus was on a possible effect arising from interactions with dark matter while additional work was conducted on the effects of variable matter distributions. Most of the computations consisted of producing plots of the effects.

5.1 Spatial Density Distribution Calculations

Calculations on spatial density effects were motivated by the idea of using the matter effect to detect exoplanets. The theory was that the passage of an exoplanet between a star and a detector would cause a shift in the pattern of neutrinos observed by the detector. The calculations were conducted with full understanding that the likelihood of an exoplanet passing directly between a star and the Earth is extremely small. Additionally, there is the essentially insurmountable problem of isolating neutrinos from a distant star. The main problem is that the signal to noise ratio is exceptionally poor. Assuming that the background consists entirely of solar neutrinos (which will be at the same energy of the proposed extra-solar neutrinos), the flux for the star10 ly away is $\phi_{star} = \frac{r_{sun}^2}{r_{star}^2}\phi_{sun} \approx 10^{-12}\phi_{sun}$. This is ignoring the contribution from every other star in

the universe, which would (presumably) be at a similar energy.

In spite of the sheer impracticality of any actual measurements being feasible, preliminary calculations were performed in order to explore the nature of the results. These were naively conducted by dividing the baseline into segments of differing potentials and then performing a (coherent) calculation of the flavour fractions at the end of each segment which would be used as the starting fraction for the next segment. It was found that the resulting patterns were independent of the actual potentials used and that deviation from the "vacuum" result (i.e. where there was a single calculation across the entire baseline) was due to the manner in which the calculations were performed. Essentially, these calculations simulated the situation where a neutrino is emitted and then captured and re-emitted a number of times before being detected, which is a far cry from the situation of interest (or indeed, one that is likely to physically exist).

After some additional thought on the matter, it was realized that the standard formalism for describing the matter effect is incapable of describing effects due to inhomogeneous matter distributions. The standard method for describing neutrino propagation is a traditional Quantum Hamiltonian, which predicts a final state given an initial state and the state of the system. In order for this to work, the analysis needs to be blind to the actions of the neutrinos along the flight-path (a Cat Problem, if you will).

That being said, there is a possibility that there will be a effect if the scale of the density fluctuations is comparable to the oscillation wavelength. The idea for this is that if the fluctuations are synchronized with the oscillations, then there will be an enhancement of the MSW effect while it will be suppressed if they are anti-synchronized. Additionally, there might be a slight mass-state distinction, given that the Weak-Interaction is energy-dependent. What the effect might be and whether it could ever be measured are matters of further study.

5.2 Mixing Modulation by Dark Matter

If there is an interaction between neutrinos and dark matter, then there could be a modulation of the mixing patterns of astrophysical neutrinos. This would result from forward coherent scattering in a manner identical to the MSW effect and thus can be treated in a similar way (in the case of WIMPs, it is precisely the MSW effect). This section contains calculations on the size of the effect with very high energy neutrinos traveling astronomical distances through very small potentials. This work is largely contained in [133].

5.2.1 Decoherent Effects

Research on this modulation has been done in recent years, specifically looking at ultra-high energy neutrinos [100]. Since these neutrinos have been produced at extremely long distances, past work has only considered the effect on decoherent neutrinos. Below is a partial replication of the past work.

The formula for decoherent wavepackets is:

$$f_\beta = \sum_{\alpha=e,\mu,\tau} \left(\sum_{i=1}^{3} \left| U_{\beta i} U_{\alpha i}^* \right|^2 f_\alpha^0 \right), \tag{5.1}$$

It is obvious at a glance that this is simply the time independent terms from the coherent flavour fraction formula.

The matter interaction Hamiltonian was parameterised as:

$$\begin{aligned} \mathcal{H}_{tot} &= \mathcal{H}_{vac} + U^\dagger \mathcal{H}_{int} U \\ &= \begin{bmatrix} E_1 & 0 & 0 \\ 0 & E_2 & 0 \\ 0 & 0 & E_3 \end{bmatrix} + U^\dagger \begin{bmatrix} V_{11} & 0 & 0 \\ 0 & V_{22} & 0 \\ 0 & 0 & 0 \end{bmatrix} U, \end{aligned} \tag{5.2}$$

where U is the PMNS matrix. The setting of the $(3,3)$ entry in $\mathcal{H}_{int}$ to zero is justified by the fact that only interaction differences can produce an effect, which means that the addition or subtraction of scalar multiples of the identity matrix will not change the result

which means that one of the values along the main diagonal can always be set to zero. The setting of the non-diagonal terms to zero is justified as this is the Hamiltonian for WIMPs only. It needs to be noted that the V terms are potentials, which are a product of the number density and the interaction cross-section.

This formula was investigated by simply plotting the difference between the vacuum result and the result in the presence of a potential across both free parameters. The range on V_{11} and V_{22} was chosen to be 10^{-33} eV to 10^{-13} eV in order to coincide with the potentials allowed by cosmological considerations [112, 113, 114]. Additionally, only the positive ranges were considered for reasons of convenience and as it suffices to describe the result (the results would be symmetric about the two axes [100]). As in [100], the starting flavour fraction composition was $(e, \mu, \tau) = (1, 0, 0)$. Two different energies were used, 1 TeV and 1 PeV, in order to show the relationship with energy. The metric to measure the effect was:

$$D_\beta = f_\beta - f_{\beta,0},\ \beta = e, \mu, \tau. \tag{5.3}$$

which is simply the difference between the fractions with and without a potential.

At 1 PeV, the minimum discernible potential is approximately 10^{-19} eV. Taking the average mass density to be 0.4 GeV cm^{-3} which is approximately the local density [134], this corresponds a scoton with a mass of 10^{-10} eV (essentially an axion) with a cross-section on the order of of 10^{-33}cm^2, which at 1 PeV is approximately at the weak scale. While not strictly outside the realm of possibility, this combination of interaction strength and scoton mass seems rather unlikely.

At 1 TeV, the minimum discernible potential has been moved up by approximately three orders of magnitude, showing that the size of the effect is proportional to the energy of the neutrinos.

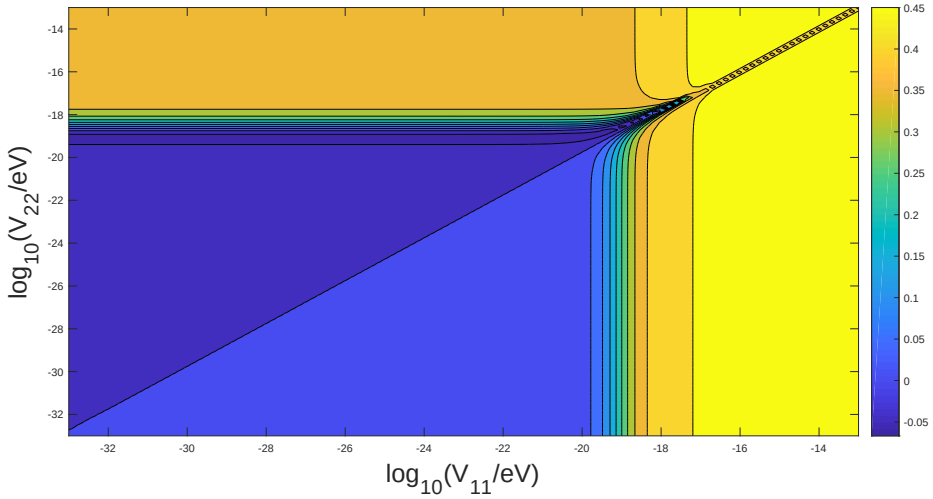

Figure 5.1: This shows D_e across flavour potentials at 1 PeV using the decoherent formula, Eq. 5.1. The regions of substantial shift are clearly visible at the top and on the right-hand side while the region of little effect is in the lower left-hand corner. The difference in colour on either side of the null-line is due to a sign change across that line. This is the same for all other plots.

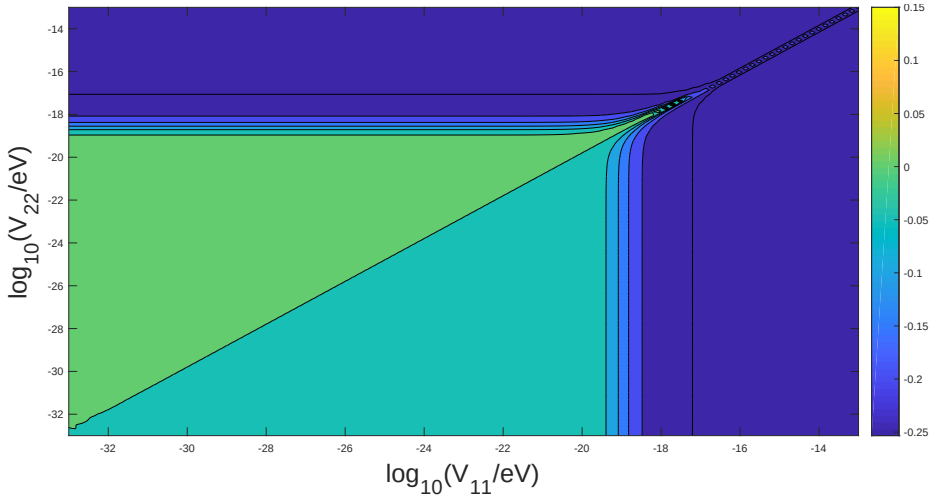

Figure 5.2: This shows D_μ across flavour potentials at 1 PeV using the decoherent formula, Eq. 5.1. The overall pattern is nearly identical to the pattern for electron neutrinos, which is expected due to the equivalence of the functions.

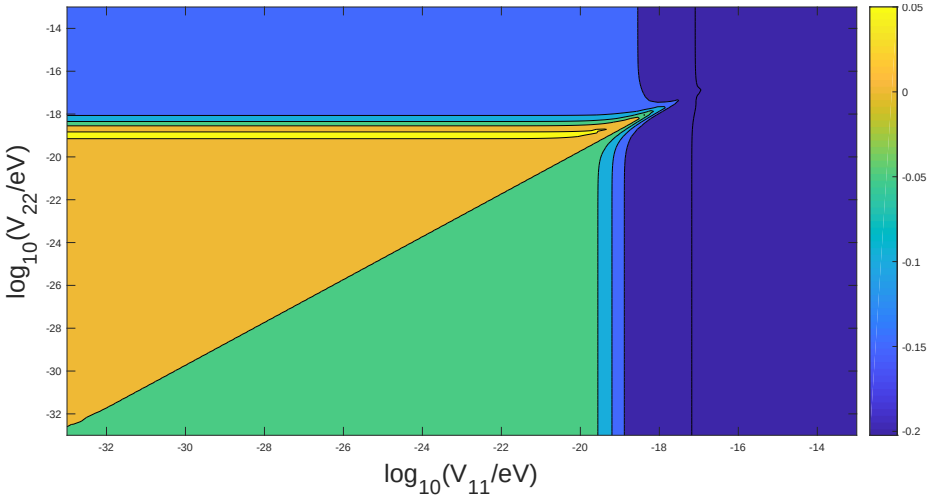

Figure 5.3: This shows D_τ across flavour potentials at 1 PeV using the decoherent formula, Eq. 5.1. The behaviour is still largely the same as for the other two flavours.

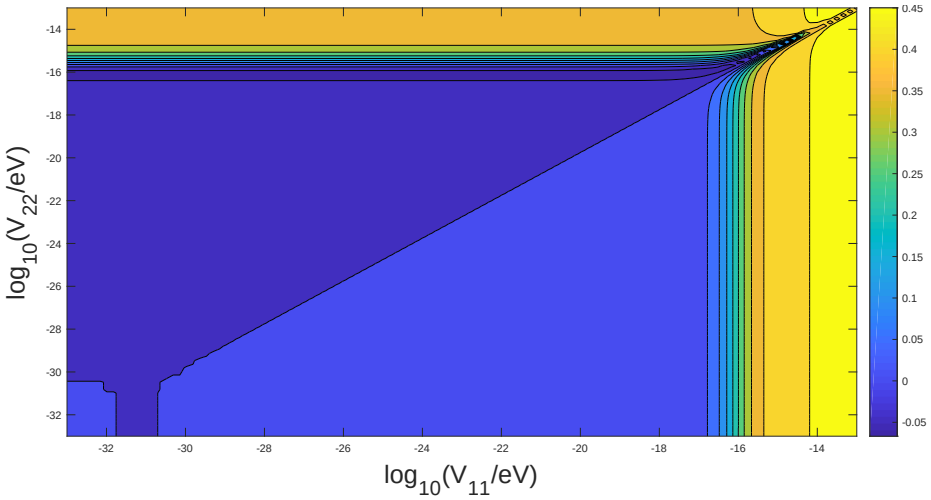

Figure 5.4: This shows D_e across flavour potentials at 1 TeV using the decoherent formula, Eq. 5.1. A comparison with figure 5.1 will quickly reveal that the effect drops off at a higher potential than for the 1 PeV case.

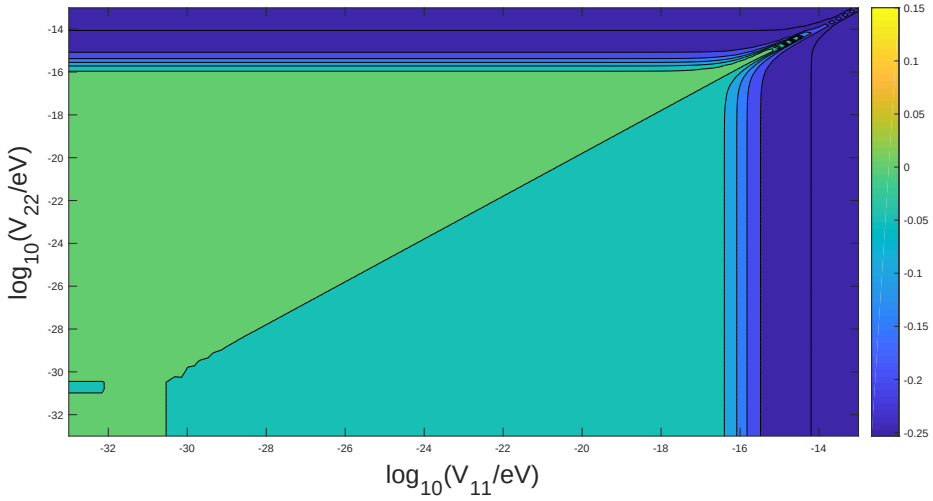

Figure 5.5: This shows D_μ across flavour potentials at 1 TeV using the decoherent formula, Eq. 5.1.

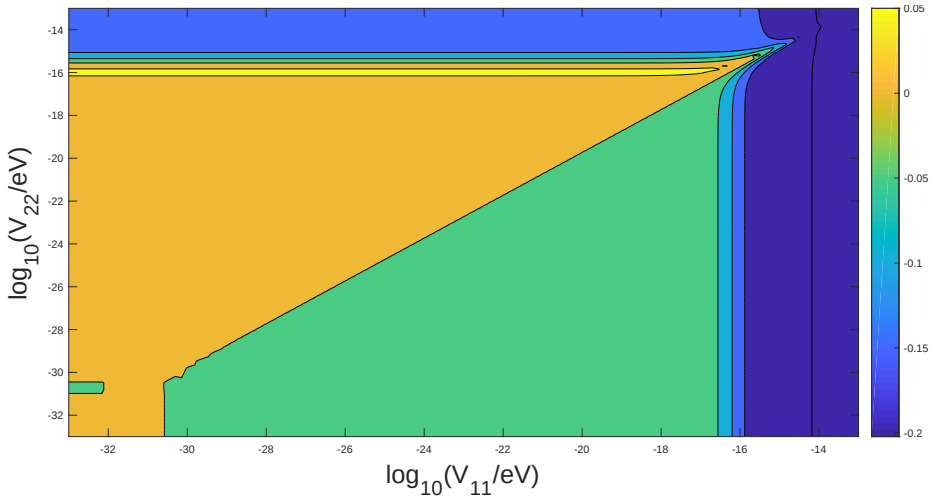

Figure 5.6: This shows D_τ across flavour potentials at 1 TeV using the decoherent formula, Eq. 5.1.

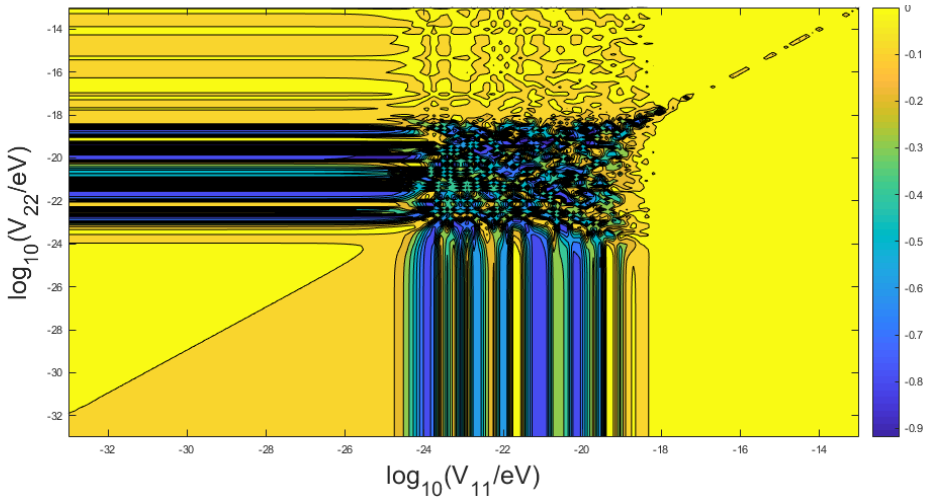

Figure 5.7: This shows D_e across flavour potentials at 1 PeV and 100 pc using the coherent formula, Eq. 2.12. The high potential effects are qualitatively the same as for the decoherent plots, as are the low potentials. The main difference is in intermediate potentials. Between 10^{-19} and 10^{-25} eV, there is a region of high variance where coherence effects produce fluctuations in the survival probability. These features are shared by all of the coherent plots.

5.2.2 Coherent Effects

This was also motivated by a desire to see if improvements could be made in the minimum detectable potential, due to a potential being high enough to be detected from decoherent effects being highly unlikely. The potentials were plotted across the same range as for the decoherent case. Plots were made across two energies and three baselines. The energies are the same as before while the baselines are 100 pc, 1 kpc and 10 kpc. This was to show the behaviour against both factors.

The results for the decoherent function (Eq. 5.1), shown in figs. 5.1 to 5.6, for D_e, D_μ and, D_τ, agree with the results reported in [100]. The results for the coherent function (Eq. 2.12) are shown in figs. 5.7 to 5.24, again for D_e, D_μ and, D_τ. Comparing with the results from using the decoherent function, one can find that the results from the coherent

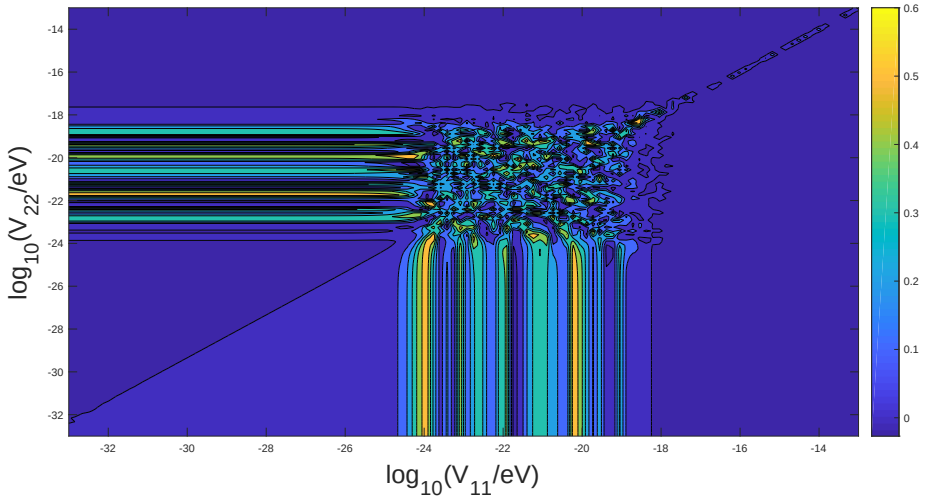

Figure 5.8: This shows D_μ across flavour potentials at 1 PeV and 100 pc using the coherent formula, Eq. 2.12..

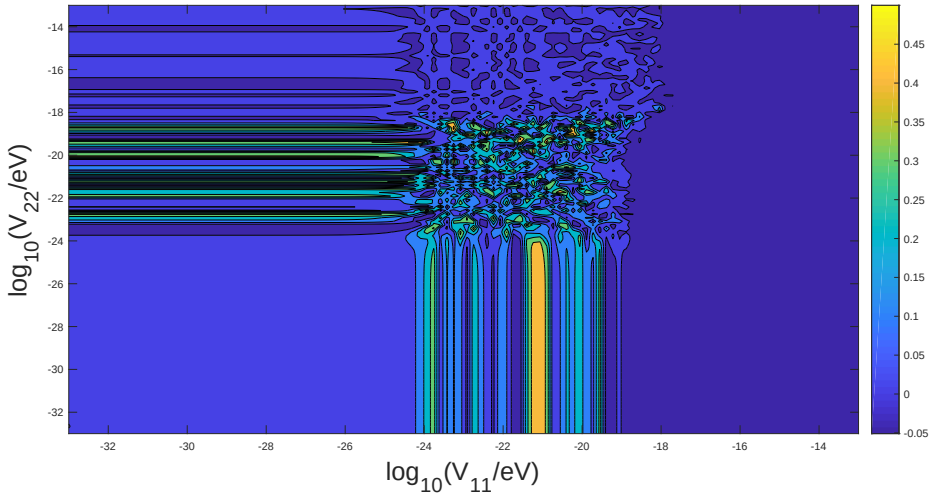

Figure 5.9: This shows D_τ across flavour potentials at 1 PeV and 100 pc using the coherent formula, Eq. 2.12.

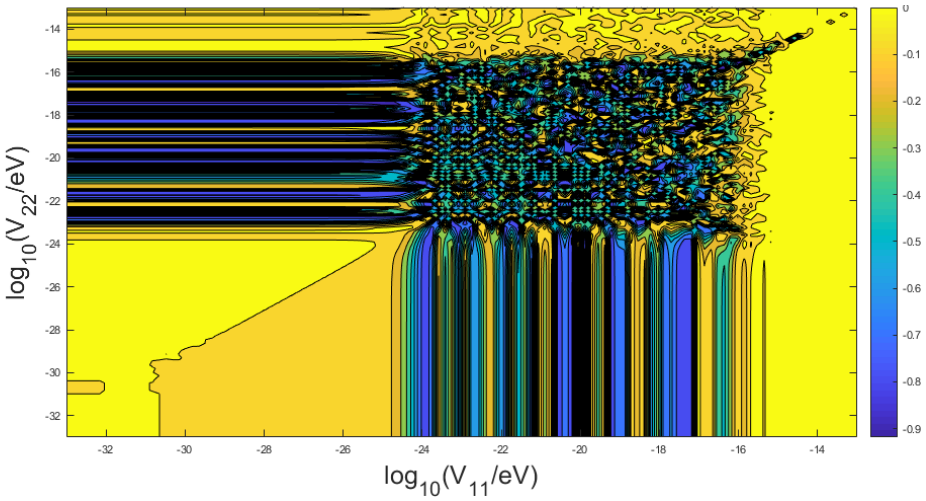

Figure 5.10: This shows D_e across flavour potentials at 1 TeV and 100 pc using the coherent formula, Eq. 2.12. The high potential region has been shifted as with the decoherent plots. However, the highly variable region has not been shifted as coherent effects do not scale with energy. Again, these features are shared with the other flavours.

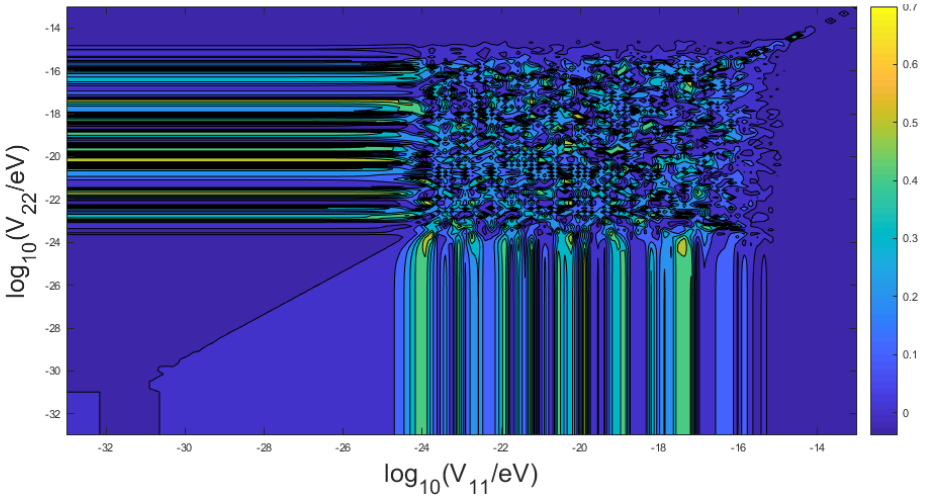

Figure 5.11: This shows D_μ across flavour potentials at 1 TeV and 100 pc using the coherent formula, Eq. 2.12.

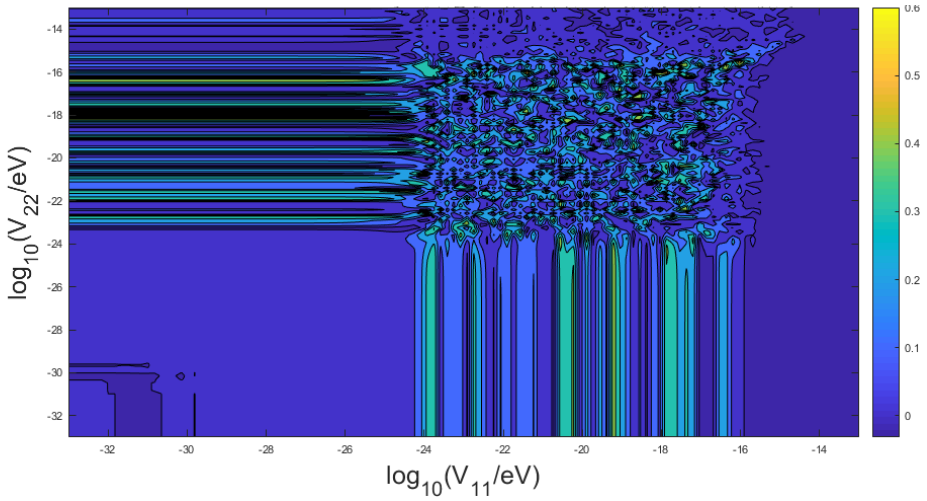

Figure 5.12: This shows D_τ across flavour potentials at 1 TeV and 100 pc using the coherent formula, Eq. 2.12.

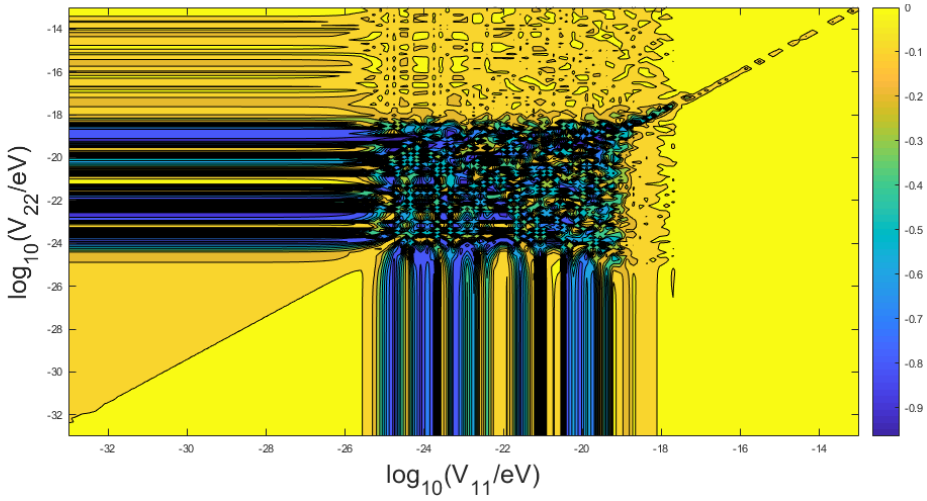

Figure 5.13: This shows D_e across flavour potentials at 1 PeV and 1 kpc using the coherent formula, Eq. 2.12. In this case, the high potential regions are the same as in the other 1 PeV plots while the variable region has now been extended downward as the coherent effects scale with baseline.

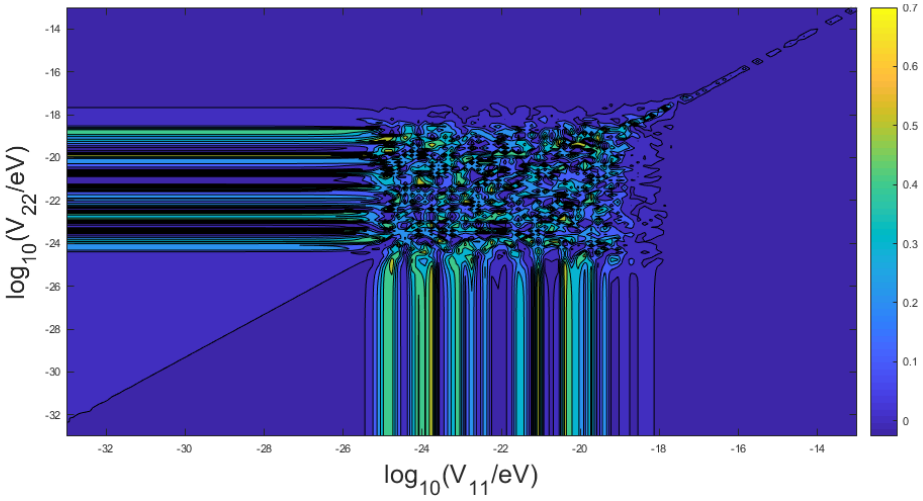

Figure 5.14: This shows D_μ across flavour potentials at 1 PeV and 1 kpc using the coherent formula, Eq. 2.12.

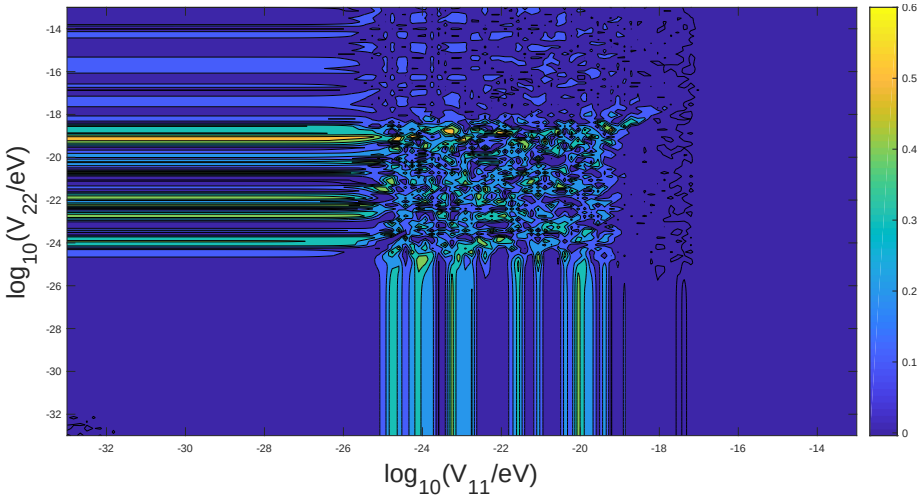

Figure 5.15: This shows D_τ across flavour potentials at 1 PeV and 1 kpc using the coherent formula, Eq. 2.12.

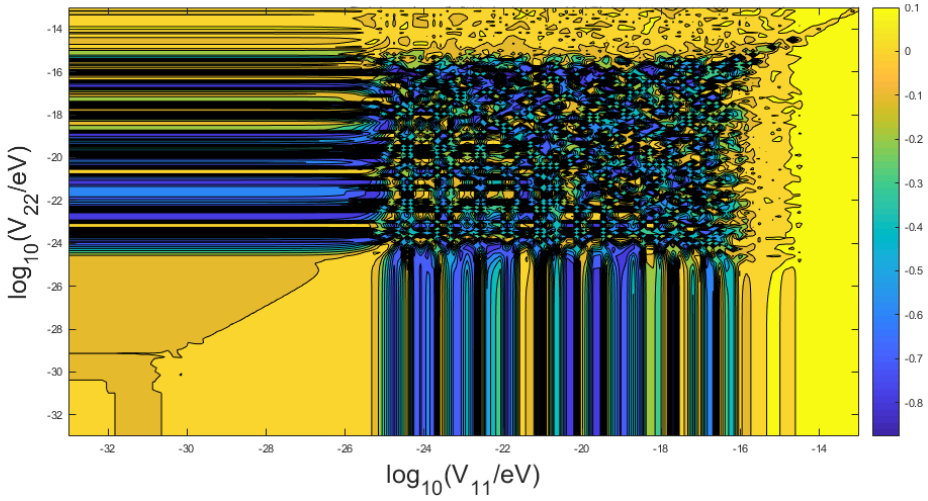

Figure 5.16: This shows D_e across flavour potentials at 1 TeV and 1 kpc using the coherent formula, Eq. 2.12. Here, both effects are now apparent.

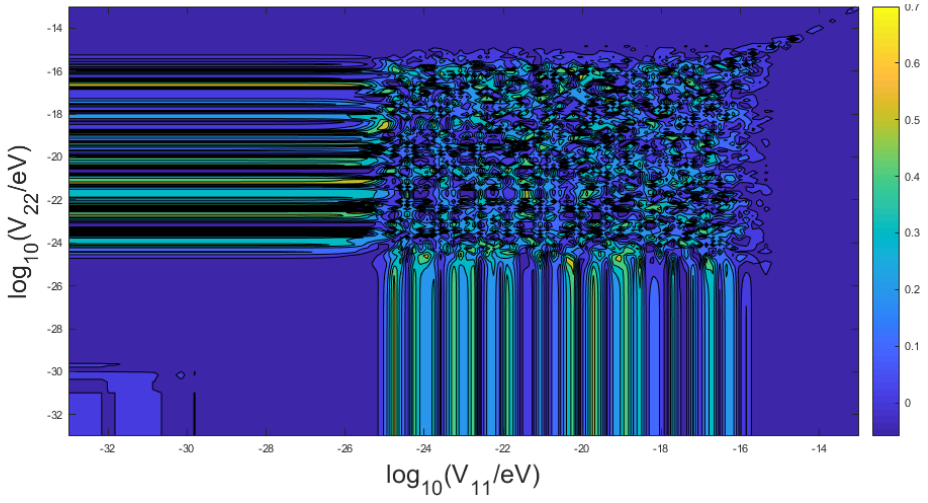

Figure 5.17: This shows D_μ across flavour potentials at 1 TeV and 1 kpc using the coherent formula, Eq. 2.12.

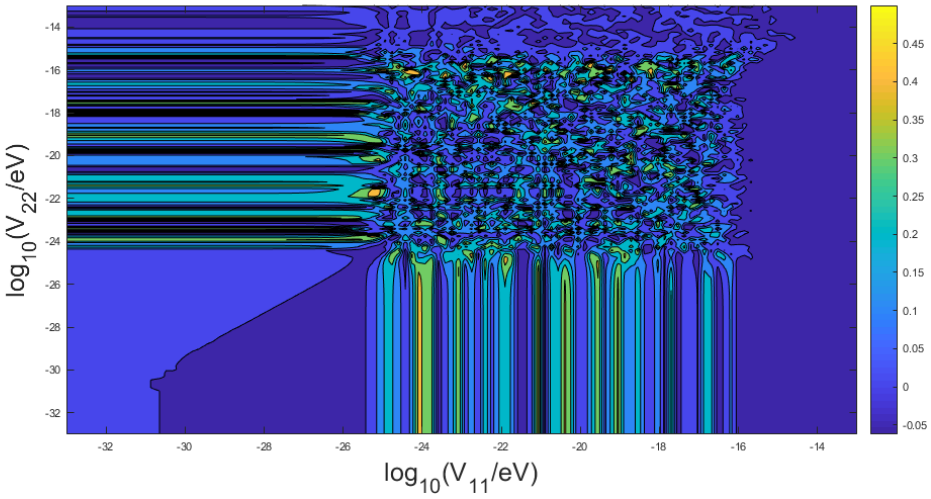

Figure 5.18: This shows D_τ across flavour potentials at 1 TeV and 1 kpc using the coherent formula, Eq. 2.12.

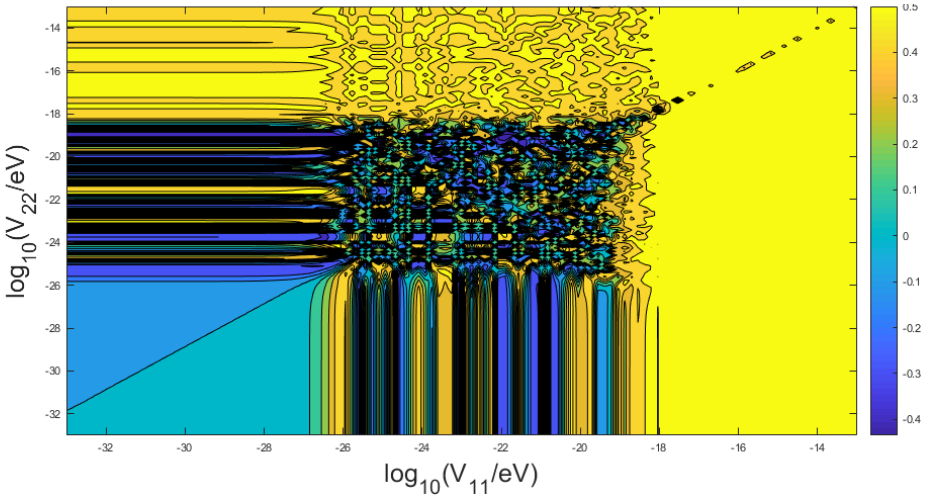

Figure 5.19: This shows D_e across flavour potentials at 1 PeV and 10 kpc using the coherent formula, Eq. 2.12. Here, the extension of the variable region is even greater due to the increase in baseline.

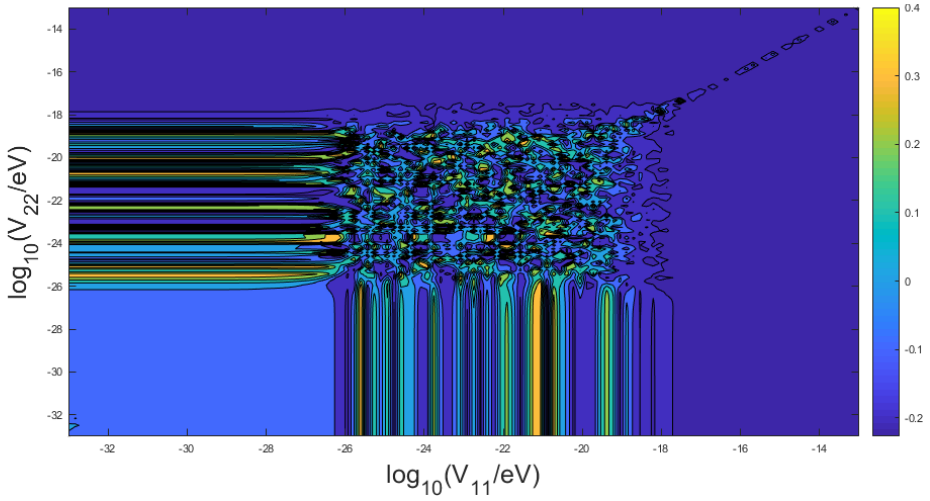

Figure 5.20: This shows D_μ across flavour potentials at 1 PeV and 10 kpc using the coherent formula, Eq. 2.12.

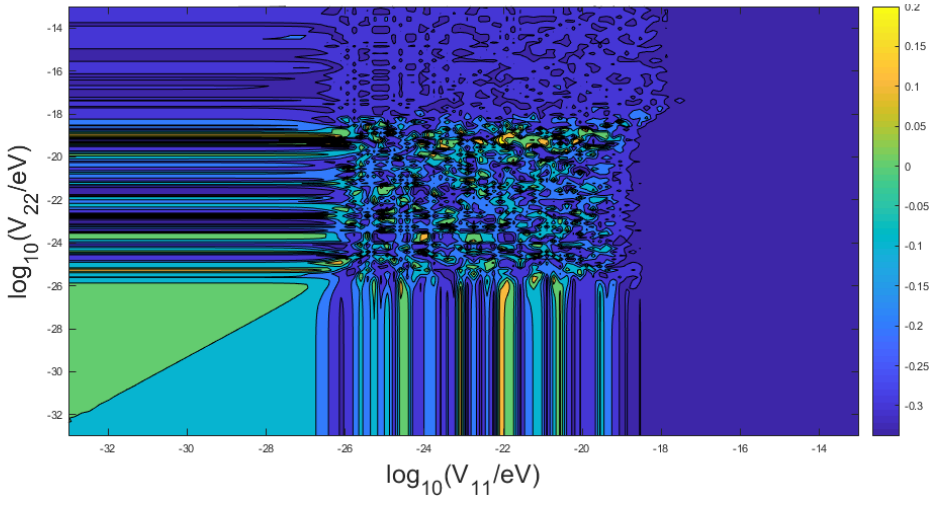

Figure 5.21: This shows D_τ across flavour potentials at 1 PeV and 10 kpc using the coherent formula, Eq. 2.12.

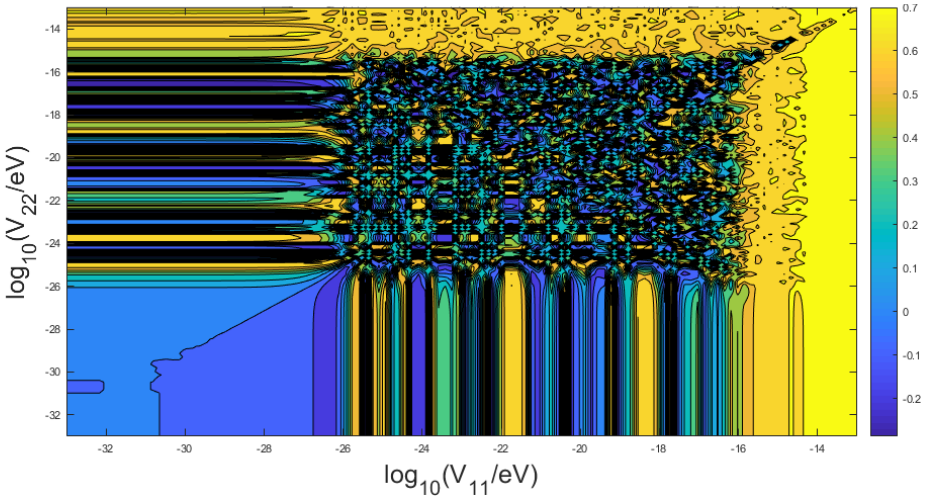

Figure 5.22: This shows D_e across flavour potentials at 1 TeV and 10 kpc using the coherent formula, Eq. 2.12.

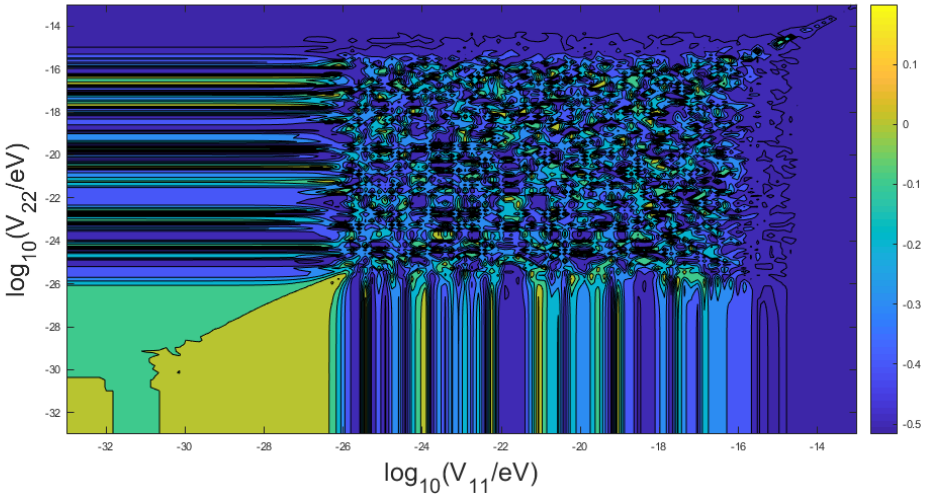

Figure 5.23: This shows D_μ across flavour potentials at 1 TeV and 10 kpc using the coherent formula, Eq. 2.12.

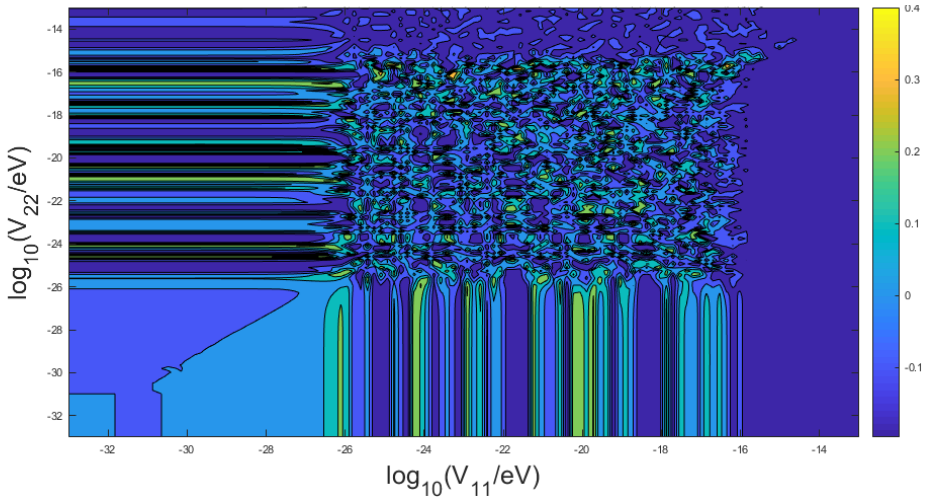

Figure 5.24: This shows D_τ across flavour potentials at 1 TeV and 10 kpc using the coherent formula, Eq. 2.12.

function have two distinguishing features. In the high potential region ($V_{11} > 10^{-18}$ eV), the coherent results for D_β have a similar structure to decoherent results, albeit with different values for D_β as the coherent results are still baseline dependent, even at high potentials. That is actually because of the definition of D_β as the difference between the flavour fraction with a potential and the fraction without. In both cases, very high potentials cause the flavours to remain fixed values. However, for the coherent case the vacuum potential is still oscillatory, causing fluctuations in D_β.

At lower potentials where the decoherent function produces very small values of D_β, the coherent function yielded highly variable values. This suggests that, even for potentials as low as 10^{-25} eV, a neutrino-Dark Matter interaction could produce a significant shift in the neutrino oscillation spectrum for coherent wavepackets. This is an improvement in interaction sensitivity over the decoherent result by approximately six orders of magnitude[1]. This effect scales with baseline, meaning that longer baselines produce bigger

[1]This seemingly coincidental convergence with the amount of improvement in energy resolution required in order to make this measurement is not particularly surprising given that both quantities scale with baseline. Thus, a one order of magnitude increase in baseline will require a one order of magnitude

effects.

5.2.3 Mass-Eigenstate Interactions.

The same procedure was repeated for mass-state interactions, which is predicted (as stated before) by scotogenic models.

The mass state interaction Hamiltonian used was:

$$\begin{aligned} \mathcal{H}_{tot} &= \mathcal{H}_{vac} + \mathcal{H}_{int} \\ &= \begin{bmatrix} E_1 & 0 & 0 \\ 0 & E_2 & 0 \\ 0 & 0 & E_3 \end{bmatrix} + \begin{bmatrix} V_{11} & 0 & 0 \\ 0 & V_{22} & 0 \\ 0 & 0 & 0 \end{bmatrix} \end{aligned} \tag{5.4}$$

which, naturally, is the same as used for flavour state interactions save for the exclusion of the PMNS matrix, U^2. The parameters used were the same as in the flavour interaction case in order to enable cross comparisons. The calculations were identical to those for the flavour case. Due to the nature of the mass state interaction Hamiltonian, the coefficients in the equation for f_β are unchanged from the vacuum, which means that the decoherent formula will remain unchanged (i.e. will always produce a null result). However, the terms inside the cosines will be changed, meaning that there will be coherence effects.

The results are shown in figs. 5.25-5.42. The patterns produced for the region of 10^{-26} eV $< V_{11} < 10^{-19}$eV are similar to the patterns shown for the same region in the flavour case, including the occurrence of significant shifts at potentials lower than can be seen with the decoherent formula. The mass state results also show more variation in D_β for the region $V_{11} > 10^{-19}$ eV than the flavour state results. This shows that the mass state effects consist entirely of the variable small scale coherence effects, as expected. Another difference between the two cases is that the massive results appear to be entirely symmetric

improvement in both energy resolution and distance measurement, separately, with the benefit of a one order of magnitude improvement in interaction sensitivity.

[2]Both Hamiltonians are presented in the mass basis representation, which is the canonical basis for the propagation Hamiltonian.

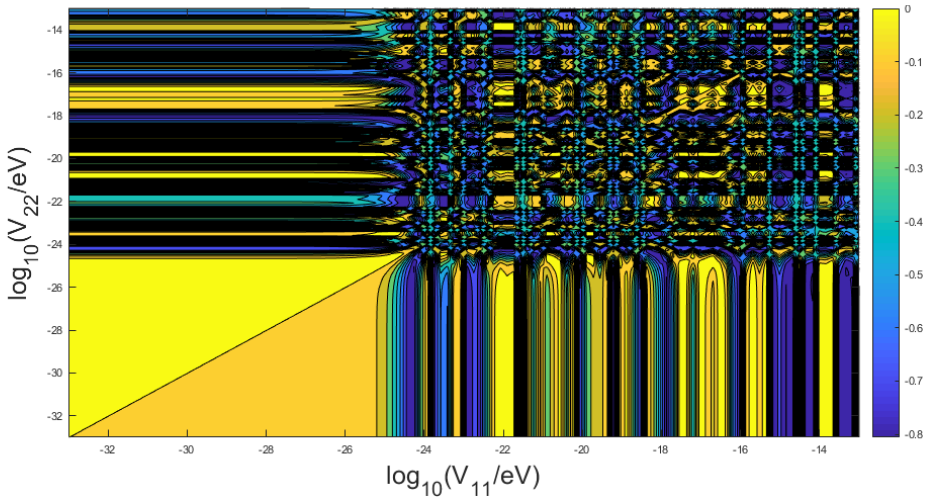

Figure 5.25: This shows D_e at 1 PeV and 100 pc for mass-eigenstate interactions. It clearly shows the lack of decoherent effects at any potential.

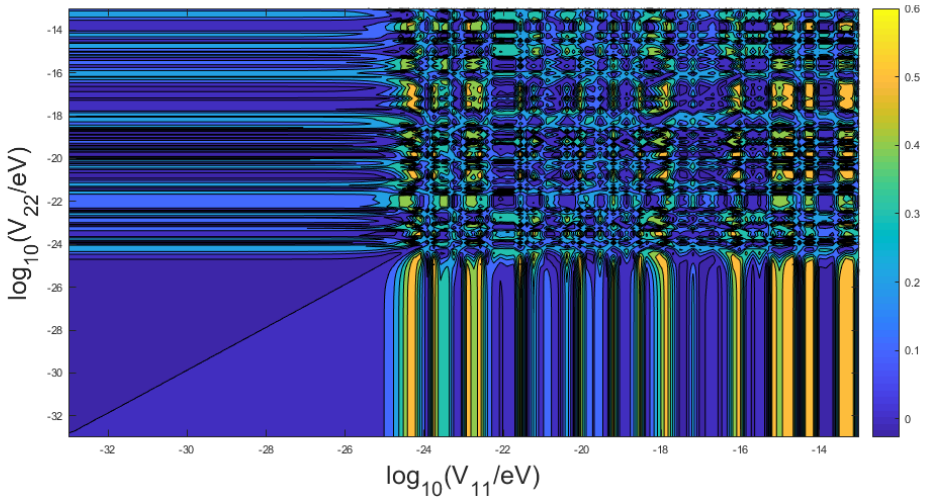

Figure 5.26: This shows D_μ at 1 PeV and 100 pc for mass-eigenstate interactions.

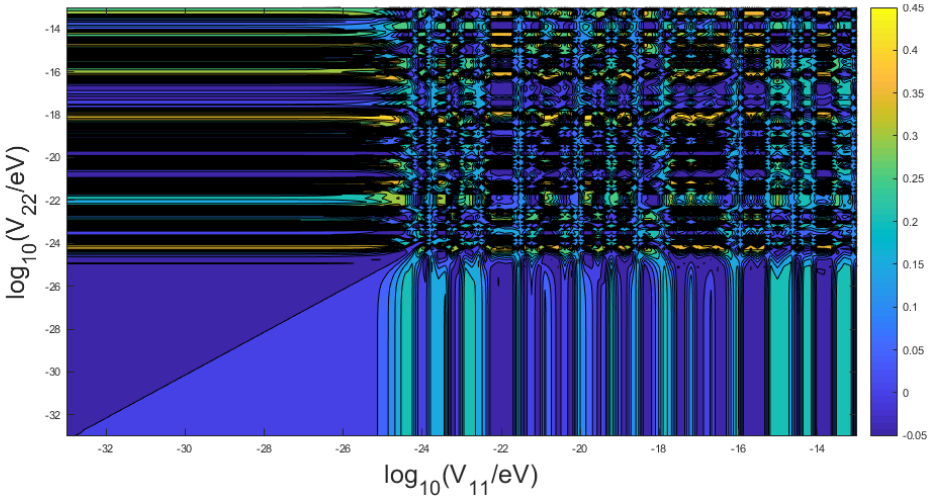

Figure 5.27: This shows D_τ at 1 PeV and 100 pc for mass-eigenstate interactions.

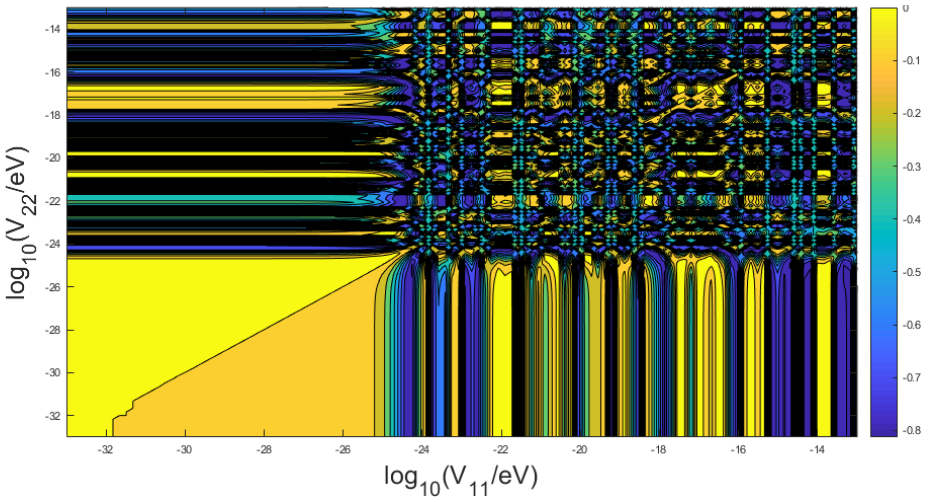

Figure 5.28: This shows D_e at 1 TeV and 100 pc for mass-eigenstate interactions. A comparison with the 1 PeV plot will show that it is identical to this plot. That is not a general feature but a fluke result unigue to this baseline.

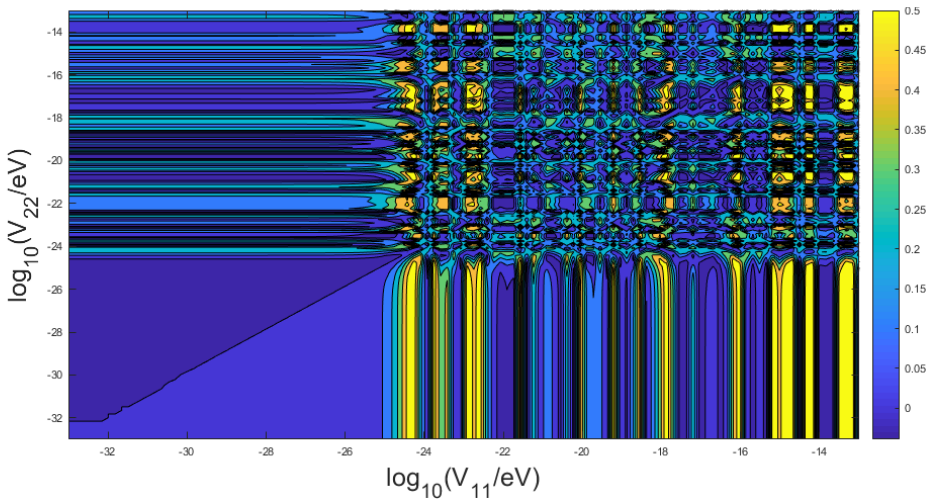

Figure 5.29: This shows D_μ at 1 TeV and 100 pc for mass-eigenstate interactions.

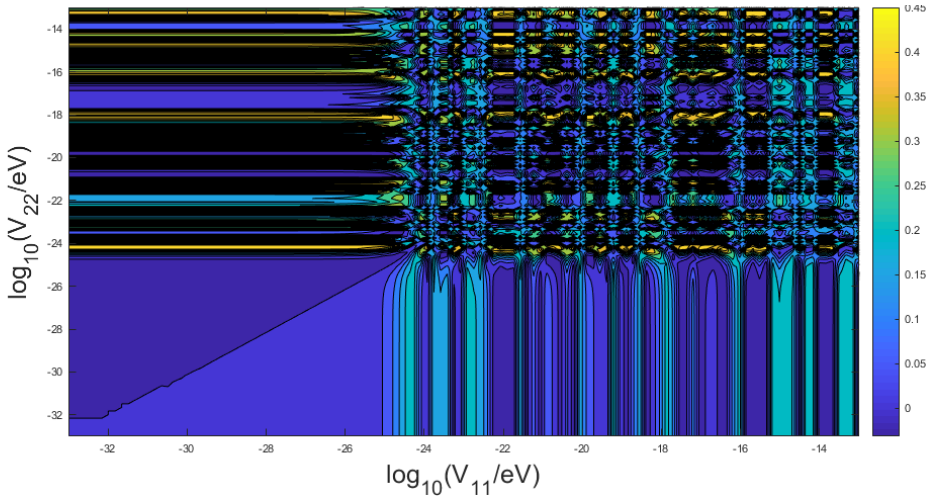

Figure 5.30: This shows D_τ at 1 TeV and 100 pc for mass-eigenstate interactions.

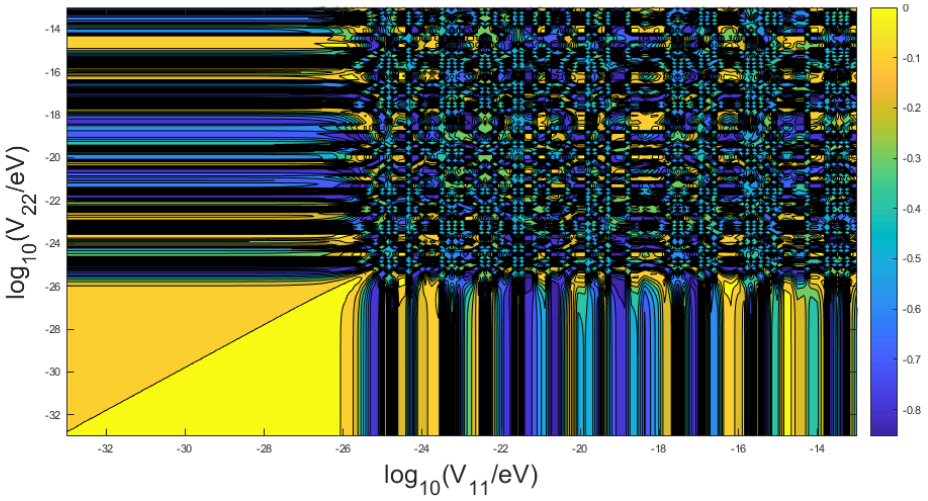

Figure 5.31: This shows D_e at 1 PeV and 1 kpc for mass-eigenstate interactions. As can clearly be seen, the is a significant extention of the region of the effect, demonstrating the baseline dependence.

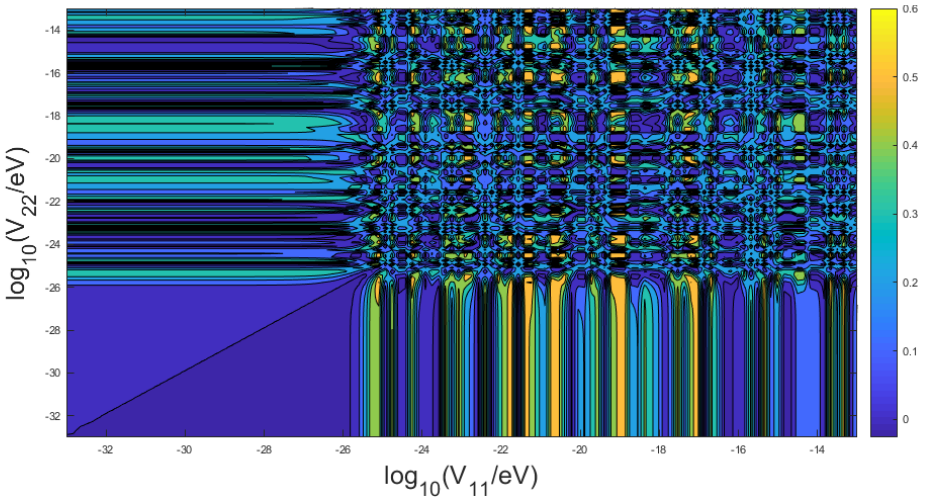

Figure 5.32: This shows D_μ at 1 PeV and 1 kpc for mass-eigenstate interactions.

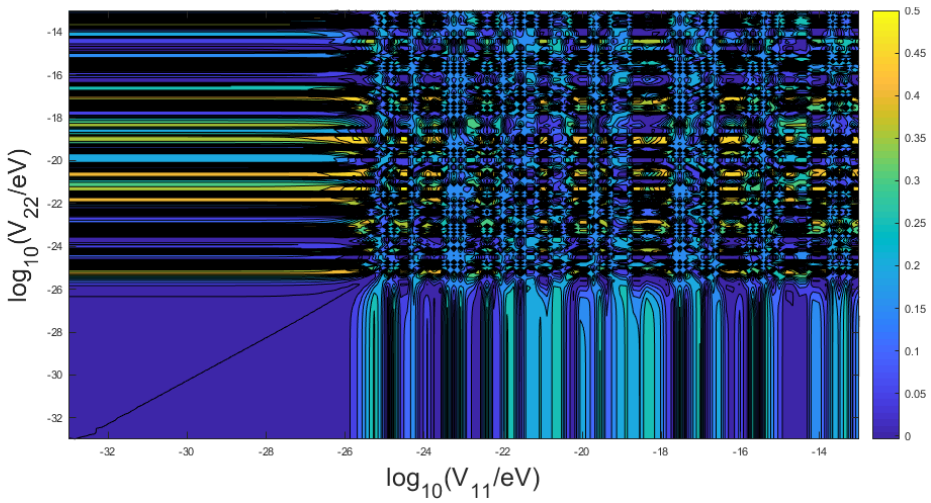

Figure 5.33: This shows D_τ at 1 PeV and 1 kpc for mass-eigenstate interactions.

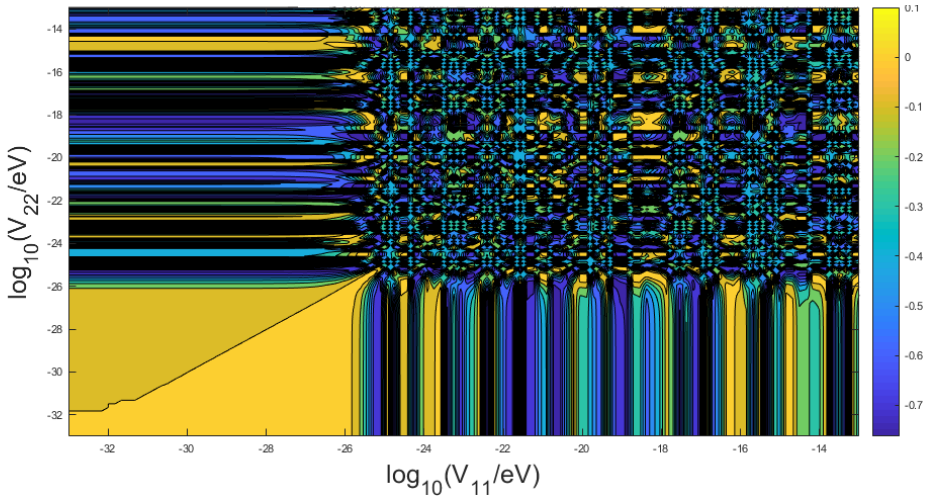

Figure 5.34: This shows D_e at 1 TeV and 1 kpc for mass-eigenstate interactions.

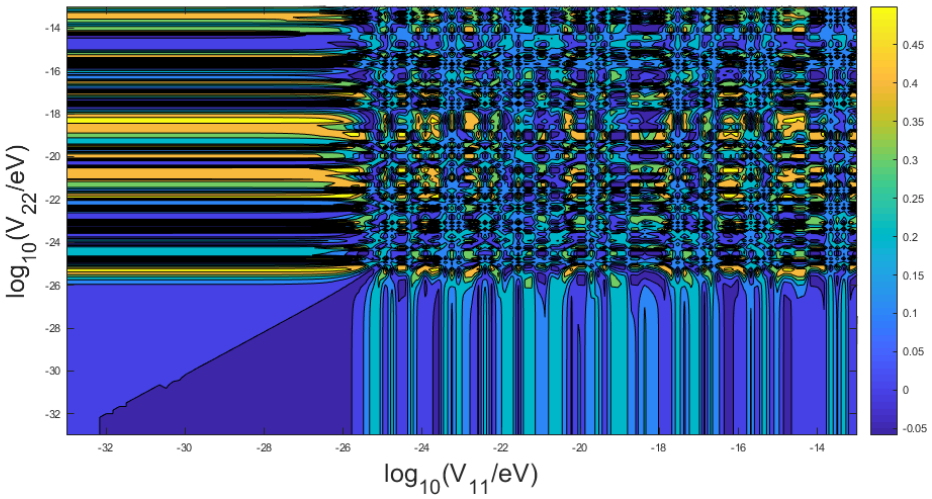

Figure 5.35: This shows D_μ at 1 TeV and 1 kpc for mass-eigenstate interactions.

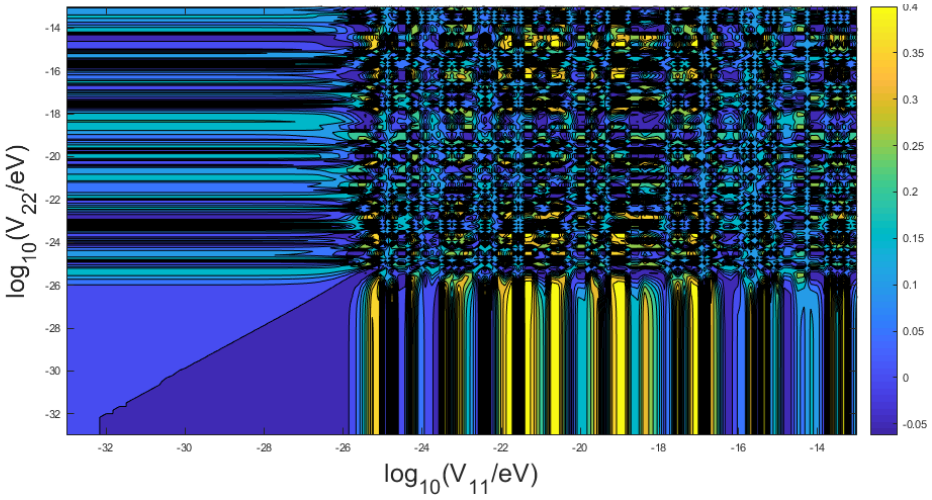

Figure 5.36: This shows D_τ at 1 TeV and 1 kpc for mass-eigenstate interactions.

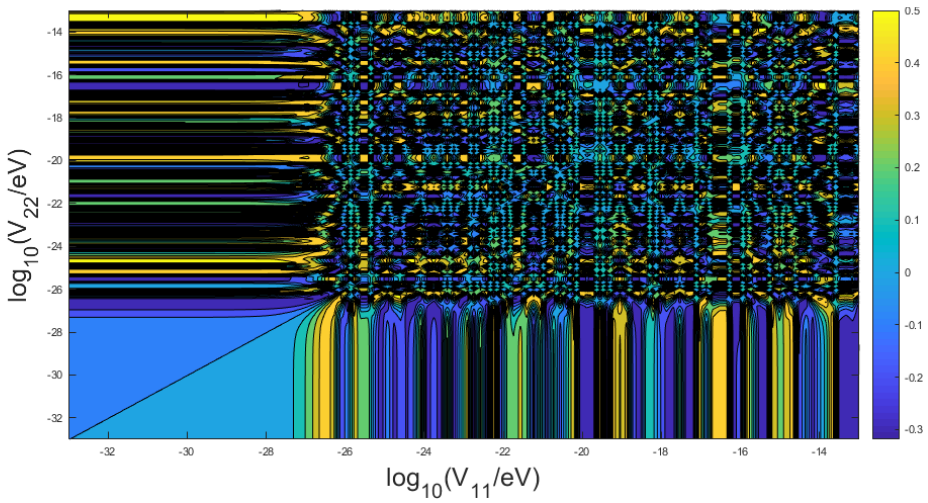

Figure 5.37: This shows D_e at 1 PeV and 10 kpc for mass-eigenstate interactions.

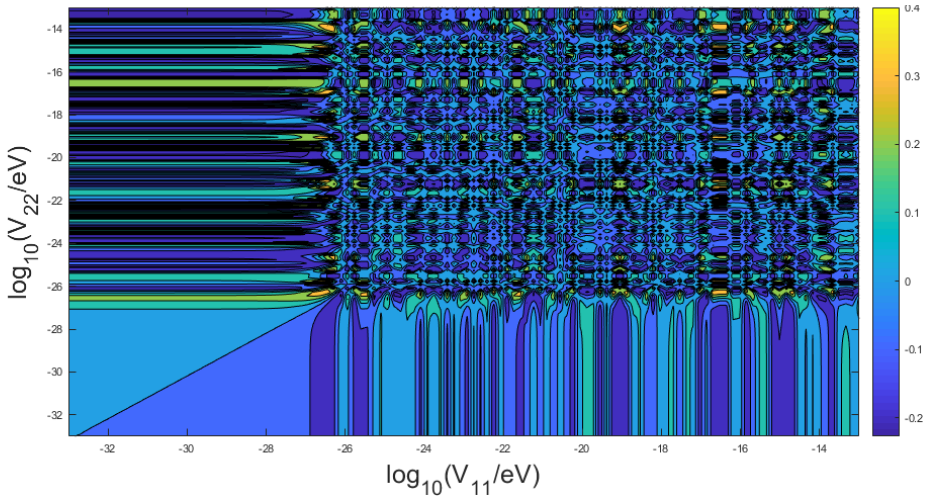

Figure 5.38: This shows D_μ at 1 PeV and 10 kpc for mass-eigenstate interactions.

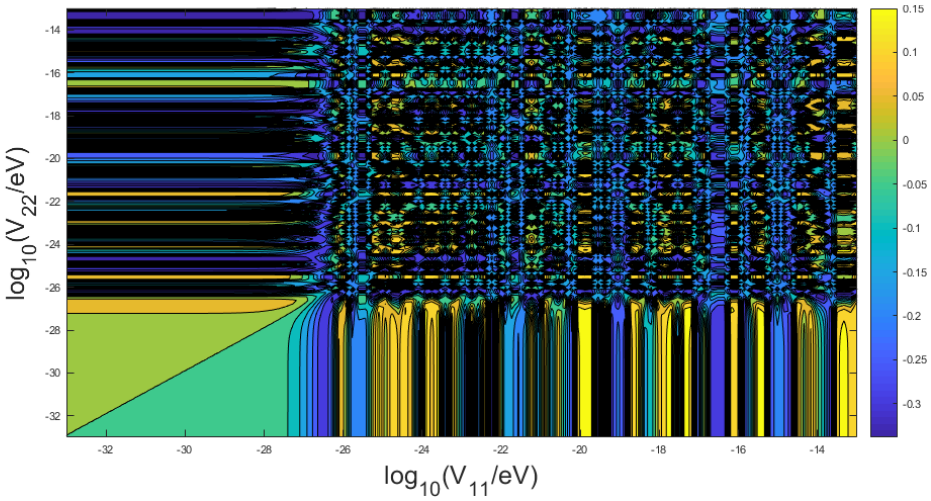

Figure 5.39: This shows D_τ at 1 PeV and 10 kpc for mass-eigenstate interactions.

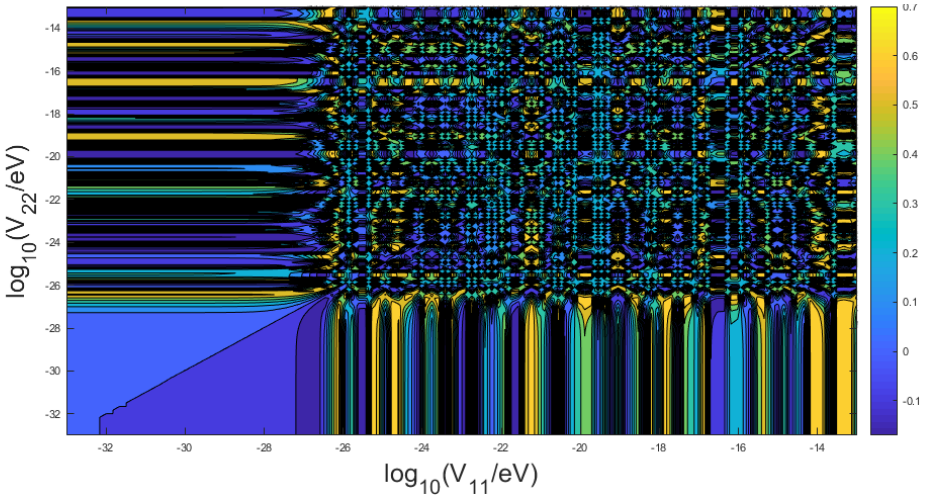

Figure 5.40: This shows D_e at 1 TeV and 10 kpc for mass-eigenstate interactions.

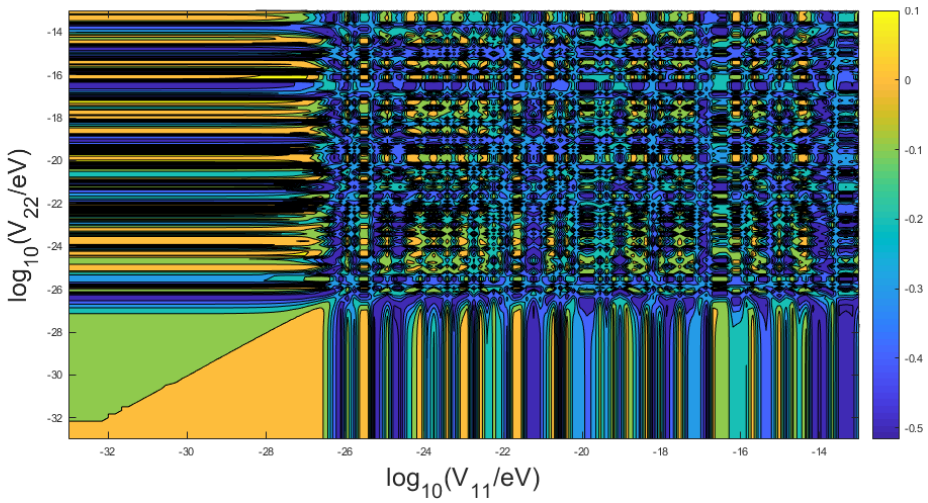

Figure 5.41: This shows D_μ at 1 TeV and 10 kpc for mass-eigenstate interactions.

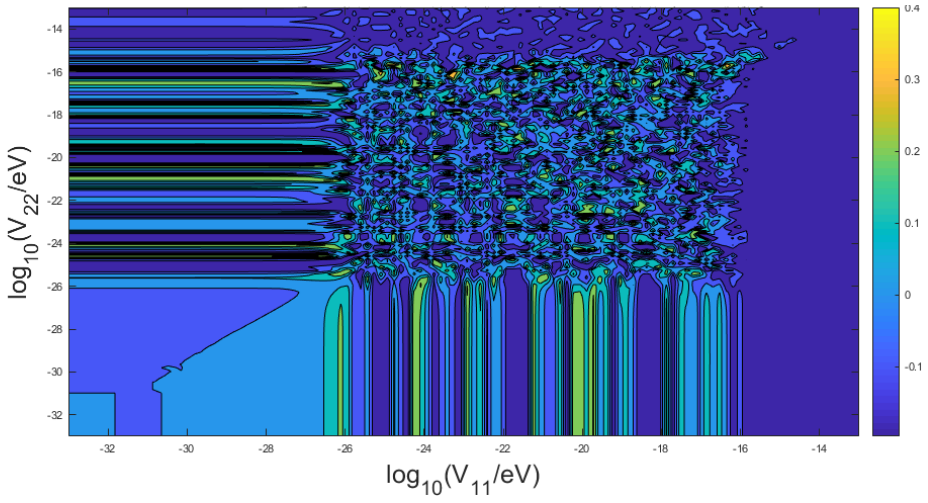

Figure 5.42: This shows D_τ at 1 TeV and 10 kpc for mass-eigenstate interactions.

about V_{11} and V_{22}. Unfortunately, the minimum cutoff in this spectrum exceeds the limits specified by Lyman-α forest measurements for fixed cross-sections, which is $\approx 10^{-38}$ eV [114][3].

5.2.4 Oscillation Patterns

In neutrino oscillations, there are two different length scales involved which are related to the two mass-squared differences[4]. The ratio of the two is generally fixed while the total scale is determined by the energy. In the case of 1 PeV neutrinos the small scale oscillations are $\approx$ 7 AU while the large-scale oscillations are $\approx$ 220 AU. The presence of an interaction introduces a shift in the oscillations. The shift is, first and foremost, in frequency, which causes the oscillations in the presence of an interaction to be out of phase with the oscillations in the absence of the interaction. The shift can also be more subtle, which seems to occur with the mass state interaction as the maximum differences are not as large as those for flavour (see fig. 5.43).

An interesting difference between the two interactions is the effect on the different flavours (see fig. 5.44). In the flavour case the biggest effect is on the electron neutrinos while in the mass case the effect on electron neutrinos is quite small. Another interesting effect is how the long range pattern for the flavour case shows a slight shift in the shape of each peak, which shows up most clearly for muon neutrinos. Due to the unphysical nature of the combination of baseline and potential (potential is related to dark matter concentration) any discussion of the long range effects are purely academic, yet this is still

[3]In [114], the cosmological constraints are given as cross-sections. However, a close examination will reveal that the mass of the speculative dark matter particle is included as a parameter. The potentials are thus a product of the mass-dependent cross-section and the average energy density of DM in the appropriate environment (the galaxy for astronomical neutrinos, the universe for blazar neutrinos).

[4]The mass-squared differences come from the ultra-relativistic approximation, $E_i t \approx \frac{m_i^2}{2E} L$, which is the standard approximation used in neutrino oscillation experiments. The term E is held common to all three species, so the relevant term (since only differences remain) is the difference of the squared masses.

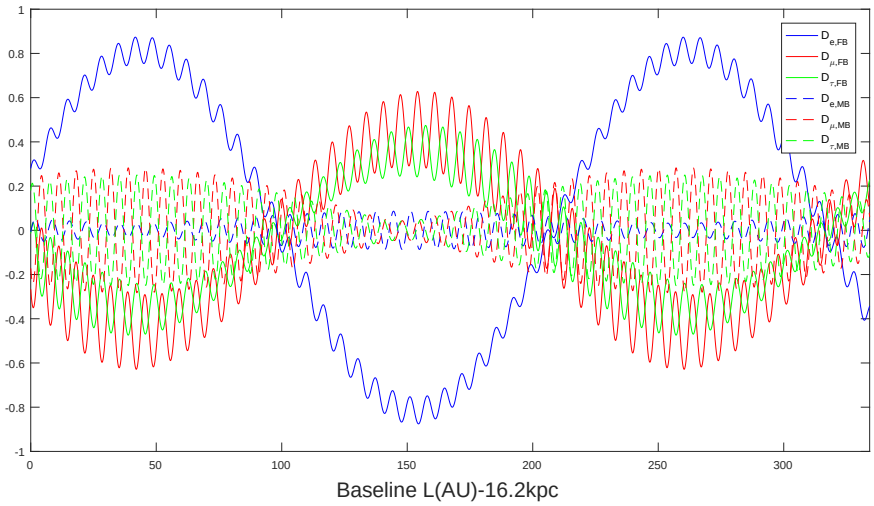

Figure 5.43: This shows the difference patterns for all three flavours in both potentials after a displacement of 16.2 kpc from the source with the baseline in AU. The two potentials (V_{11} and V_{22}) were both set to 10^{-26} eV.

an interesting result.

5.2.5 Blazar Neutrinos

A very exciting recent developement in neutrino physics was the first identification of a point source of astrophysical neutrinos. The IceCube Collaboration identified blazar TXS 0506+056 as the source for a number of high-energy (290 TeV) neutrinos observed by the group over a period of 9.5 years. In this section we present the results for D_β in the scenario where only electron neutrinos are produced at TXS 0506+056.

Blazar TXS 0506+056 has a redshift of $z = 0.3365 \pm 0.0010$, which corresponds to a baseline of $(4.384 \pm 0.013) \times 10^{25}$ m [135]). The energy was set to be 290 TeV as that was the energy reported by [136]. The potential range was changed to be in the range 10^{-40} eV $\sim 10^{-13}$ eV in order to accommodate the new results.

The results for the flavour basis are given in figs. 5.45-5.47 while the results for the mass basis are given in figs. 5.48-5.50. The overall patterns in each of the figures produced

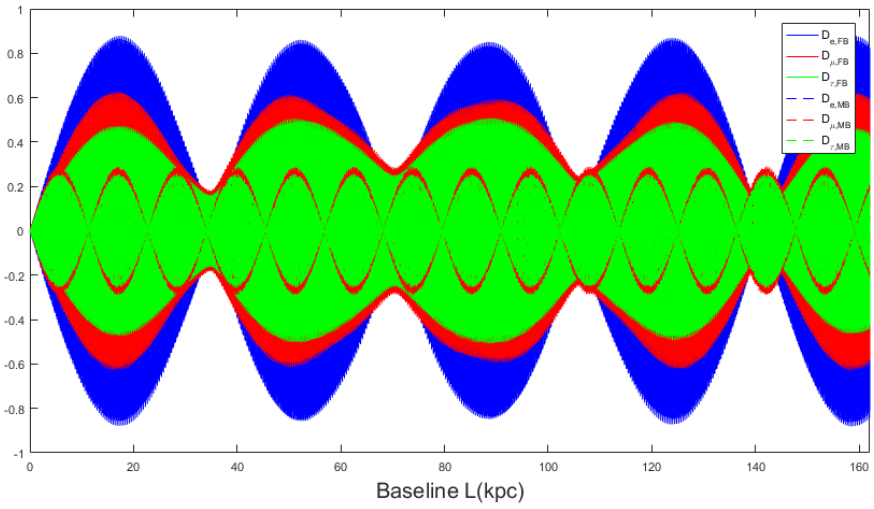

Figure 5.44: This shows the long range difference patterns for all three flavours with both potentials. The small amplitude oscillations are for the mass case and the large amplitude oscillations are for the flavour case. The potentials are the same as before. This result is of strictly academic interest as the potentials are considered unphysical at these distances.

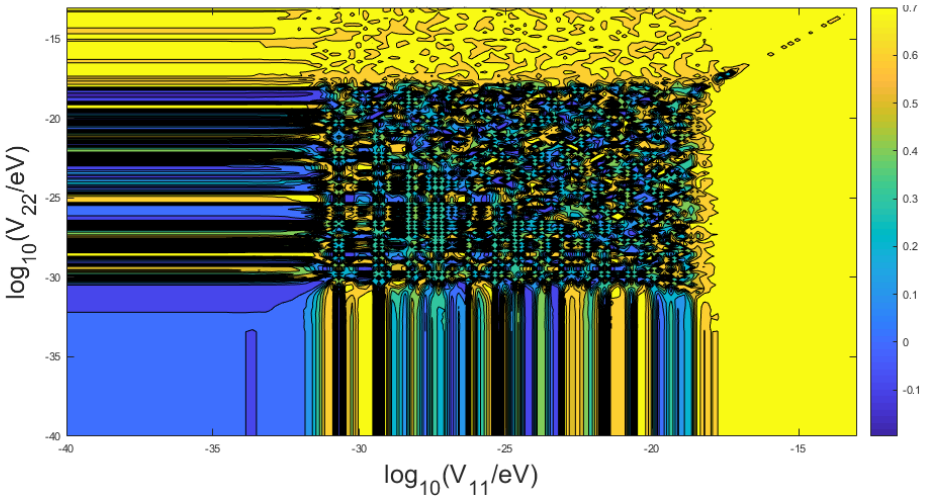

Figure 5.45: This shows D_e in the flavour basis at 290 TeV using the coherent formula. The baseline was $L = 4.384{\times}10^{25}$ m. The two kinds of effects are both still visible. The biggest difference from previously is that the region of high variability extends farther. This is due to the longer baseline.

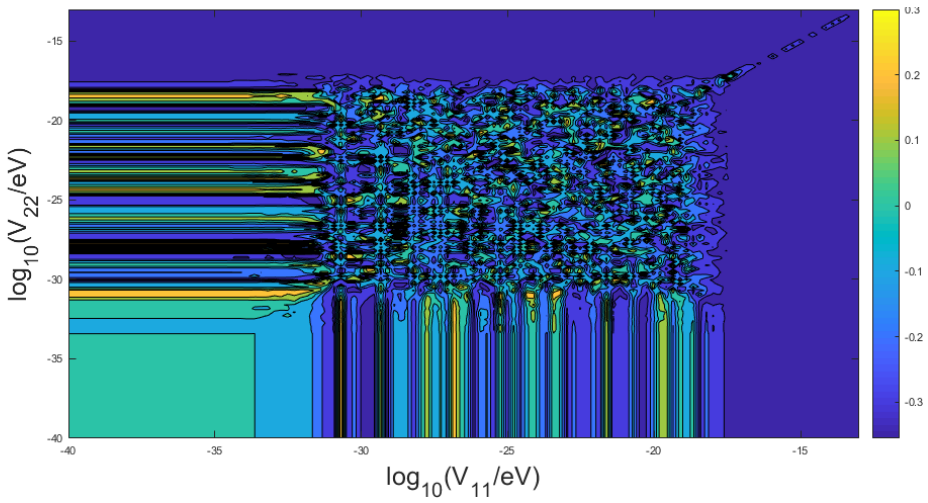

Figure 5.46: This shows D_μ in the flavour basis at 290 TeV using the full formula. The baseline was $L = 4.384{\times}10^{25}$ m. The pattern is largely the same as for the same case with electron neutrinos, as expected.

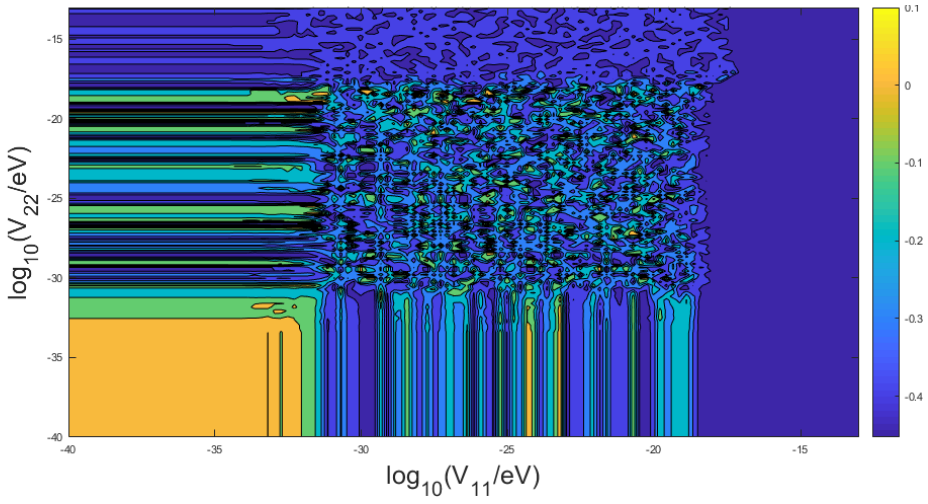

Figure 5.47: This shows D_τ in the flavour basis at 290 TeV using the full formula. The baseline was $L = 4.384{\times}10^{25}$ m

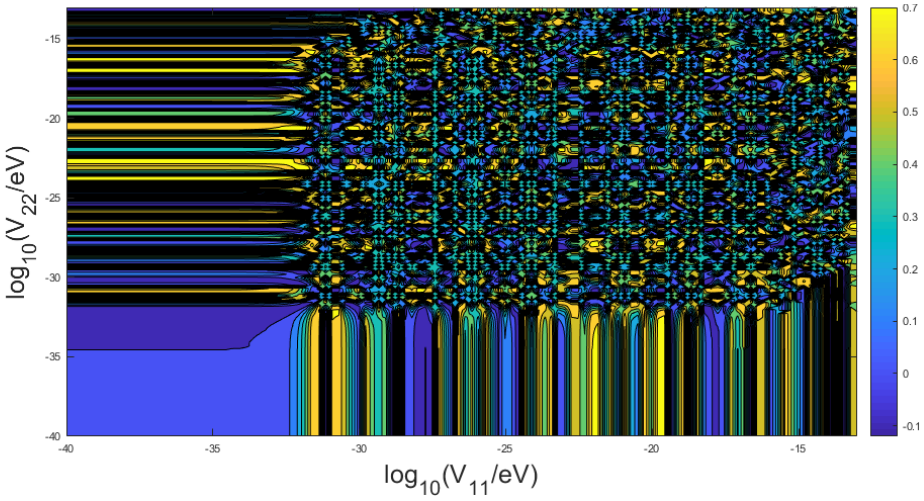

Figure 5.48: This shows D_e in the mass basis at 290 TeV using the full formula. The baseline was $L = 4.384{\times}10^{25}$ m.

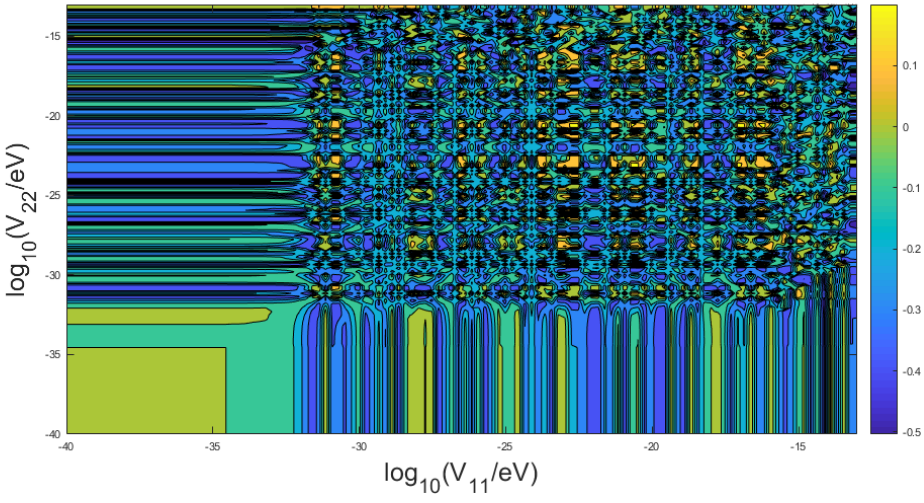

Figure 5.49: This shows D_μ in the mass basis at 290 TeV using the full formula. The baseline was $L = 4.384{\times}10^{25}$ m.

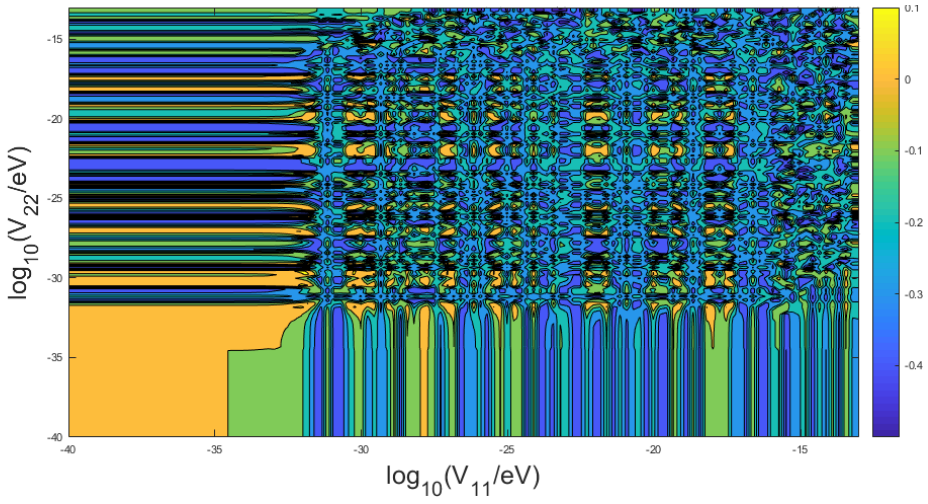

Figure 5.50: This shows D_τ in the mass basis at 290 TeV using the full formula. The baseline was $L = 4.384{\times}10^{25}m$.

for blazar neutrinos are the same as for the corresponding galactic cases. This means that the overall pattern of the field is primarily due to the function used to generate it, an unsurprising result.

The main effect was from the baseline increase, which dramatically extends the range of observability. The observable cutoff has now been lowered to $V_{11} \approx V_{22} \approx 10^{-33}$ eV.This is understandable as a longer baseline means that there is more Dark Matter for the neutrinos to scatter off of. Unfortunately, given the issues associated with such a large baseline, namely the energy resolution and the magnetic fields inside blazars, coupled with the near impossibility of determining the production point with sufficient accuracy, this is a mere thought experiment. Additionally, the potentials are proportional to the average number density along the line of flight. Given the low density of Dark Matter in inter-galactic space, the cross-section required for a potential to produce an effect is much higher than for intra-galactic baselines, meaning that a very long baseline will become counter-productive, ignoring coherence effects.

5.2.6 Conclusion

Attempting to observe a neutrino-Dark Matter interaction via modulation of the neutrino mixing patterns is highly impractical. The potentials required to observe decoherent effects are too high to be likely to exist while the observation of coherent effects would require a massive effort that is not justified by the likelihood of an observation. Other avenues would be far more practical.

That being said, it is not impossible for technology to develop enough to enable such measurements. Additionally, there is a possibility that these results might find some unforeseen application. Finally, there is no harm in contemplating the potential consequences of what should be physical effects, even if they are unobservable with current technology.

DRC 16

MASSEY UNIVERSITY
GRADUATE RESEARCH SCHOOL

STATEMENT OF CONTRIBUTION
DOCTORATE WITH PUBLICATIONS/MANUSCRIPTS

We, the candidate and the candidate's Primary Supervisor, certify that all co-authors have consented to their work being included in the thesis and they have accepted the candidate's contribution as indicated below in the *Statement of Originality*.

Name of candidate:	William S. Marks
Name/title of Primary Supervisor:	Dr. Fu-Guang Cao
Name of Research Output and full reference:	
W. S. Marks, The effects of coherent neutrino mixing modulation by dark matter. Journal of Physics: Conference Series, 1468(1): 012198, 2020.	
In which Chapter is the Manuscript /Published work:	Chapter 2 & 5
Please indicate:	
• The percentage of the manuscript/Published Work that was contributed by the candidate:	100%
and	
• Describe the contribution that the candidate has made to the Manuscript/Published Work:	
The work is a conference proceeding based on a presentation given by the Candidate at TAUP 2019.	
For manuscripts intended for publication please indicate target journal:	
Candidate's Signature:	William S Marks
Date:	19/01/21
Primary Supervisor's Signature:	Fu-Guang Cao
Date:	19/01/2021

(This form should appear at the end of each thesis chapter/section/appendix submitted as a manuscript/ publication or collected as an appendix at the end of the thesis)

GRS Version 4– January 2019

DRC 16

MASSEY UNIVERSITY
GRADUATE RESEARCH SCHOOL

STATEMENT OF CONTRIBUTION
DOCTORATE WITH PUBLICATIONS/MANUSCRIPTS

We, the candidate and the candidate's Primary Supervisor, certify that all co-authors have consented to their work being included in the thesis and they have accepted the candidate's contribution as indicated below in the *Statement of Originality*.

Name of candidate:	William S. Marks
Name/title of Primary Supervisor:	Dr. Fu-Guang Cao
Name of Research Output and full reference:	
W. S. Marks and F. G. Cao, Meaningful details: The value of adding baseline dependent to the neutrino-dark energy effect, International Journal of Theoretical Physics, 59(12): 3951–3966, 2020.	
In which Chapter is the Manuscript /Published work:	Chapters 2 and #5.2
Please indicate:	
• The percentage of the manuscript/Published Work that was contributed by the candidate:	90%
and	
• Describe the contribution that the candidate has made to the Manuscript/Published Work:	
The Candidate performed the research described in the publication. The candidate also wrote the publication in its entirety and handled the submission process. The Co-Author provided direction and feedback.	
For manuscripts intended for publication please indicate target journal:	
Candidate's Signature:	William S. Marks
Date:	19/01/21
Primary Supervisor's Signature:	Fu-Guang Cao
Date:	19/01/2021

(This form should appear at the end of each thesis chapter/section/appendix submitted as a manuscript/ publication or collected as an appendix at the end of the thesis)

Chapter 6

Conclusion

The preceding work computationally explored matters related to neutrino oscillations. These explorations included an investigation into θ_{13} extraction methods, an investigation into how the matter effect depends on the distribution of matter along the neutrino flight-path and an investigation into the inclusion of coherent effects for a very long baseline and high-energy but low potential matter effect (with the addition of investigating non-standard interactions).

6.1 θ_{13} Extraction Conclusion

The investigation into θ_{13} extraction methods was motivated by a desire, initially, to try and replicate the Daya Bay result from published data due to the discovery of a claim that it could not be. This claim from [121] was based on the fact that the values of the pull-factors were not reported by Daya Bay. It was argued that the pull-factors being unreported rendered the results un-replicable and that this was significant as spurious values could potentially influence the final result. It was also argued that the number of pull-factors was unnecessary. The research described in Chapter 4 sought to address these claims.

The claims made by [121] were based on the main publication [120]. This publication

alone did not contain all of the relevant information, it was merely the publication of results. Most of the information needed for replication was contained in the references. With the total information provided, it was possible to replicate the result, including the statistical uncertainty but not the systemic uncertainty.

The random input fit was developed during the replication process, as a summary of the exact process for the fit was never given. The random input fit was also tested on the RENO results as those are of the same experiment type as Daya Bay and used a nearly identical data analysis method. This fitting was used to test the significance of the pull-factors as it was more efficient than the standard grid-scanning fit, with the reduction in parameters dramatically decreasing the time taken for fits. These fits demonstrated that the pull-factors did not exert an undue influence on the final result. The random input fit was also more precise than the grid scanning fit, which can be explained by the fact that with the grid scan there is a contribution to the statistical uncertainty from the grid spacing. As the random fit is free-floating, it has no such issue.

The main downside to the random input fit is the amount of optimization that needs to be performed in order for the improvements to be actualized. If similar work was to be conducted in the future, this strongly suggests the development of an evolutionary algorithm to perform this process. The further development of this approach has the potential to noticeably improve precision and dramatically increase the efficiency of computational resource usage. Therefore, it should be pursued.

6.2 Mixing Modulation Conclusions

The investigation into how the matter effect depends on the distribution of matter along the flight-path started as a project to determine if neutrino oscillations can be used to detect exoplanets. This was conducted in spite of the near impossibility of isolating a detectable signal. The calculations were performed naively by dividing the baseline into

sections and performing survival probability calculations along each section. It was found that this approach doesn't work as this approach cannot replicate the vacuum result. Attempts to integrate along the baseline merely resulted in an averaging of the potential.

It was concluded from all of this that the current formalism for describing neutrino oscillations cannot accommodate a non-uniform matter distribution as it only describes the neutrinos at the start and end of flight. That is not to say that such effects cannot exist, but that they cannot be described with the standard formulas. The physical interpretation was that the MSW effect is determined by the number of opportunities for forward-coherent scattering, not when they occur. This result was included because, even though it is probably not original, previous references to it have not been found.

The investigation into mixing modulation by dark matter was conducted because this research was originally meant to search for connections between neutrinos and dark matter. The primary focus of that search was to try and find novel phenomenological consequences of neutrino dark matter interactions. However, it quickly turned out that this was a well explored field, without many practical possibilities that had yet to be explored.

The avenue that was explored was the possibility of a dark matter effect. In particular, it focused on coherent effects as those had yet to be included and the inclusion thereof was computationally straightforward. This was also motivated by the cutoff for an observable decoherent effect being rather high, to the point where a potential that high existing being quite unlikely. Additionally, it was noted that decoherent effects are strictly non-existent if the neutrino mass is scotogenic in nature, so that only a coherent effect could exist if any.

It was found that including coherent effects did improve the cutoff, with the lowering of the cut-off being proportional to baseline. Additionally, it was found that the cutoff for mass-eigenstate interactions with even remotely feasible dark matter particle mass was above the limit from cosmological observations, which rules out a MSW-like effect for scotogenic neutrinos.

6.3 Final Conclusions

For the θ_{13} extraction, it was that a Monte Carlo approach to performing minimisations could be more efficient and possibly improve the final result. For the matter effect, it was found that the standard formalism is blind to differences in matter distribution so long as the total amount of matter is the same, which wouldn't have been noticed if it wasn't for the use of coherent calculations. This implies that there is value in simply running calculations and that the act of attempting to make those calculations work can yield insight into processes. Also, the possibility of a MSW-like effect was excluded for scotogenic neutrinos.

In terms of possible extensions of this work, there are a few. The success of the random fits in θ_{13} extraction recommends the use of evolutionary algorithms in performing future fits. In terms of neutrino-dark matter interactions, the resonant absorption calculations seem promising. There is also the issue of actually confirming that the matter effect is independent of the matter distribution. It was considered but not determined one way or the other that there may be a more sophisticated way to handle neutrino propogation which can accomodate matter inhomogeneities. Additionally, it was considered that there may be an effect if the size of the inhomogeneities is comparable to the oscillation wavelength. This calls for more work.

Ultimately, the purpose of this work was, like all scientific work, to ask questions and then try to answer them. The first question was on whether the Daya Bay result from 2013 could be replicated from publications. This was answered in the affirmative. In the process, the RENO results were also replicated, the significance of certain parameters was ascertained and an improved method for χ^2 with pulls function evaluation was developed.

The second question was whether neutrinos can be used to detect exoplanets. This was answered, unsurprisingly, in the negative. In the process, it was determined that the standard method for calculating the MSW effect is incapable of accommodating matter

inhomogeneities. Whether more sophisticated methods can produce results is a matter of further study.

The third question, which received the most attention, was about the existence of a connection between neutrinos and dark matter. This turned into a question of whether there is an interaction between neutrinos and dark matter and whether it is detectable, with the main focus being on the latter. After an extensive review of the literature was conducted, it was determined that the possibility of a dark MSW effect was under-explored, with only one published work on the topic that only considered de-coherent effects. This work replicated the previous work on the subject and extended it to include coherent effects and scotogenic interactions, all with full consideration of the potential issues involved. Therefore, this work may be considered the most thorough exploration of the dark MSW effect to date.

Appendices

Appendix A

θ_{13} Extraction Programming

The following appendix contains the code used to perform the θ_{13} extraction calculations. Note that, in general, lines are ended by semi-colons (;). Many were split to fit the page.

A.1 Daya Bay Code

The following is all of the programming used to perform the θ_{13} extraction for the Daya Bay experiment.

A.1.1 Energy Spectrum.

```
function [nnu]=nuespec(E)
%This function gives the energy spectrum for emitted reactor
%anti-neutrinos.  The only independent variable is the energy.
%%
%This portion produces the emission energy spectrum, taken from
%Mueller et.al.
S235=exp(3.217-3.111*E+1.395*E.^2-3.690e-1*E.^3+4.445e-2*E.^4-2.053e-3*E.^5);
S238=exp(4.833e-1+1.927e-1*E-1.283e-1*E.^2-6.762e-3*E.^3+2.233e-3*E.^4-1.536e-4*E.^5);
S239=exp(6.413-7.432*E+3.535*E.^2-8.820e-1*E.^3+1.025e-1*E.^4-4.550e-3*E.^5);
S241=exp(3.251-3.204*E+1.428*E.^2-3.675e-1*E.^3+4.254e-2*E.^4-1.896e-3*E.^5);
```

```
%SE=0.65*S235+0.05*S238+0.25*S239+0.05*S241;
SE=0.538*S235+0.078*S238+0.328*S239+0.056*S241;
%%
%This portion produces the capture spectrum for inverse beta decay,
%taken from Vogel and Beacom.
delr=0.024;
sigma0=((((1.166*10^-11)^2)*(cos(0.2239))^2)/pi)*(1+delr);
f=1;
f2=3.706;
g=1.26;
alpha1=f^2+3*g^2;
beta1=-2*(f+f2)*g-2*f^2-8*g^2;
gamma1=-4*(f+f2)*g-2*f^2-10*g^2;
Mp=9.383*10^2;
Mn=9.396*10^2;
me=0.511;
M=(Mp+Mn)/2;
del=Mn-Mp;
Ee=E-del;
pe=(Ee.^2-me^2).^0.5;
sigmaIBD0=sigma0.*alpha1.*Ee.*pe;
sigmaIBD1=sigma0.*(alpha1+beta1.*del./M+gamma1.*Ee./M).*Ee.^2;
sigmaIBD=sigmaIBD0+sigmaIBD1;
%%
%This combines the two.
nnu=SE.*sigmaIBD;

function [NNu]=nuespece(E,dm2,L)
%This function produces the argument that includes baseline
%dependence.  The input variables are baseline, energy and, the
```

```
%mass-squared difference.
NNu=((sin(1.267*dm2.*L./E)).^2).*nuespec(E);
```

A.1.2 The Full Unreduced Function.

```
function [CHI]=DBChi(dm13,dm12,theta13,a,et1,et2,et3,et4,et5,et6,...
...al1,al2,al3,al4,al5,al6,ep1,ep2,ep3,ep4,ep5,ep6)
%This builds the chi-squared function for Daya Bay.  The free
%variables are the mass-differences squared, the mixing angle and,
%the pull terms.
%%
%This section inputs the various parameters.  omij is the fractional
%contribution to detector i from reactor j while Lij is the baseline.
%N0x is the expected number of anti-neutrinos detected at detector x
%assuming no oscillations while Mx is the number of anti-neutrinos
%actually detected at detector x.
om11=0.4069;
om12=0.3854;
om13=0.0654;
om14=0.0799;
om15=0.0291;
om16=0.0333;
om21=0.4089;
om22=0.3870;
om23=0.0643;
om24=0.0785;
om25=0.0286;
om26=0.0327;
om31=0.0330;
om32=0.0318;
om33=0.2676;
```

```
om34=0.2441;
om35=0.1882;
om36=0.2354;
om41=0.1208;
om42=0.1241;
om43=0.1894;
om44=0.1892;
om45=0.1851;
om46=0.1914;
om51=0.1201;
om52=0.1248;
om53=0.1895;
om54=0.1895;
om55=0.1847;
om56=0.1913;
om61=0.1209;
om62=0.1241;
om63=0.1892;
om64=0.1892;
om65=0.1851;
om66=0.1914;
L11=362;
L12=372;
L13=903;
L14=817;
L15=1354;
L16=1265;
L21=358;
L22=368;
L23=903;
```

```
L24=817;
L25=1354;
L26=1265;
L31=1332;
L32=1358;
L33=468;
L34=490;
L35=558;
L36=499;
L41=1920;
L42=1894;
L43=1533;
L44=1534;
L45=1551;
L46=1525;
L51=1918;
L52=1892;
L53=1535;
L54=1535;
L55=1555;
L56=1528;
L61=1925;
L62=1900;
L63=1539;
L64=1539;
L65=1556;
L66=1530;
N01=68613;
N02=69595;
N03=66402;
```

```
N04=9922.9;
N05=9940.2;
N06=9837.7;
M1=67722;
M2=68334;
M3=65367;
M4=9359;
M5=9241;
M6=9037;
sb1=157.03;
sb2=156.46;
sb3=124.53;
sb4=28.75;
sb5=28.74;
sb6=28.55;
sd1=0.002;
sd2=0.002;
sd3=0.002;
sd4=0.002;
sd5=0.002;
sd6=0.002;
sr1=0.008;
sr2=0.008;
sr3=0.008;
sr4=0.008;
sr5=0.008;
sr6=0.008;
B1=1399;
B2=1380;
B3=1106;
```

```
B4=429;
B5=428;
B6=415;
%%
%This section builds the energy dependence.  The lower limit was
%determined to be approximately the lowest value at which a real
%valued result would be produced for all of the numbers while the
%upper limit is beyond the point at which the energy spectrum
%becomes zero (to the precision of MATLAB).
Nnu=integral(@nuespec,1.810997,25,'AbsTol',1e-12,'RelTol',1e-8);
NNu111=integral(@(E)nuespece(E,dm13,L11),1.810997,25);
NNu211=integral(@(E)nuespece(E,dm13,L21),1.810997,25);
NNu311=integral(@(E)nuespece(E,dm13,L31),1.810997,25);
NNu411=integral(@(E)nuespece(E,dm13,L41),1.810997,25);
NNu511=integral(@(E)nuespece(E,dm13,L51),1.810997,25);
NNu611=integral(@(E)nuespece(E,dm13,L61),1.810997,25);
NNu121=integral(@(E)nuespece(E,dm13,L12),1.810997,25);
NNu221=integral(@(E)nuespece(E,dm13,L22),1.810997,25);
NNu321=integral(@(E)nuespece(E,dm13,L32),1.810997,25);
NNu421=integral(@(E)nuespece(E,dm13,L42),1.810997,25);
NNu521=integral(@(E)nuespece(E,dm13,L52),1.810997,25);
NNu621=integral(@(E)nuespece(E,dm13,L62),1.810997,25);
NNu131=integral(@(E)nuespece(E,dm13,L13),1.810997,25);
NNu231=integral(@(E)nuespece(E,dm13,L23),1.810997,25);
NNu331=integral(@(E)nuespece(E,dm13,L33),1.810997,25);
NNu431=integral(@(E)nuespece(E,dm13,L43),1.810997,25);
NNu531=integral(@(E)nuespece(E,dm13,L53),1.810997,25);
NNu631=integral(@(E)nuespece(E,dm13,L63),1.810997,25);
NNu141=integral(@(E)nuespece(E,dm13,L14),1.810997,25);
NNu241=integral(@(E)nuespece(E,dm13,L24),1.810997,25);
```

```
NNu341=integral(@(E)nuespece(E,dm13,L34),1.810997,25);
NNu441=integral(@(E)nuespece(E,dm13,L44),1.810997,25);
NNu541=integral(@(E)nuespece(E,dm13,L54),1.810997,25);
NNu641=integral(@(E)nuespece(E,dm13,L64),1.810997,25);
NNu151=integral(@(E)nuespece(E,dm13,L15),1.810997,25);
NNu251=integral(@(E)nuespece(E,dm13,L25),1.810997,25);
NNu351=integral(@(E)nuespece(E,dm13,L35),1.810997,25);
NNu451=integral(@(E)nuespece(E,dm13,L45),1.810997,25);
NNu551=integral(@(E)nuespece(E,dm13,L55),1.810997,25);
NNu651=integral(@(E)nuespece(E,dm13,L65),1.810997,25);
NNu161=integral(@(E)nuespece(E,dm13,L16),1.810997,25);
NNu261=integral(@(E)nuespece(E,dm13,L26),1.810997,25);
NNu361=integral(@(E)nuespece(E,dm13,L36),1.810997,25);
NNu461=integral(@(E)nuespece(E,dm13,L46),1.810997,25);
NNu561=integral(@(E)nuespece(E,dm13,L56),1.810997,25);
NNu661=integral(@(E)nuespece(E,dm13,L66),1.810997,25);
NNu112=integral(@(E)nuespece(E,dm12,L11),1.810997,25);
NNu212=integral(@(E)nuespece(E,dm12,L21),1.810997,25);
NNu312=integral(@(E)nuespece(E,dm12,L31),1.810997,25);
NNu412=integral(@(E)nuespece(E,dm12,L41),1.810997,25);
NNu512=integral(@(E)nuespece(E,dm12,L51),1.810997,25);
NNu612=integral(@(E)nuespece(E,dm12,L61),1.810997,25);
NNu122=integral(@(E)nuespece(E,dm12,L12),1.810997,25);
NNu222=integral(@(E)nuespece(E,dm12,L22),1.810997,25);
NNu322=integral(@(E)nuespece(E,dm12,L32),1.810997,25);
NNu422=integral(@(E)nuespece(E,dm12,L42),1.810997,25);
NNu522=integral(@(E)nuespece(E,dm12,L52),1.810997,25);
NNu622=integral(@(E)nuespece(E,dm12,L62),1.810997,25);
NNu132=integral(@(E)nuespece(E,dm12,L13),1.810997,25);
NNu232=integral(@(E)nuespece(E,dm12,L23),1.810997,25);
```

```
NNu332=integral(@(E)nuespece(E,dm12,L33),1.810997,25);
NNu432=integral(@(E)nuespece(E,dm12,L43),1.810997,25);
NNu532=integral(@(E)nuespece(E,dm12,L53),1.810997,25);
NNu632=integral(@(E)nuespece(E,dm12,L63),1.810997,25);
NNu142=integral(@(E)nuespece(E,dm12,L14),1.810997,25);
NNu242=integral(@(E)nuespece(E,dm12,L24),1.810997,25);
NNu342=integral(@(E)nuespece(E,dm12,L34),1.810997,25);
NNu442=integral(@(E)nuespece(E,dm12,L44),1.810997,25);
NNu542=integral(@(E)nuespece(E,dm12,L54),1.810997,25);
NNu642=integral(@(E)nuespece(E,dm12,L64),1.810997,25);
NNu152=integral(@(E)nuespece(E,dm12,L15),1.810997,25);
NNu252=integral(@(E)nuespece(E,dm12,L25),1.810997,25);
NNu352=integral(@(E)nuespece(E,dm12,L35),1.810997,25);
NNu452=integral(@(E)nuespece(E,dm12,L45),1.810997,25);
NNu552=integral(@(E)nuespece(E,dm12,L55),1.810997,25);
NNu652=integral(@(E)nuespece(E,dm12,L65),1.810997,25);
NNu162=integral(@(E)nuespece(E,dm12,L16),1.810997,25);
NNu262=integral(@(E)nuespece(E,dm12,L26),1.810997,25);
NNu362=integral(@(E)nuespece(E,dm12,L36),1.810997,25);
NNu462=integral(@(E)nuespece(E,dm12,L46),1.810997,25);
NNu562=integral(@(E)nuespece(E,dm12,L56),1.810997,25);
NNu662=integral(@(E)nuespece(E,dm12,L66),1.810997,25);
%%
%This section constructs the probability weighting.
Pdr11=1-(sin(2*theta13)^2)*NNu111/Nnu-(cos(theta13))^4*0.861*NNu112/Nnu;
Pdr21=1-(sin(2*theta13)^2)*NNu211/Nnu-(cos(theta13))^4*0.861*NNu212/Nnu;
Pdr31=1-(sin(2*theta13)^2)*NNu311/Nnu-(cos(theta13))^4*0.861*NNu312/Nnu;
Pdr41=1-(sin(2*theta13)^2)*NNu411/Nnu-(cos(theta13))^4*0.861*NNu412/Nnu;
Pdr51=1-(sin(2*theta13)^2)*NNu511/Nnu-(cos(theta13))^4*0.861*NNu512/Nnu;
Pdr61=1-(sin(2*theta13)^2)*NNu611/Nnu-(cos(theta13))^4*0.861*NNu612/Nnu;
```

```
Pdr12=1-(sin(2*theta13)^2)*NNu121/Nnu-(cos(theta13))^4*0.861*NNu122/Nnu;
Pdr22=1-(sin(2*theta13)^2)*NNu221/Nnu-(cos(theta13))^4*0.861*NNu222/Nnu;
Pdr32=1-(sin(2*theta13)^2)*NNu321/Nnu-(cos(theta13))^4*0.861*NNu322/Nnu;
Pdr42=1-(sin(2*theta13)^2)*NNu421/Nnu-(cos(theta13))^4*0.861*NNu422/Nnu;
Pdr52=1-(sin(2*theta13)^2)*NNu521/Nnu-(cos(theta13))^4*0.861*NNu522/Nnu;
Pdr62=1-(sin(2*theta13)^2)*NNu621/Nnu-(cos(theta13))^4*0.861*NNu622/Nnu;
Pdr13=1-(sin(2*theta13)^2)*NNu131/Nnu-(cos(theta13))^4*0.861*NNu132/Nnu;
Pdr23=1-(sin(2*theta13)^2)*NNu231/Nnu-(cos(theta13))^4*0.861*NNu232/Nnu;
Pdr33=1-(sin(2*theta13)^2)*NNu331/Nnu-(cos(theta13))^4*0.861*NNu332/Nnu;
Pdr43=1-(sin(2*theta13)^2)*NNu431/Nnu-(cos(theta13))^4*0.861*NNu432/Nnu;
Pdr53=1-(sin(2*theta13)^2)*NNu531/Nnu-(cos(theta13))^4*0.861*NNu532/Nnu;
Pdr63=1-(sin(2*theta13)^2)*NNu631/Nnu-(cos(theta13))^4*0.861*NNu632/Nnu;
Pdr14=1-(sin(2*theta13)^2)*NNu141/Nnu-(cos(theta13))^4*0.861*NNu142/Nnu;
Pdr24=1-(sin(2*theta13)^2)*NNu241/Nnu-(cos(theta13))^4*0.861*NNu242/Nnu;
Pdr34=1-(sin(2*theta13)^2)*NNu341/Nnu-(cos(theta13))^4*0.861*NNu342/Nnu;
Pdr44=1-(sin(2*theta13)^2)*NNu441/Nnu-(cos(theta13))^4*0.861*NNu442/Nnu;
Pdr54=1-(sin(2*theta13)^2)*NNu541/Nnu-(cos(theta13))^4*0.861*NNu542/Nnu;
Pdr64=1-(sin(2*theta13)^2)*NNu641/Nnu-(cos(theta13))^4*0.861*NNu642/Nnu;
Pdr15=1-(sin(2*theta13)^2)*NNu151/Nnu-(cos(theta13))^4*0.861*NNu152/Nnu;
Pdr25=1-(sin(2*theta13)^2)*NNu251/Nnu-(cos(theta13))^4*0.861*NNu252/Nnu;
Pdr35=1-(sin(2*theta13)^2)*NNu351/Nnu-(cos(theta13))^4*0.861*NNu352/Nnu;
Pdr45=1-(sin(2*theta13)^2)*NNu451/Nnu-(cos(theta13))^4*0.861*NNu452/Nnu;
Pdr55=1-(sin(2*theta13)^2)*NNu551/Nnu-(cos(theta13))^4*0.861*NNu552/Nnu;
Pdr65=1-(sin(2*theta13)^2)*NNu651/Nnu-(cos(theta13))^4*0.861*NNu652/Nnu;
Pdr16=1-(sin(2*theta13)^2)*NNu161/Nnu-(cos(theta13))^4*0.861*NNu162/Nnu;
Pdr26=1-(sin(2*theta13)^2)*NNu261/Nnu-(cos(theta13))^4*0.861*NNu262/Nnu;
Pdr36=1-(sin(2*theta13)^2)*NNu361/Nnu-(cos(theta13))^4*0.861*NNu362/Nnu;
Pdr46=1-(sin(2*theta13)^2)*NNu461/Nnu-(cos(theta13))^4*0.861*NNu462/Nnu;
Pdr56=1-(sin(2*theta13)^2)*NNu561/Nnu-(cos(theta13))^4*0.861*NNu562/Nnu;
Pdr66=1-(sin(2*theta13)^2)*NNu661/Nnu-(cos(theta13))^4*0.861*NNu662/Nnu;
```

```
%%
%This section constructs the theoretical prediction for each
%detector.  Daya Bay combines all of the reactor contributions into
%a single term for each detector, making reactor dependence implicit.
TF11=Pdr11*om11;
TF21=Pdr21*om21;
TF31=Pdr31*om31;
TF41=Pdr41*om41;
TF51=Pdr51*om51;
TF61=Pdr61*om61;
TF12=Pdr12*om12;
TF22=Pdr22*om22;
TF32=Pdr32*om32;
TF42=Pdr42*om42;
TF52=Pdr52*om52;
TF62=Pdr62*om62;
TF13=Pdr13*om13;
TF23=Pdr23*om23;
TF33=Pdr33*om33;
TF43=Pdr43*om43;
TF53=Pdr53*om53;
TF63=Pdr63*om63;
TF14=Pdr14*om14;
TF24=Pdr24*om24;
TF34=Pdr34*om34;
TF44=Pdr44*om44;
TF54=Pdr54*om54;
TF64=Pdr64*om64;
TF15=Pdr15*om15;
TF25=Pdr25*om25;
```

```
TF35=Pdr35*om35;
TF45=Pdr45*om45;
TF55=Pdr55*om55;
TF65=Pdr65*om65;
TF16=Pdr16*om16;
TF26=Pdr26*om26;
TF36=Pdr36*om36;
TF46=Pdr46*om46;
TF56=Pdr56*om56;
TF66=Pdr66*om66;
TF1=TF11+TF12+TF13+TF14+TF15+TF16;
TF2=TF21+TF22+TF23+TF24+TF25+TF26;
TF3=TF31+TF32+TF33+TF34+TF35+TF36;
TF4=TF41+TF42+TF43+TF44+TF45+TF46;
TF5=TF51+TF52+TF53+TF54+TF55+TF56;
TF6=TF61+TF62+TF63+TF64+TF65+TF66;
Td1=N01*TF1;
Td2=N02*TF2;
Td3=N03*TF3;
Td4=N04*TF4;
Td5=N05*TF5;
Td6=N06*TF6;
%%
%This section constructs the actual chi function, using the
%parameters defined above.
Al1=om11*al1+om12*al2+om13*al3+om14*al4+om15*al5+om16*al6;
Al2=om21*al1+om22*al2+om23*al3+om24*al4+om25*al5+om26*al6;
Al3=om31*al1+om32*al2+om33*al3+om34*al4+om35*al5+om36*al6;
Al4=om41*al1+om42*al2+om43*al3+om44*al4+om45*al5+om46*al6;
Al5=om51*al1+om52*al2+om53*al3+om54*al4+om55*al5+om56*al6;
```

```
Al6=om61*al1+om62*al2+om63*al3+om64*al4+om65*al5+om66*al6;
Chim1=((M1+ep1-Td1*(1+a+Al1+et1))^2)/(M1+B1);
Chim2=((M2+ep2-Td2*(1+a+Al2+et2))^2)/(M2+B2);
Chim3=((M3+ep3-Td3*(1+a+Al3+et3))^2)/(M3+B3);
Chim4=((M4+ep4-Td4*(1+a+Al4+et4))^2)/(M4+B4);
Chim5=((M5+ep5-Td5*(1+a+Al5+et5))^2)/(M5+B5);
Chim6=((M6+ep6-Td6*(1+a+Al6+et6))^2)/(M6+B6);
Chim=Chim1+Chim2+Chim3+Chim4+Chim5+Chim6;
Chial=(al1/sr1)^2+(al2/sr2)^2+(al3/sr3)^2+(al4/sr4)^2+(al5/sr5)^2+(al6/sr6)^2;
Chiet=(et1/sd1)^2+(et2/sd2)^2+(et3/sd3)^2+(et4/sd4)^2+(et5/sd5)^2+(et6/sd6)^2;
Chiep=(ep1/sb1)^2+(ep2/sb2)^2+(ep3/sb3)^2+(ep4/sb4)^2+(ep5/sb5)^2+(ep6/sb6)^2;
CHI=Chim+Chial+Chiet+Chiep;

function [Chi]=DBChib(terms,dm13,dm12)
%This function formats the Daya Bay function to make it usable by the
%command "fminsearch".
Chi=DBChi(dm13,dm12,terms(1,1),terms(2,1),terms(3,1),terms(4,1),...
...terms(5,1),terms(6,1),terms(7,1),terms(8,1),terms(9,1),terms(10,1),...
...terms(11,1),terms(12,1),terms(13,1),terms(14,1),terms(15,1),terms(16,1),...
...terms(17,1),terms(18,1),terms(19,1),terms(20,1));

function [Smean,Sstd,Sste,Xmean,Xstd,Chimean,Chistd]=...
...dbchigood(dm13,dm12,N,q,acc)
%This function performs the minimization of the Daya Bay function
%given the mass-squared differences (dm13 and dm12); the number of
%minimizations to be collected (N); the scale factor of the random
%inputs (q) and, the accuracy level required for a minimization to
%be included in the average (acc).
bannana=@(terms)DBChib(terms,dm13,dm12);
option=optimset('MaxIter',100000,'MaxFunEvals',10000);
```

```
Xtot=zeros(20,N);
CHIi=zeros(1,N);
S231=zeros(1,N);
s=0;
while s < N
    rng('shuffle');
    ter=q*rand(20,1);
    [X,Chi]=fminsearch(bannana,ter,option);
    if Chi <= acc
        if X(1,1) >= 0
        s=s+1;
        Xtot(:,s)=X;
        CHIi(1,s)=Chi;
        S231(1,s)=sin(2*X(1,1))^2;
        end
    end
end
Xmean=mean(Xtot,2);
Xstd=std(Xtot,0,2);
Smean=mean(S231,2);
Sstd=std(S231,0,2);
Chimean=mean(CHIi,2);
Chistd=std(CHIi,0,2);
Sste=Sstd/(sqrt(N));
```

A.1.3 First Reduced Function Coding

```
function [CHI]=DBChid1(dm13,dm12,theta13,a,et,...
...al1,al2,al3,al4,al5,al6,ep1,ep2,ep3,ep4,ep5,ep6)
%This function is the first reduced form of DBChi.
om11=0.4069;
```

```
om12=0.3854;
om13=0.0654;
om14=0.0799;
om15=0.0291;
om16=0.0333;
om21=0.4089;
om22=0.3870;
om23=0.0643;
om24=0.0785;
om25=0.0286;
om26=0.0327;
om31=0.0330;
om32=0.0318;
om33=0.2676;
om34=0.2441;
om35=0.1882;
om36=0.2354;
om41=0.1208;
om42=0.1241;
om43=0.1894;
om44=0.1892;
om45=0.1851;
om46=0.1914;
om51=0.1201;
om52=0.1248;
om53=0.1895;
om54=0.1895;
om55=0.1847;
om56=0.1913;
om61=0.1209;
```

```
om62=0.1241;
om63=0.1892;
om64=0.1892;
om65=0.1851;
om66=0.1914;
L11=362;
L12=372;
L13=903;
L14=817;
L15=1354;
L16=1265;
L21=358;
L22=368;
L23=903;
L24=817;
L25=1354;
L26=1265;
L31=1332;
L32=1358;
L33=468;
L34=490;
L35=558;
L36=499;
L41=1920;
L42=1894;
L43=1533;
L44=1534;
L45=1551;
L46=1525;
L51=1918;
```

```
L52=1892;
L53=1535;
L54=1535;
L55=1555;
L56=1528;
L61=1925;
L62=1900;
L63=1539;
L64=1539;
L65=1556;
L66=1530;
N01=68613;
N02=69595;
N03=66402;
N04=9922.9;
N05=9940.2;
N06=9837.7;
M1=67722;
M2=68334;
M3=65367;
M4=9359;
M5=9241;
M6=9037;
sb1=157.03;
sb2=156.46;
sb3=124.53;
sb4=28.75;
sb5=28.74;
sb6=28.55;
sd=0.002;
```

```
sr1=0.008;
sr2=0.008;
sr3=0.008;
sr4=0.008;
sr5=0.008;
sr6=0.008;
B1=1399;
B2=1380;
B3=1106;
B4=429;
B5=428;
B6=415;
Nnu=integral(@nuespec,1.810997,25,'AbsTol',1e-12,'RelTol',1e-8);
NNu111=integral(@(E)nuespece(E,dm13,L11),1.810997,25);
NNu211=integral(@(E)nuespece(E,dm13,L21),1.810997,25);
NNu311=integral(@(E)nuespece(E,dm13,L31),1.810997,25);
NNu411=integral(@(E)nuespece(E,dm13,L41),1.810997,25);
NNu511=integral(@(E)nuespece(E,dm13,L51),1.810997,25);
NNu611=integral(@(E)nuespece(E,dm13,L61),1.810997,25);
NNu121=integral(@(E)nuespece(E,dm13,L12),1.810997,25);
NNu221=integral(@(E)nuespece(E,dm13,L22),1.810997,25);
NNu321=integral(@(E)nuespece(E,dm13,L32),1.810997,25);
NNu421=integral(@(E)nuespece(E,dm13,L42),1.810997,25);
NNu521=integral(@(E)nuespece(E,dm13,L52),1.810997,25);
NNu621=integral(@(E)nuespece(E,dm13,L62),1.810997,25);
NNu131=integral(@(E)nuespece(E,dm13,L13),1.810997,25);
NNu231=integral(@(E)nuespece(E,dm13,L23),1.810997,25);
NNu331=integral(@(E)nuespece(E,dm13,L33),1.810997,25);
NNu431=integral(@(E)nuespece(E,dm13,L43),1.810997,25);
NNu531=integral(@(E)nuespece(E,dm13,L53),1.810997,25);
```

```
NNu631=integral(@(E)nuespece(E,dm13,L63),1.810997,25);
NNu141=integral(@(E)nuespece(E,dm13,L14),1.810997,25);
NNu241=integral(@(E)nuespece(E,dm13,L24),1.810997,25);
NNu341=integral(@(E)nuespece(E,dm13,L34),1.810997,25);
NNu441=integral(@(E)nuespece(E,dm13,L44),1.810997,25);
NNu541=integral(@(E)nuespece(E,dm13,L54),1.810997,25);
NNu641=integral(@(E)nuespece(E,dm13,L64),1.810997,25);
NNu151=integral(@(E)nuespece(E,dm13,L15),1.810997,25);
NNu251=integral(@(E)nuespece(E,dm13,L25),1.810997,25);
NNu351=integral(@(E)nuespece(E,dm13,L35),1.810997,25);
NNu451=integral(@(E)nuespece(E,dm13,L45),1.810997,25);
NNu551=integral(@(E)nuespece(E,dm13,L55),1.810997,25);
NNu651=integral(@(E)nuespece(E,dm13,L65),1.810997,25);
NNu161=integral(@(E)nuespece(E,dm13,L16),1.810997,25);
NNu261=integral(@(E)nuespece(E,dm13,L26),1.810997,25);
NNu361=integral(@(E)nuespece(E,dm13,L36),1.810997,25);
NNu461=integral(@(E)nuespece(E,dm13,L46),1.810997,25);
NNu561=integral(@(E)nuespece(E,dm13,L56),1.810997,25);
NNu661=integral(@(E)nuespece(E,dm13,L66),1.810997,25);
NNu112=integral(@(E)nuespece(E,dm12,L11),1.810997,25);
NNu212=integral(@(E)nuespece(E,dm12,L21),1.810997,25);
NNu312=integral(@(E)nuespece(E,dm12,L31),1.810997,25);
NNu412=integral(@(E)nuespece(E,dm12,L41),1.810997,25);
NNu512=integral(@(E)nuespece(E,dm12,L51),1.810997,25);
NNu612=integral(@(E)nuespece(E,dm12,L61),1.810997,25);
NNu122=integral(@(E)nuespece(E,dm12,L12),1.810997,25);
NNu222=integral(@(E)nuespece(E,dm12,L22),1.810997,25);
NNu322=integral(@(E)nuespece(E,dm12,L32),1.810997,25);
NNu422=integral(@(E)nuespece(E,dm12,L42),1.810997,25);
NNu522=integral(@(E)nuespece(E,dm12,L52),1.810997,25);
```

```
NNu622=integral(@(E)nuespece(E,dm12,L62),1.810997,25);
NNu132=integral(@(E)nuespece(E,dm12,L13),1.810997,25);
NNu232=integral(@(E)nuespece(E,dm12,L23),1.810997,25);
NNu332=integral(@(E)nuespece(E,dm12,L33),1.810997,25);
NNu432=integral(@(E)nuespece(E,dm12,L43),1.810997,25);
NNu532=integral(@(E)nuespece(E,dm12,L53),1.810997,25);
NNu632=integral(@(E)nuespece(E,dm12,L63),1.810997,25);
NNu142=integral(@(E)nuespece(E,dm12,L14),1.810997,25);
NNu242=integral(@(E)nuespece(E,dm12,L24),1.810997,25);
NNu342=integral(@(E)nuespece(E,dm12,L34),1.810997,25);
NNu442=integral(@(E)nuespece(E,dm12,L44),1.810997,25);
NNu542=integral(@(E)nuespece(E,dm12,L54),1.810997,25);
NNu642=integral(@(E)nuespece(E,dm12,L64),1.810997,25);
NNu152=integral(@(E)nuespece(E,dm12,L15),1.810997,25);
NNu252=integral(@(E)nuespece(E,dm12,L25),1.810997,25);
NNu352=integral(@(E)nuespece(E,dm12,L35),1.810997,25);
NNu452=integral(@(E)nuespece(E,dm12,L45),1.810997,25);
NNu552=integral(@(E)nuespece(E,dm12,L55),1.810997,25);
NNu652=integral(@(E)nuespece(E,dm12,L65),1.810997,25);
NNu162=integral(@(E)nuespece(E,dm12,L16),1.810997,25);
NNu262=integral(@(E)nuespece(E,dm12,L26),1.810997,25);
NNu362=integral(@(E)nuespece(E,dm12,L36),1.810997,25);
NNu462=integral(@(E)nuespece(E,dm12,L46),1.810997,25);
NNu562=integral(@(E)nuespece(E,dm12,L56),1.810997,25);
NNu662=integral(@(E)nuespece(E,dm12,L66),1.810997,25);
Pdr11=1-(sin(2*theta13)^2)*NNu111/Nnu-(cos(theta13))^4*0.861*NNu112/Nnu;
Pdr21=1-(sin(2*theta13)^2)*NNu211/Nnu-(cos(theta13))^4*0.861*NNu212/Nnu;
Pdr31=1-(sin(2*theta13)^2)*NNu311/Nnu-(cos(theta13))^4*0.861*NNu312/Nnu;
Pdr41=1-(sin(2*theta13)^2)*NNu411/Nnu-(cos(theta13))^4*0.861*NNu412/Nnu;
Pdr51=1-(sin(2*theta13)^2)*NNu511/Nnu-(cos(theta13))^4*0.861*NNu512/Nnu;
```

```
Pdr61=1-(sin(2*theta13)^2)*NNu611/Nnu-(cos(theta13))^4*0.861*NNu612/Nnu;
Pdr12=1-(sin(2*theta13)^2)*NNu121/Nnu-(cos(theta13))^4*0.861*NNu122/Nnu;
Pdr22=1-(sin(2*theta13)^2)*NNu221/Nnu-(cos(theta13))^4*0.861*NNu222/Nnu;
Pdr32=1-(sin(2*theta13)^2)*NNu321/Nnu-(cos(theta13))^4*0.861*NNu322/Nnu;
Pdr42=1-(sin(2*theta13)^2)*NNu421/Nnu-(cos(theta13))^4*0.861*NNu422/Nnu;
Pdr52=1-(sin(2*theta13)^2)*NNu521/Nnu-(cos(theta13))^4*0.861*NNu522/Nnu;
Pdr62=1-(sin(2*theta13)^2)*NNu621/Nnu-(cos(theta13))^4*0.861*NNu622/Nnu;
Pdr13=1-(sin(2*theta13)^2)*NNu131/Nnu-(cos(theta13))^4*0.861*NNu132/Nnu;
Pdr23=1-(sin(2*theta13)^2)*NNu231/Nnu-(cos(theta13))^4*0.861*NNu232/Nnu;
Pdr33=1-(sin(2*theta13)^2)*NNu331/Nnu-(cos(theta13))^4*0.861*NNu332/Nnu;
Pdr43=1-(sin(2*theta13)^2)*NNu431/Nnu-(cos(theta13))^4*0.861*NNu432/Nnu;
Pdr53=1-(sin(2*theta13)^2)*NNu531/Nnu-(cos(theta13))^4*0.861*NNu532/Nnu;
Pdr63=1-(sin(2*theta13)^2)*NNu631/Nnu-(cos(theta13))^4*0.861*NNu632/Nnu;
Pdr14=1-(sin(2*theta13)^2)*NNu141/Nnu-(cos(theta13))^4*0.861*NNu142/Nnu;
Pdr24=1-(sin(2*theta13)^2)*NNu241/Nnu-(cos(theta13))^4*0.861*NNu242/Nnu;
Pdr34=1-(sin(2*theta13)^2)*NNu341/Nnu-(cos(theta13))^4*0.861*NNu342/Nnu;
Pdr44=1-(sin(2*theta13)^2)*NNu441/Nnu-(cos(theta13))^4*0.861*NNu442/Nnu;
Pdr54=1-(sin(2*theta13)^2)*NNu541/Nnu-(cos(theta13))^4*0.861*NNu542/Nnu;
Pdr64=1-(sin(2*theta13)^2)*NNu641/Nnu-(cos(theta13))^4*0.861*NNu642/Nnu;
Pdr15=1-(sin(2*theta13)^2)*NNu151/Nnu-(cos(theta13))^4*0.861*NNu152/Nnu;
Pdr25=1-(sin(2*theta13)^2)*NNu251/Nnu-(cos(theta13))^4*0.861*NNu252/Nnu;
Pdr35=1-(sin(2*theta13)^2)*NNu351/Nnu-(cos(theta13))^4*0.861*NNu352/Nnu;
Pdr45=1-(sin(2*theta13)^2)*NNu451/Nnu-(cos(theta13))^4*0.861*NNu452/Nnu;
Pdr55=1-(sin(2*theta13)^2)*NNu551/Nnu-(cos(theta13))^4*0.861*NNu552/Nnu;
Pdr65=1-(sin(2*theta13)^2)*NNu651/Nnu-(cos(theta13))^4*0.861*NNu652/Nnu;
Pdr16=1-(sin(2*theta13)^2)*NNu161/Nnu-(cos(theta13))^4*0.861*NNu162/Nnu;
Pdr26=1-(sin(2*theta13)^2)*NNu261/Nnu-(cos(theta13))^4*0.861*NNu262/Nnu;
Pdr36=1-(sin(2*theta13)^2)*NNu361/Nnu-(cos(theta13))^4*0.861*NNu362/Nnu;
Pdr46=1-(sin(2*theta13)^2)*NNu461/Nnu-(cos(theta13))^4*0.861*NNu462/Nnu;
Pdr56=1-(sin(2*theta13)^2)*NNu561/Nnu-(cos(theta13))^4*0.861*NNu562/Nnu;
```

```
Pdr66=1-(sin(2*theta13)^2)*NNu661/Nnu-(cos(theta13))^4*0.861*NNu662/Nnu;

TF11=Pdr11*om11;

TF21=Pdr21*om21;

TF31=Pdr31*om31;

TF41=Pdr41*om41;

TF51=Pdr51*om51;

TF61=Pdr61*om61;

TF12=Pdr12*om12;

TF22=Pdr22*om22;

TF32=Pdr32*om32;

TF42=Pdr42*om42;

TF52=Pdr52*om52;

TF62=Pdr62*om62;

TF13=Pdr13*om13;

TF23=Pdr23*om23;

TF33=Pdr33*om33;

TF43=Pdr43*om43;

TF53=Pdr53*om53;

TF63=Pdr63*om63;

TF14=Pdr14*om14;

TF24=Pdr24*om24;

TF34=Pdr34*om34;

TF44=Pdr44*om44;

TF54=Pdr54*om54;

TF64=Pdr64*om64;

TF15=Pdr15*om15;

TF25=Pdr25*om25;

TF35=Pdr35*om35;

TF45=Pdr45*om45;

TF55=Pdr55*om55;
```

```
TF65=Pdr65*om65;
TF16=Pdr16*om16;
TF26=Pdr26*om26;
TF36=Pdr36*om36;
TF46=Pdr46*om46;
TF56=Pdr56*om56;
TF66=Pdr66*om66;
TF1=TF11+TF12+TF13+TF14+TF15+TF16;
TF2=TF21+TF22+TF23+TF24+TF25+TF26;
TF3=TF31+TF32+TF33+TF34+TF35+TF36;
TF4=TF41+TF42+TF43+TF44+TF45+TF46;
TF5=TF51+TF52+TF53+TF54+TF55+TF56;
TF6=TF61+TF62+TF63+TF64+TF65+TF66;
Td1=N01*TF1;
Td2=N02*TF2;
Td3=N03*TF3;
Td4=N04*TF4;
Td5=N05*TF5;
Td6=N06*TF6;
Al1=om11*al1+om12*al2+om13*al3+om14*al4+om15*al5+om16*al6;
Al2=om21*al1+om22*al2+om23*al3+om24*al4+om25*al5+om26*al6;
Al3=om31*al1+om32*al2+om33*al3+om34*al4+om35*al5+om36*al6;
Al4=om41*al1+om42*al2+om43*al3+om44*al4+om45*al5+om46*al6;
Al5=om51*al1+om52*al2+om53*al3+om54*al4+om55*al5+om56*al6;
Al6=om61*al1+om62*al2+om63*al3+om64*al4+om65*al5+om66*al6;
Chim1=((M1+ep1-Td1*(1+a+Al1+et))^2)/(M1+B1);
Chim2=((M2+ep2-Td2*(1+a+Al2+et))^2)/(M2+B2);
Chim3=((M3+ep3-Td3*(1+a+Al3+et))^2)/(M3+B3);
Chim4=((M4+ep4-Td4*(1+a+Al4+et))^2)/(M4+B4);
Chim5=((M5+ep5-Td5*(1+a+Al5+et))^2)/(M5+B5);
```

```
Chim6=((M6+ep6-Td6*(1+a+Al6+et))^2)/(M6+B6);
Chim=Chim1+Chim2+Chim3+Chim4+Chim5+Chim6;
Chial=(al1/sr1)^2+(al2/sr2)^2+(al3/sr3)^2+(al4/sr4)^2+(al5/sr5)^2+(al6/sr6)^2;
Chiet=6*(et/sd)^2;
Chiep=(ep1/sb1)^2+(ep2/sb2)^2+(ep3/sb3)^2+(ep4/sb4)^2+(ep5/sb5)^2+(ep6/sb6)^2;
CHI=Chim+Chial+Chiet+Chiep;

function [Chi]=DBChibd1(terms,dm13,dm12)
%This function is the first reduced form of DBChib.
Chi=DBChid1(dm13,dm12,terms(1,1),terms(2,1),terms(3,1),terms(4,1),...
...terms(5,1),terms(6,1),terms(7,1),terms(8,1),terms(9,1),terms(10,1),...
...terms(11,1),terms(12,1),terms(13,1),terms(14,1),terms(15,1));

function [Smean,Sstd,Sste,Xmean,Xstd,Chimean,Chistd]=...
...dbchigoodd1(dm13,dm12,N,q,acc)
%This is the frist reduced form of dbchigood.
bannana=@(terms)DBChibd1(terms,dm13,dm12);
option=optimset('MaxIter',100000,'MaxFunEvals',10000);
Xtot=zeros(15,N);
CHIi=zeros(1,N);
S231=zeros(1,N);
s=0;
while s < N
    rng('shuffle');
    ter=q*rand(15,1);
    [X,Chi]=fminsearch(bannana,ter,option);
    if Chi <= acc
        if X(1,1) >= 0
        s=s+1;
        Xtot(:,s)=X;
```

```
        CHIi(1,s)=Chi;
        S231(1,s)=sin(2*X(1,1))^2;
        end
    end
end
Xmean=mean(Xtot,2);
Xstd=std(Xtot,0,2);
Smean=mean(S231,2);
Sstd=std(S231,0,2);
Chimean=mean(CHIi,2);
Chistd=std(CHIi,0,2);
Sste=Sstd/(sqrt(N));
```

A.1.4 Second Reduced Function Coding

```
function [CHI]=DBChid2(dm13,dm12,theta13,a,et,...
...al1,al2,al3,ep1,ep2,ep3,ep4,ep5,ep6)
%This function is the second reduced version of DBChi.
om11=0.4069;
om12=0.3854;
om13=0.0654;
om14=0.0799;
om15=0.0291;
om16=0.0333;
om21=0.4089;
om22=0.3870;
om23=0.0643;
om24=0.0785;
om25=0.0286;
om26=0.0327;
om31=0.0330;
```

```
om32=0.0318;
om33=0.2676;
om34=0.2441;
om35=0.1882;
om36=0.2354;
om41=0.1208;
om42=0.1241;
om43=0.1894;
om44=0.1892;
om45=0.1851;
om46=0.1914;
om51=0.1201;
om52=0.1248;
om53=0.1895;
om54=0.1895;
om55=0.1847;
om56=0.1913;
om61=0.1209;
om62=0.1241;
om63=0.1892;
om64=0.1892;
om65=0.1851;
om66=0.1914;
L11=362;
L12=372;
L13=903;
L14=817;
L15=1354;
L16=1265;
L21=358;
```

```
L22=368;
L23=903;
L24=817;
L25=1354;
L26=1265;
L31=1332;
L32=1358;
L33=468;
L34=490;
L35=558;
L36=499;
L41=1920;
L42=1894;
L43=1533;
L44=1534;
L45=1551;
L46=1525;
L51=1918;
L52=1892;
L53=1535;
L54=1535;
L55=1555;
L56=1528;
L61=1925;
L62=1900;
L63=1539;
L64=1539;
L65=1556;
L66=1530;
N01=68613;
```

```
N02=69595;
N03=66402;
N04=9922.9;
N05=9940.2;
N06=9837.7;
M1=67722;
M2=68334;
M3=65367;
M4=9359;
M5=9241;
M6=9037;
sb1=157.03;
sb2=156.46;
sb3=124.53;
sb4=28.75;
sb5=28.74;
sb6=28.55;
sd=0.002;
sr1=0.008;
sr2=0.008;
sr3=0.008;
B1=1399;
B2=1380;
B3=1106;
B4=429;
B5=428;
B6=415;
Nnu=integral(@nuespec,1.810997,25,'AbsTol',1e-12,'RelTol',1e-8);
NNu111=integral(@(E)nuespece(E,dm13,L11),1.810997,25);
NNu211=integral(@(E)nuespece(E,dm13,L21),1.810997,25);
```

```
NNu311=integral(@(E)nuespece(E,dm13,L31),1.810997,25);
NNu411=integral(@(E)nuespece(E,dm13,L41),1.810997,25);
NNu511=integral(@(E)nuespece(E,dm13,L51),1.810997,25);
NNu611=integral(@(E)nuespece(E,dm13,L61),1.810997,25);
NNu121=integral(@(E)nuespece(E,dm13,L12),1.810997,25);
NNu221=integral(@(E)nuespece(E,dm13,L22),1.810997,25);
NNu321=integral(@(E)nuespece(E,dm13,L32),1.810997,25);
NNu421=integral(@(E)nuespece(E,dm13,L42),1.810997,25);
NNu521=integral(@(E)nuespece(E,dm13,L52),1.810997,25);
NNu621=integral(@(E)nuespece(E,dm13,L62),1.810997,25);
NNu131=integral(@(E)nuespece(E,dm13,L13),1.810997,25);
NNu231=integral(@(E)nuespece(E,dm13,L23),1.810997,25);
NNu331=integral(@(E)nuespece(E,dm13,L33),1.810997,25);
NNu431=integral(@(E)nuespece(E,dm13,L43),1.810997,25);
NNu531=integral(@(E)nuespece(E,dm13,L53),1.810997,25);
NNu631=integral(@(E)nuespece(E,dm13,L63),1.810997,25);
NNu141=integral(@(E)nuespece(E,dm13,L14),1.810997,25);
NNu241=integral(@(E)nuespece(E,dm13,L24),1.810997,25);
NNu341=integral(@(E)nuespece(E,dm13,L34),1.810997,25);
NNu441=integral(@(E)nuespece(E,dm13,L44),1.810997,25);
NNu541=integral(@(E)nuespece(E,dm13,L54),1.810997,25);
NNu641=integral(@(E)nuespece(E,dm13,L64),1.810997,25);
NNu151=integral(@(E)nuespece(E,dm13,L15),1.810997,25);
NNu251=integral(@(E)nuespece(E,dm13,L25),1.810997,25);
NNu351=integral(@(E)nuespece(E,dm13,L35),1.810997,25);
NNu451=integral(@(E)nuespece(E,dm13,L45),1.810997,25);
NNu551=integral(@(E)nuespece(E,dm13,L55),1.810997,25);
NNu651=integral(@(E)nuespece(E,dm13,L65),1.810997,25);
NNu161=integral(@(E)nuespece(E,dm13,L16),1.810997,25);
NNu261=integral(@(E)nuespece(E,dm13,L26),1.810997,25);
```

```
NNu361=integral(@(E)nuespece(E,dm13,L36),1.810997,25);
NNu461=integral(@(E)nuespece(E,dm13,L46),1.810997,25);
NNu561=integral(@(E)nuespece(E,dm13,L56),1.810997,25);
NNu661=integral(@(E)nuespece(E,dm13,L66),1.810997,25);
NNu112=integral(@(E)nuespece(E,dm12,L11),1.810997,25);
NNu212=integral(@(E)nuespece(E,dm12,L21),1.810997,25);
NNu312=integral(@(E)nuespece(E,dm12,L31),1.810997,25);
NNu412=integral(@(E)nuespece(E,dm12,L41),1.810997,25);
NNu512=integral(@(E)nuespece(E,dm12,L51),1.810997,25);
NNu612=integral(@(E)nuespece(E,dm12,L61),1.810997,25);
NNu122=integral(@(E)nuespece(E,dm12,L12),1.810997,25);
NNu222=integral(@(E)nuespece(E,dm12,L22),1.810997,25);
NNu322=integral(@(E)nuespece(E,dm12,L32),1.810997,25);
NNu422=integral(@(E)nuespece(E,dm12,L42),1.810997,25);
NNu522=integral(@(E)nuespece(E,dm12,L52),1.810997,25);
NNu622=integral(@(E)nuespece(E,dm12,L62),1.810997,25);
NNu132=integral(@(E)nuespece(E,dm12,L13),1.810997,25);
NNu232=integral(@(E)nuespece(E,dm12,L23),1.810997,25);
NNu332=integral(@(E)nuespece(E,dm12,L33),1.810997,25);
NNu432=integral(@(E)nuespece(E,dm12,L43),1.810997,25);
NNu532=integral(@(E)nuespece(E,dm12,L53),1.810997,25);
NNu632=integral(@(E)nuespece(E,dm12,L63),1.810997,25);
NNu142=integral(@(E)nuespece(E,dm12,L14),1.810997,25);
NNu242=integral(@(E)nuespece(E,dm12,L24),1.810997,25);
NNu342=integral(@(E)nuespece(E,dm12,L34),1.810997,25);
NNu442=integral(@(E)nuespece(E,dm12,L44),1.810997,25);
NNu542=integral(@(E)nuespece(E,dm12,L54),1.810997,25);
NNu642=integral(@(E)nuespece(E,dm12,L64),1.810997,25);
NNu152=integral(@(E)nuespece(E,dm12,L15),1.810997,25);
NNu252=integral(@(E)nuespece(E,dm12,L25),1.810997,25);
```

```
NNu352=integral(@(E)nuespece(E,dm12,L35),1.810997,25);
NNu452=integral(@(E)nuespece(E,dm12,L45),1.810997,25);
NNu552=integral(@(E)nuespece(E,dm12,L55),1.810997,25);
NNu652=integral(@(E)nuespece(E,dm12,L65),1.810997,25);
NNu162=integral(@(E)nuespece(E,dm12,L16),1.810997,25);
NNu262=integral(@(E)nuespece(E,dm12,L26),1.810997,25);
NNu362=integral(@(E)nuespece(E,dm12,L36),1.810997,25);
NNu462=integral(@(E)nuespece(E,dm12,L46),1.810997,25);
NNu562=integral(@(E)nuespece(E,dm12,L56),1.810997,25);
NNu662=integral(@(E)nuespece(E,dm12,L66),1.810997,25);
Pdr11=1-(sin(2*theta13)^2)*NNu111/Nnu-(cos(theta13))^4*0.861*NNu112/Nnu;
Pdr21=1-(sin(2*theta13)^2)*NNu211/Nnu-(cos(theta13))^4*0.861*NNu212/Nnu;
Pdr31=1-(sin(2*theta13)^2)*NNu311/Nnu-(cos(theta13))^4*0.861*NNu312/Nnu;
Pdr41=1-(sin(2*theta13)^2)*NNu411/Nnu-(cos(theta13))^4*0.861*NNu412/Nnu;
Pdr51=1-(sin(2*theta13)^2)*NNu511/Nnu-(cos(theta13))^4*0.861*NNu512/Nnu;
Pdr61=1-(sin(2*theta13)^2)*NNu611/Nnu-(cos(theta13))^4*0.861*NNu612/Nnu;
Pdr12=1-(sin(2*theta13)^2)*NNu121/Nnu-(cos(theta13))^4*0.861*NNu122/Nnu;
Pdr22=1-(sin(2*theta13)^2)*NNu221/Nnu-(cos(theta13))^4*0.861*NNu222/Nnu;
Pdr32=1-(sin(2*theta13)^2)*NNu321/Nnu-(cos(theta13))^4*0.861*NNu322/Nnu;
Pdr42=1-(sin(2*theta13)^2)*NNu421/Nnu-(cos(theta13))^4*0.861*NNu422/Nnu;
Pdr52=1-(sin(2*theta13)^2)*NNu521/Nnu-(cos(theta13))^4*0.861*NNu522/Nnu;
Pdr62=1-(sin(2*theta13)^2)*NNu621/Nnu-(cos(theta13))^4*0.861*NNu622/Nnu;
Pdr13=1-(sin(2*theta13)^2)*NNu131/Nnu-(cos(theta13))^4*0.861*NNu132/Nnu;
Pdr23=1-(sin(2*theta13)^2)*NNu231/Nnu-(cos(theta13))^4*0.861*NNu232/Nnu;
Pdr33=1-(sin(2*theta13)^2)*NNu331/Nnu-(cos(theta13))^4*0.861*NNu332/Nnu;
Pdr43=1-(sin(2*theta13)^2)*NNu431/Nnu-(cos(theta13))^4*0.861*NNu432/Nnu;
Pdr53=1-(sin(2*theta13)^2)*NNu531/Nnu-(cos(theta13))^4*0.861*NNu532/Nnu;
Pdr63=1-(sin(2*theta13)^2)*NNu631/Nnu-(cos(theta13))^4*0.861*NNu632/Nnu;
Pdr14=1-(sin(2*theta13)^2)*NNu141/Nnu-(cos(theta13))^4*0.861*NNu142/Nnu;
Pdr24=1-(sin(2*theta13)^2)*NNu241/Nnu-(cos(theta13))^4*0.861*NNu242/Nnu;
```

```
Pdr34=1-(sin(2*theta13)^2)*NNu341/Nnu-(cos(theta13))^4*0.861*NNu342/Nnu;
Pdr44=1-(sin(2*theta13)^2)*NNu441/Nnu-(cos(theta13))^4*0.861*NNu442/Nnu;
Pdr54=1-(sin(2*theta13)^2)*NNu541/Nnu-(cos(theta13))^4*0.861*NNu542/Nnu;
Pdr64=1-(sin(2*theta13)^2)*NNu641/Nnu-(cos(theta13))^4*0.861*NNu642/Nnu;
Pdr15=1-(sin(2*theta13)^2)*NNu151/Nnu-(cos(theta13))^4*0.861*NNu152/Nnu;
Pdr25=1-(sin(2*theta13)^2)*NNu251/Nnu-(cos(theta13))^4*0.861*NNu252/Nnu;
Pdr35=1-(sin(2*theta13)^2)*NNu351/Nnu-(cos(theta13))^4*0.861*NNu352/Nnu;
Pdr45=1-(sin(2*theta13)^2)*NNu451/Nnu-(cos(theta13))^4*0.861*NNu452/Nnu;
Pdr55=1-(sin(2*theta13)^2)*NNu551/Nnu-(cos(theta13))^4*0.861*NNu552/Nnu;
Pdr65=1-(sin(2*theta13)^2)*NNu651/Nnu-(cos(theta13))^4*0.861*NNu652/Nnu;
Pdr16=1-(sin(2*theta13)^2)*NNu161/Nnu-(cos(theta13))^4*0.861*NNu162/Nnu;
Pdr26=1-(sin(2*theta13)^2)*NNu261/Nnu-(cos(theta13))^4*0.861*NNu262/Nnu;
Pdr36=1-(sin(2*theta13)^2)*NNu361/Nnu-(cos(theta13))^4*0.861*NNu362/Nnu;
Pdr46=1-(sin(2*theta13)^2)*NNu461/Nnu-(cos(theta13))^4*0.861*NNu462/Nnu;
Pdr56=1-(sin(2*theta13)^2)*NNu561/Nnu-(cos(theta13))^4*0.861*NNu562/Nnu;
Pdr66=1-(sin(2*theta13)^2)*NNu661/Nnu-(cos(theta13))^4*0.861*NNu662/Nnu;
TF11=Pdr11*om11;
TF21=Pdr21*om21;
TF31=Pdr31*om31;
TF41=Pdr41*om41;
TF51=Pdr51*om51;
TF61=Pdr61*om61;
TF12=Pdr12*om12;
TF22=Pdr22*om22;
TF32=Pdr32*om32;
TF42=Pdr42*om42;
TF52=Pdr52*om52;
TF62=Pdr62*om62;
TF13=Pdr13*om13;
TF23=Pdr23*om23;
```

```
TF33=Pdr33*om33;
TF43=Pdr43*om43;
TF53=Pdr53*om53;
TF63=Pdr63*om63;
TF14=Pdr14*om14;
TF24=Pdr24*om24;
TF34=Pdr34*om34;
TF44=Pdr44*om44;
TF54=Pdr54*om54;
TF64=Pdr64*om64;
TF15=Pdr15*om15;
TF25=Pdr25*om25;
TF35=Pdr35*om35;
TF45=Pdr45*om45;
TF55=Pdr55*om55;
TF65=Pdr65*om65;
TF16=Pdr16*om16;
TF26=Pdr26*om26;
TF36=Pdr36*om36;
TF46=Pdr46*om46;
TF56=Pdr56*om56;
TF66=Pdr66*om66;
TF1=TF11+TF12+TF13+TF14+TF15+TF16;
TF2=TF21+TF22+TF23+TF24+TF25+TF26;
TF3=TF31+TF32+TF33+TF34+TF35+TF36;
TF4=TF41+TF42+TF43+TF44+TF45+TF46;
TF5=TF51+TF52+TF53+TF54+TF55+TF56;
TF6=TF61+TF62+TF63+TF64+TF65+TF66;
Td1=N01*TF1;
Td2=N02*TF2;
```

```
Td3=N03*TF3;

Td4=N04*TF4;

Td5=N05*TF5;

Td6=N06*TF6;

Al1=om11*al1+om12*al1+om13*al2+om14*al2+om15*al3+om16*al3;

Al2=om21*al1+om22*al1+om23*al2+om24*al2+om25*al3+om26*al3;

Al3=om31*al1+om32*al1+om33*al2+om34*al2+om35*al3+om36*al3;

Al4=om41*al1+om42*al1+om43*al2+om44*al2+om45*al3+om46*al3;

Al5=om51*al1+om52*al1+om53*al2+om54*al2+om55*al3+om56*al3;

Al6=om61*al1+om62*al1+om63*al2+om64*al2+om65*al3+om66*al3;

Chim1=((M1+ep1-Td1*(1+a+Al1+et))^2)/(M1+B1);

Chim2=((M2+ep2-Td2*(1+a+Al2+et))^2)/(M2+B2);

Chim3=((M3+ep3-Td3*(1+a+Al3+et))^2)/(M3+B3);

Chim4=((M4+ep4-Td4*(1+a+Al4+et))^2)/(M4+B4);

Chim5=((M5+ep5-Td5*(1+a+Al5+et))^2)/(M5+B5);

Chim6=((M6+ep6-Td6*(1+a+Al6+et))^2)/(M6+B6);

Chim=Chim1+Chim2+Chim3+Chim4+Chim5+Chim6;

Chial=2*(al1/sr1)^2+2*(al2/sr2)^2+2*(al3/sr3)^2;

Chiet=6*(et/sd)^2;

Chiep=(ep1/sb1)^2+(ep2/sb2)^2+(ep3/sb3)^2+(ep4/sb4)^2+(ep5/sb5)^2+(ep6/sb6)^2;

CHI=Chim+Chial+Chiet+Chiep;


function [Chi]=DBChibd2(terms,dm13,dm12)

%This function is the second reduced form of DBChib.

Chi=DBChid2(dm13,dm12,terms(1,1),terms(2,1),terms(3,1),terms(4,1),...

...terms(5,1),terms(6,1),terms(7,1),terms(8,1),terms(9,1),terms(10,1),...

...terms(11,1),terms(12,1));


function [Smean,Sstd,Sste,Xmean,Xstd,Chimean,Chistd]=...

...dbchigoodd2(dm13,dm12,N,... ...q,acc)
```

```
%This function is the second reduced form of dbchigood.
bannana=@(terms)DBChibd2(terms,dm13,dm12);
option=optimset('MaxIter',100000,'MaxFunEvals',10000);
Xtot=zeros(12,N);
CHIi=zeros(1,N);
S231=zeros(1,N);
s=0;
while s < N
    rng('shuffle');
    ter=q*rand(12,1);
    [X,Chi]=fminsearch(bannana,ter,option);
    if Chi <= acc
        if X(1,1) >= 0
        s=s+1;
        Xtot(:,s)=X;
        CHIi(1,s)=Chi;
        S231(1,s)=sin(2*X(1,1))^2;
        end
    end
end
Xmean=mean(Xtot,2);
Xstd=std(Xtot,0,2);
Smean=mean(S231,2);
Sstd=std(S231,0,2);
Chimean=mean(CHIi,2);
Chistd=std(CHIi,0,2);
Sste=Sstd/(sqrt(N));
```

A.1.5 Fully Reduced Function Coding

```
function [CHI]=DBChiden(dm13,dm12,theta13,a,et,al,...
```

```
...ep1,ep2,ep3,ep4,ep5,ep6)
%This function is the fully reduced form of DBChi.
om11=0.4069;
om12=0.3854;
om13=0.0654;
om14=0.0799;
om15=0.0291;
om16=0.0333;
om21=0.4089;
om22=0.3870;
om23=0.0643;
om24=0.0785;
om25=0.0286;
om26=0.0327;
om31=0.0330;
om32=0.0318;
om33=0.2676;
om34=0.2441;
om35=0.1882;
om36=0.2354;
om41=0.1208;
om42=0.1241;
om43=0.1894;
om44=0.1892;
om45=0.1851;
om46=0.1914;
om51=0.1201;
om52=0.1248;
om53=0.1895;
om54=0.1895;
```

```
om55=0.1847;
om56=0.1913;
om61=0.1209;
om62=0.1241;
om63=0.1892;
om64=0.1892;
om65=0.1851;
om66=0.1914;
L11=362;
L12=372;
L13=903;
L14=817;
L15=1354;
L16=1265;
L21=358;
L22=368;
L23=903;
L24=817;
L25=1354;
L26=1265;
L31=1332;
L32=1358;
L33=468;
L34=490;
L35=558;
L36=499;
L41=1920;
L42=1894;
L43=1533;
L44=1534;
```

```
L45=1551;
L46=1525;
L51=1918;
L52=1892;
L53=1535;
L54=1535;
L55=1555;
L56=1528;
L61=1925;
L62=1900;
L63=1539;
L64=1539;
L65=1556;
L66=1530;
N01=68613;
N02=69595;
N03=66402;
N04=9922.9;
N05=9940.2;
N06=9837.7;
M1=67722;
M2=68334;
M3=65367;
M4=9359;
M5=9241;
M6=9037;
sb1=157.03;
sb2=156.46;
sb3=124.53;
sb4=28.75;
```

```
sb5=28.74;
sb6=28.55;
sd=0.002;
sr=0.008;
B1=1399;
B2=1380;
B3=1106;
B4=429;
B5=428;
B6=415;
Nnu=integral(@nuespec,1.810997,25,'AbsTol',1e-12,'RelTol',1e-8);
NNu111=integral(@(E)nuespece(E,dm13,L11),1.810997,25);
NNu211=integral(@(E)nuespece(E,dm13,L21),1.810997,25);
NNu311=integral(@(E)nuespece(E,dm13,L31),1.810997,25);
NNu411=integral(@(E)nuespece(E,dm13,L41),1.810997,25);
NNu511=integral(@(E)nuespece(E,dm13,L51),1.810997,25);
NNu611=integral(@(E)nuespece(E,dm13,L61),1.810997,25);
NNu121=integral(@(E)nuespece(E,dm13,L12),1.810997,25);
NNu221=integral(@(E)nuespece(E,dm13,L22),1.810997,25);
NNu321=integral(@(E)nuespece(E,dm13,L32),1.810997,25);
NNu421=integral(@(E)nuespece(E,dm13,L42),1.810997,25);
NNu521=integral(@(E)nuespece(E,dm13,L52),1.810997,25);
NNu621=integral(@(E)nuespece(E,dm13,L62),1.810997,25);
NNu131=integral(@(E)nuespece(E,dm13,L13),1.810997,25);
NNu231=integral(@(E)nuespece(E,dm13,L23),1.810997,25);
NNu331=integral(@(E)nuespece(E,dm13,L33),1.810997,25);
NNu431=integral(@(E)nuespece(E,dm13,L43),1.810997,25);
NNu531=integral(@(E)nuespece(E,dm13,L53),1.810997,25);
NNu631=integral(@(E)nuespece(E,dm13,L63),1.810997,25);
NNu141=integral(@(E)nuespece(E,dm13,L14),1.810997,25);
```

```
NNu241=integral(@(E)nuespece(E,dm13,L24),1.810997,25);
NNu341=integral(@(E)nuespece(E,dm13,L34),1.810997,25);
NNu441=integral(@(E)nuespece(E,dm13,L44),1.810997,25);
NNu541=integral(@(E)nuespece(E,dm13,L54),1.810997,25);
NNu641=integral(@(E)nuespece(E,dm13,L64),1.810997,25);
NNu151=integral(@(E)nuespece(E,dm13,L15),1.810997,25);
NNu251=integral(@(E)nuespece(E,dm13,L25),1.810997,25);
NNu351=integral(@(E)nuespece(E,dm13,L35),1.810997,25);
NNu451=integral(@(E)nuespece(E,dm13,L45),1.810997,25);
NNu551=integral(@(E)nuespece(E,dm13,L55),1.810997,25);
NNu651=integral(@(E)nuespece(E,dm13,L65),1.810997,25);
NNu161=integral(@(E)nuespece(E,dm13,L16),1.810997,25);
NNu261=integral(@(E)nuespece(E,dm13,L26),1.810997,25);
NNu361=integral(@(E)nuespece(E,dm13,L36),1.810997,25);
NNu461=integral(@(E)nuespece(E,dm13,L46),1.810997,25);
NNu561=integral(@(E)nuespece(E,dm13,L56),1.810997,25);
NNu661=integral(@(E)nuespece(E,dm13,L66),1.810997,25);
NNu112=integral(@(E)nuespece(E,dm12,L11),1.810997,25);
NNu212=integral(@(E)nuespece(E,dm12,L21),1.810997,25);
NNu312=integral(@(E)nuespece(E,dm12,L31),1.810997,25);
NNu412=integral(@(E)nuespece(E,dm12,L41),1.810997,25);
NNu512=integral(@(E)nuespece(E,dm12,L51),1.810997,25);
NNu612=integral(@(E)nuespece(E,dm12,L61),1.810997,25);
NNu122=integral(@(E)nuespece(E,dm12,L12),1.810997,25);
NNu222=integral(@(E)nuespece(E,dm12,L22),1.810997,25);
NNu322=integral(@(E)nuespece(E,dm12,L32),1.810997,25);
NNu422=integral(@(E)nuespece(E,dm12,L42),1.810997,25);
NNu522=integral(@(E)nuespece(E,dm12,L52),1.810997,25);
NNu622=integral(@(E)nuespece(E,dm12,L62),1.810997,25);
NNu132=integral(@(E)nuespece(E,dm12,L13),1.810997,25);
```

```
NNu232=integral(@(E)nuespece(E,dm12,L23),1.810997,25);
NNu332=integral(@(E)nuespece(E,dm12,L33),1.810997,25);
NNu432=integral(@(E)nuespece(E,dm12,L43),1.810997,25);
NNu532=integral(@(E)nuespece(E,dm12,L53),1.810997,25);
NNu632=integral(@(E)nuespece(E,dm12,L63),1.810997,25);
NNu142=integral(@(E)nuespece(E,dm12,L14),1.810997,25);
NNu242=integral(@(E)nuespece(E,dm12,L24),1.810997,25);
NNu342=integral(@(E)nuespece(E,dm12,L34),1.810997,25);
NNu442=integral(@(E)nuespece(E,dm12,L44),1.810997,25);
NNu542=integral(@(E)nuespece(E,dm12,L54),1.810997,25);
NNu642=integral(@(E)nuespece(E,dm12,L64),1.810997,25);
NNu152=integral(@(E)nuespece(E,dm12,L15),1.810997,25);
NNu252=integral(@(E)nuespece(E,dm12,L25),1.810997,25);
NNu352=integral(@(E)nuespece(E,dm12,L35),1.810997,25);
NNu452=integral(@(E)nuespece(E,dm12,L45),1.810997,25);
NNu552=integral(@(E)nuespece(E,dm12,L55),1.810997,25);
NNu652=integral(@(E)nuespece(E,dm12,L65),1.810997,25);
NNu162=integral(@(E)nuespece(E,dm12,L16),1.810997,25);
NNu262=integral(@(E)nuespece(E,dm12,L26),1.810997,25);
NNu362=integral(@(E)nuespece(E,dm12,L36),1.810997,25);
NNu462=integral(@(E)nuespece(E,dm12,L46),1.810997,25);
NNu562=integral(@(E)nuespece(E,dm12,L56),1.810997,25);
NNu662=integral(@(E)nuespece(E,dm12,L66),1.810997,25);
Pdr11=1-(sin(2*theta13)^2)*NNu111/Nnu-(cos(theta13))^4*0.861*NNu112/Nnu;
Pdr21=1-(sin(2*theta13)^2)*NNu211/Nnu-(cos(theta13))^4*0.861*NNu212/Nnu;
Pdr31=1-(sin(2*theta13)^2)*NNu311/Nnu-(cos(theta13))^4*0.861*NNu312/Nnu;
Pdr41=1-(sin(2*theta13)^2)*NNu411/Nnu-(cos(theta13))^4*0.861*NNu412/Nnu;
Pdr51=1-(sin(2*theta13)^2)*NNu511/Nnu-(cos(theta13))^4*0.861*NNu512/Nnu;
Pdr61=1-(sin(2*theta13)^2)*NNu611/Nnu-(cos(theta13))^4*0.861*NNu612/Nnu;
Pdr12=1-(sin(2*theta13)^2)*NNu121/Nnu-(cos(theta13))^4*0.861*NNu122/Nnu;
```

```
Pdr22=1-(sin(2*theta13)^2)*NNu221/Nnu-(cos(theta13))^4*0.861*NNu222/Nnu;
Pdr32=1-(sin(2*theta13)^2)*NNu321/Nnu-(cos(theta13))^4*0.861*NNu322/Nnu;
Pdr42=1-(sin(2*theta13)^2)*NNu421/Nnu-(cos(theta13))^4*0.861*NNu422/Nnu;
Pdr52=1-(sin(2*theta13)^2)*NNu521/Nnu-(cos(theta13))^4*0.861*NNu522/Nnu;
Pdr62=1-(sin(2*theta13)^2)*NNu621/Nnu-(cos(theta13))^4*0.861*NNu622/Nnu;
Pdr13=1-(sin(2*theta13)^2)*NNu131/Nnu-(cos(theta13))^4*0.861*NNu132/Nnu;
Pdr23=1-(sin(2*theta13)^2)*NNu231/Nnu-(cos(theta13))^4*0.861*NNu232/Nnu;
Pdr33=1-(sin(2*theta13)^2)*NNu331/Nnu-(cos(theta13))^4*0.861*NNu332/Nnu;
Pdr43=1-(sin(2*theta13)^2)*NNu431/Nnu-(cos(theta13))^4*0.861*NNu432/Nnu;
Pdr53=1-(sin(2*theta13)^2)*NNu531/Nnu-(cos(theta13))^4*0.861*NNu532/Nnu;
Pdr63=1-(sin(2*theta13)^2)*NNu631/Nnu-(cos(theta13))^4*0.861*NNu632/Nnu;
Pdr14=1-(sin(2*theta13)^2)*NNu141/Nnu-(cos(theta13))^4*0.861*NNu142/Nnu;
Pdr24=1-(sin(2*theta13)^2)*NNu241/Nnu-(cos(theta13))^4*0.861*NNu242/Nnu;
Pdr34=1-(sin(2*theta13)^2)*NNu341/Nnu-(cos(theta13))^4*0.861*NNu342/Nnu;
Pdr44=1-(sin(2*theta13)^2)*NNu441/Nnu-(cos(theta13))^4*0.861*NNu442/Nnu;
Pdr54=1-(sin(2*theta13)^2)*NNu541/Nnu-(cos(theta13))^4*0.861*NNu542/Nnu;
Pdr64=1-(sin(2*theta13)^2)*NNu641/Nnu-(cos(theta13))^4*0.861*NNu642/Nnu;
Pdr15=1-(sin(2*theta13)^2)*NNu151/Nnu-(cos(theta13))^4*0.861*NNu152/Nnu;
Pdr25=1-(sin(2*theta13)^2)*NNu251/Nnu-(cos(theta13))^4*0.861*NNu252/Nnu;
Pdr35=1-(sin(2*theta13)^2)*NNu351/Nnu-(cos(theta13))^4*0.861*NNu352/Nnu;
Pdr45=1-(sin(2*theta13)^2)*NNu451/Nnu-(cos(theta13))^4*0.861*NNu452/Nnu;
Pdr55=1-(sin(2*theta13)^2)*NNu551/Nnu-(cos(theta13))^4*0.861*NNu552/Nnu;
Pdr65=1-(sin(2*theta13)^2)*NNu651/Nnu-(cos(theta13))^4*0.861*NNu652/Nnu;
Pdr16=1-(sin(2*theta13)^2)*NNu161/Nnu-(cos(theta13))^4*0.861*NNu162/Nnu;
Pdr26=1-(sin(2*theta13)^2)*NNu261/Nnu-(cos(theta13))^4*0.861*NNu262/Nnu;
Pdr36=1-(sin(2*theta13)^2)*NNu361/Nnu-(cos(theta13))^4*0.861*NNu362/Nnu;
Pdr46=1-(sin(2*theta13)^2)*NNu461/Nnu-(cos(theta13))^4*0.861*NNu462/Nnu;
Pdr56=1-(sin(2*theta13)^2)*NNu561/Nnu-(cos(theta13))^4*0.861*NNu562/Nnu;
Pdr66=1-(sin(2*theta13)^2)*NNu661/Nnu-(cos(theta13))^4*0.861*NNu662/Nnu;
TF11=Pdr11*om11;
```

```
TF21=Pdr21*om21;

TF31=Pdr31*om31;

TF41=Pdr41*om41;

TF51=Pdr51*om51;

TF61=Pdr61*om61;

TF12=Pdr12*om12;

TF22=Pdr22*om22;

TF32=Pdr32*om32;

TF42=Pdr42*om42;

TF52=Pdr52*om52;

TF62=Pdr62*om62;

TF13=Pdr13*om13;

TF23=Pdr23*om23;

TF33=Pdr33*om33;

TF43=Pdr43*om43;

TF53=Pdr53*om53;

TF63=Pdr63*om63;

TF14=Pdr14*om14;

TF24=Pdr24*om24;

TF34=Pdr34*om34;

TF44=Pdr44*om44;

TF54=Pdr54*om54;

TF64=Pdr64*om64;

TF15=Pdr15*om15;

TF25=Pdr25*om25;

TF35=Pdr35*om35;

TF45=Pdr45*om45;

TF55=Pdr55*om55;

TF65=Pdr65*om65;

TF16=Pdr16*om16;
```

```
TF26=Pdr26*om26;

TF36=Pdr36*om36;

TF46=Pdr46*om46;

TF56=Pdr56*om56;

TF66=Pdr66*om66;

TF1=TF11+TF12+TF13+TF14+TF15+TF16;

TF2=TF21+TF22+TF23+TF24+TF25+TF26;

TF3=TF31+TF32+TF33+TF34+TF35+TF36;

TF4=TF41+TF42+TF43+TF44+TF45+TF46;

TF5=TF51+TF52+TF53+TF54+TF55+TF56;

TF6=TF61+TF62+TF63+TF64+TF65+TF66;

Td1=N01*TF1;

Td2=N02*TF2;

Td3=N03*TF3;

Td4=N04*TF4;

Td5=N05*TF5;

Td6=N06*TF6;

Chim1=((M1+ep1-Td1*(1+a+al+et))^2)/(M1+B1);

Chim2=((M2+ep2-Td2*(1+a+al+et))^2)/(M2+B2);

Chim3=((M3+ep3-Td3*(1+a+al+et))^2)/(M3+B3);

Chim4=((M4+ep4-Td4*(1+a+al+et))^2)/(M4+B4);

Chim5=((M5+ep5-Td5*(1+a+al+et))^2)/(M5+B5);

Chim6=((M6+ep6-Td6*(1+a+al+et))^2)/(M6+B6);

Chim=Chim1+Chim2+Chim3+Chim4+Chim5+Chim6;

Chial=6*(al^2)/(sr^2);

Chiet=6*(et^2)/(sd^2);

Chiep=(ep1/sb1)^2+(ep2/sb2)^2+(ep3/sb3)^2+(ep4/sb4)^2+(ep5/sb5)^2+(ep6/sb6)^2;

CHI=Chim+Chial+Chiet+Chiep;


function [Chi]=DBChibden(terms,dm13,dm12)
```

```
%This is the fully reduced version of DBChib.
Chi=DBChiden(dm13,dm12,terms(1,1),terms(2,1),terms(3,1),terms(4,1),...
...terms(5,1),terms(6,1),terms(7,1),terms(8,1),terms(9,1),terms(10,1));

function [Smeanden,Sstdden,Sste,Xmeanden,Xstdden,Chimeanden,Chistdden]=...
...dbchigoodden(dm13,dm12,N,q,acc)
%This is the fully reduced version of dbchigood.
bannana=@(terms)DBChibden(terms,dm13,dm12);
option=optimset('MaxIter',100000,'MaxFunEvals',10000);
Xtot=zeros(10,N);
CHIi=zeros(1,N);
S231=zeros(1,N);
s=0;
while s < N
    rng('shuffle');
    ter=q*rand(10,1);
    [X,Chi]=fminsearch(bannana,ter,option);
    if Chi <= acc
        if X(1,1) >= 0
        s=s+1;
        Xtot(:,s)=X;
        CHIi(1,s)=Chi;
        S231(1,s)=sin(2*X(1,1))^2;
        end
    end
end
Xmeanden=mean(Xtot,2);
Xstdden=std(Xtot,0,2);
Smeanden=mean(S231,2);
Sstdden=std(S231,0,2);
```

```
Chimeanden=mean(CHIi,2);
Chistdden=std(CHIi,0,2);
Sste=Sstdden/(sqrt(N));
```

A.2 RENO Programming.

A.2.1 Full Function Coding

```
function [Chi]=renochi(theta13,dm13,a,e1,e2,b1,b2,f1,f2,f3,f4,f5,f6)
%This builds the chi squared function for RENO.  The independent variables
%are the mixing angle, the mass difference squared and, the pull terms.
%%
%This section contains the parameters relating to the experimental results.
%The Nxe0 values are the prediction for detector x assuming no
%oscillations.  Ne0ij is the contribution of this amount to detector j from
%reactor i.  Lij is the distance from reactor i to detector j.  sigmad is
%the uncorrelated uncertainty for each detector, sigma r is the
%uncorrelated uncertainty for each reactor and, sigmabx is the uncorrelated
%uncertainty in the background for detector x.
N1e0=151723.54;
N2e0=17565.72;
Ne011=0.0678*N1e0;
Ne021=0.1493*N1e0;
Ne031=0.3419*N1e0;
Ne041=0.2701*N1e0;
Ne051=0.1150*N1e0;
Ne061=0.0558*N1e0;
Ne012=0.1373*N2e0;
Ne022=0.1574*N2e0;
Ne032=0.1809*N2e0;
```

```
Ne042=0.1856*N2e0;
Ne052=0.1780*N2e0;
Ne062=0.1608*N2e0;
Nobs1=149902.86;
Nobs2=16160.46;
sigmad=0.002;
sigmar=0.009;
sigmab1=1141.05;
sigmab2=166.54;
L11=667.9;
L21=451.8;
L31=304.8;
L41=336.1;
L51=513.9;
L61=739.1;
L12=1556.5;
L22=1456.2;
L32=1395.9;
L42=1381.3;
L52=1413.8;
L62=1490.1;
%%
%This section builds the energy dependence.  Nnu is the normalization
%factor.  NNuij is the energy weighting for the flux from reactor i to
%detector j.  1.806 is the stated minimum value from [26].
Nnu=integral(@nuespec,1.811,8,'AbsTol',1e-12,'RelTol',1e-8);
NNu11=integral(@(E)nuespece(E,dm13,L11),1.811,8);
NNu21=integral(@(E)nuespece(E,dm13,L21),1.811,8);
NNu31=integral(@(E)nuespece(E,dm13,L31),1.811,8);
NNu41=integral(@(E)nuespece(E,dm13,L41),1.811,8);
```

```
NNu51=integral(@(E)nuespece(E,dm13,L51),1.811,8);
NNu61=integral(@(E)nuespece(E,dm13,L61),1.811,8);
NNu12=integral(@(E)nuespece(E,dm13,L12),1.811,8);
NNu22=integral(@(E)nuespece(E,dm13,L22),1.811,8);
NNu32=integral(@(E)nuespece(E,dm13,L32),1.811,8);
NNu42=integral(@(E)nuespece(E,dm13,L42),1.811,8);
NNu52=integral(@(E)nuespece(E,dm13,L52),1.811,8);
NNu62=integral(@(E)nuespece(E,dm13,L62),1.811,8);
%%
%This section constructs the probability weighting for the total neutrino
%flux, which is the portion that includes the mixing angle.  Pdrij is the
%probability of reactor anti-neutrino disappearence between reactor i and
%detector j.
Pdr11=1-(sin(2*theta13))^2*(NNu11/Nnu);
Pdr21=1-(sin(2*theta13))^2*(NNu21/Nnu);
Pdr31=1-(sin(2*theta13))^2*(NNu31/Nnu);
Pdr41=1-(sin(2*theta13))^2*(NNu41/Nnu);
Pdr51=1-(sin(2*theta13))^2*(NNu51/Nnu);
Pdr61=1-(sin(2*theta13))^2*(NNu61/Nnu);
Pdr12=1-(sin(2*theta13))^2*(NNu12/Nnu);
Pdr22=1-(sin(2*theta13))^2*(NNu22/Nnu);
Pdr32=1-(sin(2*theta13))^2*(NNu32/Nnu);
Pdr42=1-(sin(2*theta13))^2*(NNu42/Nnu);
Pdr52=1-(sin(2*theta13))^2*(NNu52/Nnu);
Pdr62=1-(sin(2*theta13))^2*(NNu62/Nnu);
%%
%This section weights the expected flux with the probability, each for
%the appropriate reactor-detector combination.
Ne11=Ne011*Pdr11;
Ne21=Ne021*Pdr21;
```

```
Ne31=Ne031*Pdr31;
Ne41=Ne041*Pdr41;
Ne51=Ne051*Pdr51;
Ne61=Ne061*Pdr61;
Ne12=Ne012*Pdr12;
Ne22=Ne022*Pdr22;
Ne32=Ne032*Pdr32;
Ne42=Ne042*Pdr42;
Ne52=Ne052*Pdr52;
Ne62=Ne062*Pdr62;
%%
%This section combines the results of the previous sections to produce the
%function.
NE1=Ne11*(1+f1)+Ne21*(1+f2)+Ne31*(1+f3)+Ne41*(1+f4)+Ne51*(1+f5)+Ne61*(1+f6);
NE2=Ne12*(1+f1)+Ne22*(1+f2)+Ne32*(1+f3)+Ne42*(1+f4)+Ne52*(1+f5)+Ne62*(1+f6);
Chi=((Nobs1+b1-(1+a+e1)*NE1)^2)/Nobs1+((Nobs2+b2-(1+a+e2)*NE2)^2)/Nobs2+...
...+(e1^2)/(sigmad^2)+(e2^2)/(sigmad^2)+(b1^2)/(sigmab1^2)+(b2^2)/(sigmab2^2)+...
...+(f1/sigmar)^2+(f2/sigmar)^2+(f3/sigmar)^2+(f4/sigmar)^2+(f5/sigmar)^2+(f6/sigmar)^2;

function [Chi]=RChib(terms,dm13)
%This function converts the function renochi into one with a vector
%argument, so that it can be used with fminsearch.
Chi=renochi(terms(1,1),dm13,terms(2,1),terms(3,1),terms(4,1),terms(5,1),...
...terms(6,1),terms(7,1),terms(8,1),terms(9,1),terms(10,1),terms(11,1),terms(12,1));

function [Smean,Sstd,Sste,Xmean,Xstd,Chimean,Chistd]=...
...renogood(dm13,N,q,acc)
%This function actually performs the minimisation using as inputs the
%mass difference squared from MINOS, the number of minimisations to be
%performed, the scale factor for the random inputs (see below) and, the
```

```
%level of accuracy required for a minimisation to be counted.
bannana=@(terms)RChib(terms,dm13);
option=optimset('MaxIter',100000,'MaxFunEvals',10000);
Xtot=zeros(12,N);
CHIi=zeros(1,N);
S231=zeros(1,N);
s=0;
while s < N
    rng('shuffle');
    ter=q*rand(12,1);
    %Random inputs are used because an initial guess is required for the
    %fminsearch algorithm.
    [X,Chi]=fminsearch(bannana,ter,option);
    if Chi <= acc
        if X(1,1) >= 0
        s=s+1;
        Xtot(:,s)=X;
        CHIi(1,s)=Chi;
        S231(1,s)=sin(2*X(1,1))^2;
        end
    end
end
Xmean=mean(Xtot,2);
Xstd=std(Xtot,0,2);
Smean=mean(S231,2);
Sstd=std(S231,0,2);
Chimean=mean(CHIi,2);
Chistd=std(CHIi,0,2);
Sste=Sstd/(sqrt(N));
```

A.2.2 Reduced Function Coding

```
function [Chi]=renochiden(theta13,dm13,a,e,b1,b2,f)
%This builds the simplified chi squared function for RENO.  The independent
%variables are the mixing angle, the mass difference squared and, the
%averaged pull terms.  This code is identical to the code for the full
%function except for the number of pull terms and the final function.
N1e0=151723.54;
N2e0=17565.72;
Ne011=0.0678*N1e0;
Ne021=0.1493*N1e0;
Ne031=0.3419*N1e0;
Ne041=0.2701*N1e0;
Ne051=0.1150*N1e0;
Ne061=0.0558*N1e0;
Ne012=0.1373*N2e0;
Ne022=0.1574*N2e0;
Ne032=0.1809*N2e0;
Ne042=0.1856*N2e0;
Ne052=0.1780*N2e0;
Ne062=0.1608*N2e0;
Nobs1=149902.86;
Nobs2=16160.46;
sigmad=0.002;
sigmar=0.009;
sigmab1=1141.05;
sigmab2=166.54;
L11=667.9;
L21=451.8;
L31=304.8;
L41=336.1;
```

```
L51=513.9;
L61=739.1;
L12=1556.5;
L22=1456.2;
L32=1395.9;
L42=1381.3;
L52=1413.8;
L62=1490.1;
Nnu=integral(@nuespec,1.811,8,'AbsTol',1e-12,'RelTol',1e-8);
NNu11=integral(@(E)nuespece(E,dm13,L11),1.811,8);
NNu21=integral(@(E)nuespece(E,dm13,L21),1.811,8);
NNu31=integral(@(E)nuespece(E,dm13,L31),1.811,8);
NNu41=integral(@(E)nuespece(E,dm13,L41),1.811,8);
NNu51=integral(@(E)nuespece(E,dm13,L51),1.811,8);
NNu61=integral(@(E)nuespece(E,dm13,L61),1.811,8);
NNu12=integral(@(E)nuespece(E,dm13,L12),1.811,8);
NNu22=integral(@(E)nuespece(E,dm13,L22),1.811,8);
NNu32=integral(@(E)nuespece(E,dm13,L32),1.811,8);
NNu42=integral(@(E)nuespece(E,dm13,L42),1.811,8);
NNu52=integral(@(E)nuespece(E,dm13,L52),1.811,8);
NNu62=integral(@(E)nuespece(E,dm13,L62),1.811,8);
Pdr11=1-(sin(2*theta13))^2*(NNu11/Nnu);
Pdr21=1-(sin(2*theta13))^2*(NNu21/Nnu);
Pdr31=1-(sin(2*theta13))^2*(NNu31/Nnu);
Pdr41=1-(sin(2*theta13))^2*(NNu41/Nnu);
Pdr51=1-(sin(2*theta13))^2*(NNu51/Nnu);
Pdr61=1-(sin(2*theta13))^2*(NNu61/Nnu);
Pdr12=1-(sin(2*theta13))^2*(NNu12/Nnu);
Pdr22=1-(sin(2*theta13))^2*(NNu22/Nnu);
Pdr32=1-(sin(2*theta13))^2*(NNu32/Nnu);
```

```
Pdr42=1-(sin(2*theta13))^2*(NNu42/Nnu);

Pdr52=1-(sin(2*theta13))^2*(NNu52/Nnu);

Pdr62=1-(sin(2*theta13))^2*(NNu62/Nnu);

Ne11=Ne011*Pdr11;

Ne21=Ne021*Pdr21;

Ne31=Ne031*Pdr31;

Ne41=Ne041*Pdr41;

Ne51=Ne051*Pdr51;

Ne61=Ne061*Pdr61;

Ne12=Ne012*Pdr12;

Ne22=Ne022*Pdr22;

Ne32=Ne032*Pdr32;

Ne42=Ne042*Pdr42;

Ne52=Ne052*Pdr52;

Ne62=Ne062*Pdr62;

NE1=Ne11*(1+f)+Ne21*(1+f)+Ne31*(1+f)+Ne41*(1+f)+Ne51*(1+f)+Ne61*(1+f);

NE2=Ne12*(1+f)+Ne22*(1+f)+Ne32*(1+f)+Ne42*(1+f)+Ne52*(1+f)+Ne62*(1+f);

Chi=((Nobs1+b1-(1+a+e)*NE1)^2)/Nobs1+((Nobs2+b2-(1+a+e)*NE2)^2)/Nobs2+...

...+2*(e^2)/(sigmad^2)+(b1^2)/(sigmab1^2)+(b2^2)/(sigmab2^2)+6*(f/sigmar)^2;
```

Appendix B

Mixing Modulation by Dark Matter Code

This appendix contains the programming related to the matter effect calculations. Note that, in general, lines are ended by semi-colons (;). Many were split to fit the page.

B.1 Matter Effect Functions

This section contains the functions written to perform the matter effect calculations.

B.1.1 Decoherent Function

```
function [Pe,Pu,Pt]=menunhsurprobtoteVpotSLT...
   ...(E,dm12,dm13,fe,fu,ft,V11,V12,V13,V21,V22,V23,V31,V32,V33)
   %Note that E is in MeV and L is in m.
   Pot=[V11,V12,V13;V21,V22,V23;V31,V32,V33];
   theta12=0.5944;
   theta13=0.1515;
   theta23=0.7854;
   PMNS=[cos(theta12)*cos(theta13) sin(theta12)*cos(theta13) sin(theta13);
   -sin(theta12)*cos(theta23)-cos(theta12)*sin(theta23)*sin(theta13)...
   cos(theta12)*cos(theta23)-sin(theta12)*sin(theta23)*sin(theta13)...
   ...sin(theta23)*cos(theta13);
```

```
sin(theta12)*sin(theta23)-cos(theta12)*cos(theta23)*sin(theta13)...
-cos(theta12)*sin(theta23)-sin(theta12)*cos(theta23)*sin(theta13)...
...cos(theta23)*cos(theta13)];
```

Note: The preceding matrix is edited from the version used for clarity.

```
PMNST=PMNS';
H1=1.267*sqrt(2)*10^6*Pot;
H0=[0 0 0; 0 2*1.267*dm12/(E) 0; 0 0 2*1.267*dm13/(E)];
Ht=PMNS*H0*PMNST-H1;
[U,D]=eig(Ht);
V=U;
IV=inv(U);
dM12=D(1,1)-D(2,2);
dM13=D(1,1)-D(3,3);
dM23=D(2,2)-D(3,3);
Pee=fe*((V(1,1)*IV(1,1))^2+(V(1,2)*IV(2,1))^2+(V(1,3)*IV(3,1))^2);
Peu=fe*((V(2,1)*IV(1,1))^2+(V(2,2)*IV(2,1))^2+(V(2,3)*IV(3,1))^2);
Pet=fe*((V(3,1)*IV(1,1))^2+(V(3,2)*IV(2,1))^2+(V(3,3)*IV(3,1))^2);
Pue=fu*((V(1,1)*IV(1,2))^2+(V(1,2)*IV(2,2))^2+(V(1,3)*IV(3,2))^2);
Puu=fu*((V(2,1)*IV(1,2))^2+(V(2,2)*IV(2,2))^2+(V(2,3)*IV(3,2))^2);
Put=fu*((V(3,1)*IV(1,2))^2+(V(3,2)*IV(2,2))^2+(V(3,3)*IV(3,2))^2);
Pte=ft*((V(1,1)*IV(1,3))^2+(V(1,2)*IV(2,3))^2+(V(1,3)*IV(3,3))^2);
Ptu=ft*((V(2,1)*IV(1,3))^2+(V(2,2)*IV(2,3))^2+(V(2,3)*IV(3,3))^2);
Ptt=ft*((V(3,1)*IV(1,3))^2+(V(3,2)*IV(2,3))^2+(V(3,3)*IV(3,3))^2);
Pe=Pee+Pue+Pte;
Pu=Peu+Puu+Ptu;
Pt=Pet+Put+Ptt;
```

B.1.2 Coherent Flavour State Function.

```
function [Pe,Pu,Pt]=menunhsurprobtoteVpotFBas...
   ...(L,E,dm12,dm13,fe,fu,ft,V11,V12,V13,V21,V22,V23,V31,V32,V33)
```

```
%Note that E is in MeV and L is in m.
Pot=[V11,V12,V13;V21,V22,V23;V31,V32,V33];
theta12=0.5944;
theta13=0.1515;
theta23=0.7854;
PMNS=[cos(theta12)*cos(theta13) sin(theta12)*cos(theta13) sin(theta13);
-sin(theta12)*cos(theta23)-cos(theta12)*sin(theta23)*sin(theta13)...
cos(theta12)*cos(theta23)-sin(theta12)*sin(theta23)*sin(theta13)
sin(theta23)*cos(theta13);
sin(theta12)*sin(theta23)-cos(theta12)*cos(theta23)*sin(theta13)...
-cos(theta12)*sin(theta23)-sin(theta12)*cos(theta23)*sin(theta13)...
cos(theta23)*cos(theta13)];
```

Note: The preceding matrix is edited from the version used for clarity.

```
PMNST=PMNS';
H1=1.267*sqrt(2).*10.^6*Pot;
H0=[0 0 0; 0 2*1.267*dm12./(E) 0; 0 0 2*1.267*dm13./(E)];
Ht=PMNS*H0*PMNST-H1;
[U,D]=eig(Ht);
V=U;
IV=inv(U);
dM12=D(1,1)-D(2,2);
dM13=D(1,1)-D(3,3);
dM23=D(2,2)-D(3,3);
Pee=fe*((V(1,1)*IV(1,1))^2+(V(1,2)*IV(2,1))^2+(V(1,3)*IV(3,1))^2+...
...+2*V(1,1)*IV(1,1)*V(1,2)*IV(2,1)*cos(dM12*L)+...
...+2*V(1,1)*IV(1,1)*V(1,3)*IV(3,1)*cos(dM13*L)+...
...+2*V(1,2)*IV(2,1)*V(1,3)*IV(3,1)*cos(dM23*L));
Peu=fe*((V(2,1)*IV(1,1))^2+(V(2,2)*IV(2,1))^2+(V(2,3)*IV(3,1))^2+...
...+2*V(2,1)*IV(1,1)*V(2,2)*IV(2,1)*cos(dM12*L)+...
...+2*V(2,1)*IV(1,1)*V(2,3)*IV(3,1)*cos(dM13*L)+...
```

```
...+2*V(2,2)*IV(2,1)*V(2,3)*IV(3,1)*cos(dM23*L));
Pet=fe*((V(3,1)*IV(1,1))^2+(V(3,2)*IV(2,1))^2+(V(3,3)*IV(3,1))^2+...
...+2*V(3,1)*IV(1,1)*V(3,2)*IV(2,1)*cos(dM12*L)+...
...+2*V(3,1)*IV(1,1)*V(3,3)*IV(3,1)*cos(dM13*L)+...
...+2*V(3,2)*IV(2,1)*V(3,3)*IV(3,1)*cos(dM23*L));
Pue=fu*((V(1,1)*IV(1,2))^2+(V(1,2)*IV(2,2))^2+(V(1,3)*IV(3,2))^2+...
...+2*V(1,1)*IV(1,2)*V(1,2)*IV(2,2)*cos(dM12*L)+...
...+2*V(1,1)*IV(1,2)*V(1,3)*IV(3,2)*cos(dM13*L)+...
...+2*V(1,2)*IV(2,2)*V(1,3)*IV(3,2)*cos(dM23*L));
Puu=fu*((V(2,1)*IV(1,2))^2+(V(2,2)*IV(2,2))^2+(V(2,3)*IV(3,2))^2+...
...+2*V(2,1)*IV(1,2)*V(2,2)*IV(2,2)*cos(dM12*L)+...
...+2*V(2,1)*IV(1,2)*V(2,3)*IV(3,2)*cos(dM13*L)+...
...+2*V(2,2)*IV(2,2)*V(2,3)*IV(3,2)*cos(dM23*L));
Put=fu*((V(3,1)*IV(1,2))^2+(V(3,2)*IV(2,2))^2+(V(3,3)*IV(3,2))^2+...
...+2*V(3,1)*IV(1,2)*V(3,2)*IV(2,2)*cos(dM12*L)+...
...+2*V(3,1)*IV(1,2)*V(3,3)*IV(3,2)*cos(dM13*L)+...
...+2*V(3,2)*IV(2,2)*V(3,3)*IV(3,2)*cos(dM23*L));
Pte=ft*((V(1,1)*IV(1,3))^2+(V(1,2)*IV(2,3))^2+(V(1,3)*IV(3,3))^2+...
...+2*V(1,1)*IV(1,3)*V(1,2)*IV(2,3)*cos(dM12*L)+...
...+2*V(1,1)*IV(1,3)*V(1,3)*IV(3,3)*cos(dM13*L)+...
...+2*V(1,2)*IV(2,3)*V(1,3)*IV(3,3)*cos(dM23*L));
Ptu=ft*((V(2,1)*IV(1,3))^2+(V(2,2)*IV(2,3))^2+(V(2,3)*IV(3,3))^2+...
...+2*V(2,1)*IV(1,3)*V(2,2)*IV(2,3)*cos(dM12*L)+...
...+2*V(2,1)*IV(1,3)*V(2,3)*IV(3,3)*cos(dM13*L)+...
...+2*V(2,2)*IV(2,3)*V(2,3)*IV(3,3)*cos(dM23*L));
Ptt=ft*((V(3,1)*IV(1,3))^2+(V(3,2)*IV(2,3))^2+(V(3,3)*IV(3,3))^2+...
...+2*V(3,1)*IV(1,3)*V(3,2)*IV(2,3)*cos(dM12*L)+...
...+2*V(3,1)*IV(1,3)*V(3,3)*IV(3,3)*cos(dM13*L)+...
...+2*V(3,2)*IV(2,3)*V(3,3)*IV(3,3)*cos(dM23*L));
Pe=Pee+Pue+Pte;
```

```
Pu=Peu+Puu+Ptu;
Pt=Pet+Put+Ptt;
```

B.1.3 Coherent Mass State Function

```
function [Pe,Pu,Pt]=menunhsurprobtoteVpot...
...(L,E,dm12,dm13,fe,fu,ft,V11,V12,V13,V21,V22,V23,V31,V32,V33)
%Note that E is in MeV and L is in m.
Pot=[V11,V12,V13;V21,V22,V23;V31,V32,V33];
H1=1.267*sqrt(2)*10\^6.*Pot;
H0=[0 0 0; 0 2*1.267*dm12./(E) 0; 0 0 2*1.267*dm13./(E)];
Ht=H0-H1;
[U,D]=eig(Ht);
theta12=0.5944;
theta13=0.1515;
theta23=0.7854;
PMNS=[cos(theta12)*cos(theta13) sin(theta12)*cos(theta13) sin(theta13);
-sin(theta12)*cos(theta23)-cos(theta12)*sin(theta23)*sin(theta13)...
cos(theta12)*cos(theta23)-sin(theta12)*sin(theta23)*sin(theta13)
sin(theta23)*cos(theta13);
sin(theta12)*sin(theta23)-cos(theta12)*cos(theta23)*sin(theta13)...
-cos(theta12)*sin(theta23)-sin(theta12)*cos(theta23)*sin(theta13)...
cos(theta23)*cos(theta13)];
```

Note: The preceding matrix is edited from the version used for clarity.

```
PMNST=PMNS';
V=PMNS*U;
IV=U\PMNST;
dM12=D(1,1)-D(2,2);
dM13=D(1,1)-D(3,3);
dM23=D(2,2)-D(3,3);
Pee=fe*((V(1,1)*IV(1,1))^2+(V(1,2)*IV(2,1))^2+(V(1,3)*IV(3,1))^2+...
```

```
...+2*V(1,1)*IV(1,1)*V(1,2)*IV(2,1)*cos(dM12*L)+...
...+2*V(1,1)*IV(1,1)*V(1,3)*IV(3,1)*cos(dM13*L)+...
...+2*V(1,2)*IV(2,1)*V(1,3)*IV(3,1)*cos(dM23*L));
Peu=fe*((V(2,1)*IV(1,1))^2+(V(2,2)*IV(2,1))^2+(V(2,3)*IV(3,1))^2+...
...+2*V(2,1)*IV(1,1)*V(2,2)*IV(2,1)*cos(dM12*L)+...
...+2*V(2,1)*IV(1,1)*V(2,3)*IV(3,1)*cos(dM13*L)+...
...+2*V(2,2)*IV(2,1)*V(2,3)*IV(3,1)*cos(dM23*L));
Pet=fe*((V(3,1)*IV(1,1))^2+(V(3,2)*IV(2,1))^2+(V(3,3)*IV(3,1))^2+...
...+2*V(3,1)*IV(1,1)*V(3,2)*IV(2,1)*cos(dM12*L)+...
...+2*V(3,1)*IV(1,1)*V(3,3)*IV(3,1)*cos(dM13*L)+...
...+2*V(3,2)*IV(2,1)*V(3,3)*IV(3,1)*cos(dM23*L));
Pue=fu*((V(1,1)*IV(1,2))^2+(V(1,2)*IV(2,2))^2+(V(1,3)*IV(3,2))^2+...
...+2*V(1,1)*IV(1,2)*V(1,2)*IV(2,2)*cos(dM12*L)+...
...+2*V(1,1)*IV(1,2)*V(1,3)*IV(3,2)*cos(dM13*L)+...
...+2*V(1,2)*IV(2,2)*V(1,3)*IV(3,2)*cos(dM23*L));
Puu=fu*((V(2,1)*IV(1,2))^2+(V(2,2)*IV(2,2))^2+(V(2,3)*IV(3,2))^2+...
...+2*V(2,1)*IV(1,2)*V(2,2)*IV(2,2)*cos(dM12*L)+...
...+2*V(2,1)*IV(1,2)*V(2,3)*IV(3,2)*cos(dM13*L)+...
...+2*V(2,2)*IV(2,2)*V(2,3)*IV(3,2)*cos(dM23*L));
Put=fu*((V(3,1)*IV(1,2))^2+(V(3,2)*IV(2,2))^2+(V(3,3)*IV(3,2))^2+...
...+2*V(3,1)*IV(1,2)*V(3,2)*IV(2,2)*cos(dM12*L)+...
...+2*V(3,1)*IV(1,2)*V(3,3)*IV(3,2)*cos(dM13*L)+...
...+2*V(3,2)*IV(2,2)*V(3,3)*IV(3,2)*cos(dM23*L));
Pte=ft*((V(1,1)*IV(1,3))^2+(V(1,2)*IV(2,3))^2+(V(1,3)*IV(3,3))^2+...
...+2*V(1,1)*IV(1,3)*V(1,2)*IV(2,3)*cos(dM12*L)+...
...+2*V(1,1)*IV(1,3)*V(1,3)*IV(3,3)*cos(dM13*L)+...
...+2*V(1,2)*IV(2,3)*V(1,3)*IV(3,3)*cos(dM23*L));
Ptu=ft*((V(2,1)*IV(1,3))^2+(V(2,2)*IV(2,3))^2+(V(2,3)*IV(3,3))^2+...
...+2*V(2,1)*IV(1,3)*V(2,2)*IV(2,3)*cos(dM12*L)+...
...+2*V(2,1)*IV(1,3)*V(2,3)*IV(3,3)*cos(dM13*L)+...
```

```
...+2*V(2,2)*IV(2,3)*V(2,3)*IV(3,3)*cos(dM23*L));
Ptt=ft*((V(3,1)*IV(1,3))^2+(V(3,2)*IV(2,3))^2+(V(3,3)*IV(3,3))^2+...
...+2*V(3,1)*IV(1,3)*V(3,2)*IV(2,3)*cos(dM12*L)+...
...+2*V(3,1)*IV(1,3)*V(3,3)*IV(3,3)*cos(dM13*L)+...
...+2*V(3,2)*IV(2,3)*V(3,3)*IV(3,3)*cos(dM23*L));
Pe=Pee+Pue+Pte;
Pu=Peu+Puu+Ptu;
Pt=Pet+Put+Ptt;
dm12=7.59e-5;
dm13=2.43e-3;
```

B.2 Plotting Programs

This section contains the programs that used the previously mentioned functions to produce the plots.

B.2.1 Decoherent Plotting Program 1

```
E=1e9;%2.9e8;
   fe=1;
   fu=0;
   ft=0;
   n=120;
   V11=logspace(-33,-13,n);
   V12=0;
   V13=0;
   V21=V12;
   V22=logspace(-33,-13,n);
   V23=0;
   V31=V13;
   V32=V23;
```

```
V33=0;
Pe=zeros(n,n);
Pu=zeros(n,n);
Pt=zeros(n,n);
Pe0=zeros(n,n);
Pu0=zeros(n,n);
Pt0=zeros(n,n);
De=zeros(n,n);
Du=zeros(n,n);
Dt=zeros(n,n);
for j=1:n
for k=1:n
[Pe(j,k),Pu(j,k),Pt(j,k)]=menunhsurprobtoteVpotSLT...
...(E,dm12,dm13,fe,fu,ft,V11(k),V12,V13,V21,V22(j),V23,V31,V32,V33);
[Pe0(j,k),Pu0(j,k),Pt0(j,k)]=menunhsurprobtoteVpotSLT...
...(E,dm12,dm13,fe,fu,ft,0,0,0,0,0,0,0,0,0);
De(j,k)=(Pe(j,k)-Pe0(j,k));
Du(j,k)=(Pu(j,k)-Pu0(j,k));
Dt(j,k)=(Pt(j,k)-Pt0(j,k));
end
end
LV11=log10(V11);
LV22=log10(V22);
figure(1)
contourf(LV11,LV22,De)
colorbar
xlabel('log\_{10}(V\_{11}/{eV})','FontSize',28)
ylabel('log\_{10}(V\_{22}/{eV})','FontSize',28)
figure(2)
contourf(LV11,LV22,Du)
```

```
xlabel('log\_{10}(V\_{11}/{eV})','FontSize',28)
ylabel('log\_{10}(V\_{22}/{eV})','FontSize',28)
colorbar
figure(3)
contourf(LV11,LV22,Dt)
xlabel('log\_{10}(V\_{11}/{eV})','FontSize',28)
ylabel('log\_{10}(V\_{22}/{eV})','FontSize',28)
colorbar
```

B.2.2 Coherent Flavour State Plotting Program 1

```
dm12=7.59e-5;
dm13=2.43e-3;
L=4.384e25;%3e19;%2.55e20;%;%5e20;
E=2.9e8;%1e9;
fe=1;
fu=0;
ft=0;
n=120;
V11=logspace(-40,-13,n);
V12=0;
V13=0;
V21=V12;
V22=logspace(-40,-13,n);
V23=0;
V31=V13;
V32=V23;
V33=0;
Pe=zeros(n,n);
Pu=zeros(n,n);
Pt=zeros(n,n);
```

```
Pe0=zeros(n,n);
Pu0=zeros(n,n);
Pt0=zeros(n,n);
Re=zeros(n,n);
Ru=zeros(n,n);
Rt=zeros(n,n);
De=zeros(n,n);
Du=zeros(n,n);
Dt=zeros(n,n);
for j=1:n
for k=1:n
[Pe(j,k),Pu(j,k),Pt(j,k)]=menunhsurprobtoteVpotFBas...
...(L,E,dm12,dm13,fe,fu,ft,V11(k),V12,V13,V21,V22(j),V23,V31,V32,V33);
[Pe0(j,k),Pu0(j,k),Pt0(j,k)]=menunhsurprobtoteVpotFBas...
...(L,E,dm12,dm13,fe,fu,ft,0,0,0,0,0,0,0,0,0);
Re(j,k)=(Pe(j,k)-Pe0(j,k))/Pe0(j,k);
Ru(j,k)=(Pu(j,k)-Pu0(j,k))/Pu0(j,k);
Rt(j,k)=(Pt(j,k)-Pt0(j,k))/Pt0(j,k);
De(j,k)=(Pe(j,k)-Pe0(j,k));
Du(j,k)=(Pu(j,k)-Pu0(j,k));
Dt(j,k)=(Pt(j,k)-Pt0(j,k));
end
end
LV11=log10(V11);
LV22=log10(V22);
%Z=linspace(-1,1,41);
figure(4)
contourf(LV11,LV22,De)%,Z)
colorbar
xlabel('log_{10}(V_{11}/{eV})','FontSize',28)
```

```
ylabel('log_{10}(V_{22}/{eV})','FontSize',28)
%title('D_{e} with E=10 EeV','FontSize',24)
%surf(De)
figure(5)
contourf(LV11,LV22,Du)%,Z)
xlabel('log_{10}(V_{11}/{eV})','FontSize',28)
ylabel('log_{10}(V_{22}/{eV})','FontSize',28)
%title('D_{\mu} with E=10 EeV','FontSize',24)
colorbar
%surf(Du)
figure(6)
contourf(LV11,LV22,Dt)%,Z)
xlabel('log_{10}(V_{11}/{eV})','FontSize',28)
ylabel('log_{10}(V_{22}/{eV})','FontSize',28)
%title('D_{\tau} with E=10 EeV','FontSize',24)
colorbar
%surf(Dt)
```

B.2.3 Coherent Mass State Plotting Program 1

```
dm12=7.59e-5;
dm13=2.43e-3;
L=3e19;%4.384e25;%5e20;%2.55e20;4.384e25
E=1e9;%2.9e8;
fe=1;
fu=0;
ft=0;
n=120;
V11=logspace(-33,-13,n);
V12=0;
V13=0;
```

```
V21=V12;
V22=logspace(-33,-13,n);
V23=0;
V31=V13;
V32=V23;
V33=0;
Pe=zeros(n,n);
Pu=zeros(n,n);
Pt=zeros(n,n);
Pe0=zeros(n,n);
Pu0=zeros(n,n);
Pt0=zeros(n,n);
Re=zeros(n,n);
Ru=zeros(n,n);
Rt=zeros(n,n);
De=zeros(n,n);
Du=zeros(n,n);
Dt=zeros(n,n);
for j=1:n
for k=1:n
[Pe(j,k),Pu(j,k),Pt(j,k)]=menunhsurprobtoteVpot...
...(L,E,dm12,dm13,fe,fu,ft,V11(k),V12,V13,V21,V22(j),V23,V31,V32,V33);
[Pe0(j,k),Pu0(j,k),Pt0(j,k)]=menunhsurprobtoteVpot...
...(L,E,dm12,dm13,fe,fu,ft,0,0,0,0,0,0,0,0,0);
Re(j,k)=(Pe(j,k)-Pe0(j,k))/Pe0(j,k);
Ru(j,k)=(Pu(j,k)-Pu0(j,k))/Pu0(j,k);
Rt(j,k)=(Pt(j,k)-Pt0(j,k))/Pt0(j,k);
De(j,k)=(Pe(j,k)-Pe0(j,k));
Du(j,k)=(Pu(j,k)-Pu0(j,k));
Dt(j,k)=(Pt(j,k)-Pt0(j,k));
```

```
end
end
LV11=log10(V11);
LV22=log10(V22);
figure(1)
contourf(LV11,LV22,De)
colorbar
xlabel('log_{10}(V_{11}/{eV})','FontSize',28)
ylabel('log_{10}(V_{22}/{eV})','FontSize',28)
%title('D_{e} with L=5{\times}10^{20}m and E=10 EeV','FontSize',32)
%surf(De)
figure(2)
contourf(LV11,LV22,Du)
xlabel('log_{10}(V_{11}/{eV})','FontSize',28)
ylabel('log_{10}(V_{22}/{eV})','FontSize',28)
%title('D_{\mu} with L=5{\times}10^{20}m and E=10 EeV','FontSize',24)
colorbar
%surf(Du)
figure(3)
contourf(LV11,LV22,Dt)
xlabel('log_{10}(V_{11}/{eV})','FontSize',28)
ylabel('log_{10}(V_{22}/{eV})','FontSize',28)
%title('D_{\tau} with L=5{\times}10^{20}m and E=10 EeV','FontSize',24)
colorbar
%surf(Dt)
```

B.2.4 Large Overfunction

This overfunction produced the plots in chapter 5.

```
dm12=7.59e-5;
dm13=2.43e-3;
```

```
fe=1;
fu=0;
ft=0;
n=120;
V11=logspace(-33,-13,n);
V12=0;
V13=0;
V21=V12;
V22=logspace(-33,-13,n);
V23=0;
V31=V13;
V32=V23;
V33=0;
LV11=log10(V11);
LV22=log10(V22);
Pede=zeros(n,n);
Pude=zeros(n,n);
Ptde=zeros(n,n);
Pe0de=zeros(n,n);
Pu0de=zeros(n,n);
Pt0de=zeros(n,n);
Dede=zeros(n,n);
Dude=zeros(n,n);
Dtde=zeros(n,n);
Peco=zeros(n,n);
Puco=zeros(n,n);
Ptco=zeros(n,n);
Pe0co=zeros(n,n);
Pu0co=zeros(n,n);
Pt0co=zeros(n,n);
```

```
Deco=zeros(n,n);
Duco=zeros(n,n);
Dtco=zeros(n,n);
Pemb=zeros(n,n);
Pumb=zeros(n,n);
Ptmb=zeros(n,n);
Pe0mb=zeros(n,n);
Pu0mb=zeros(n,n);
Pt0=zeros(n,n);
Demb=zeros(n,n);
Dumb=zeros(n,n);
Dtmb=zeros(n,n);
q=0;
for h=1:3
    E=10^(6+3*(h-1));
for l=1:3
    L=3*10^(17+l);
    q=q+1;
for j=1:n
for k=1:n
[Pede(j,k),Pude(j,k),Ptde(j,k)]=menunhsurprobtoteVpotSLT...
...(E,dm12,dm13,fe,fu,ft,V11(k),V12,V13,V21,V22(j),V23,V31,V32,V33);
[Pe0de(j,k),Pu0de(j,k),Pt0de(j,k)]=menunhsurprobtoteVpotSLT...
...(E,dm12,dm13,fe,fu,ft,0,0,0,0,0,0,0,0,0);
Dede(j,k)=(Pede(j,k)-Pe0de(j,k));
Dude(j,k)=(Pude(j,k)-Pu0de(j,k));
Dtde(j,k)=(Ptde(j,k)-Pt0de(j,k));
[Peco(j,k),Puco(j,k),Ptco(j,k)]=menunhsurprobtoteVpotFBas...
...(L,E,dm12,dm13,fe,fu,ft,V11(k),V12,V13,V21,V22(j),V23,V31,V32,V33);
[Pe0co(j,k),Pu0co(j,k),Pt0co(j,k)]=menunhsurprobtoteVpotFBas...
```

```
...(L,E,dm12,dm13,fe,fu,ft,0,0,0,0,0,0,0,0,0);
Deco(j,k)=(Peco(j,k)-Pe0co(j,k));
Duco(j,k)=(Puco(j,k)-Pu0co(j,k));
Dtco(j,k)=(Ptco(j,k)-Pt0co(j,k));
[Pemb(j,k),Pumb(j,k),Ptmb(j,k)]=menunhsurprobtoteVpot...
...(L,E,dm12,dm13,fe,fu,ft,V11(k),V12,V13,V21,V22(j),V23,V31,V32,V33);
[Pe0mb(j,k),Pu0mb(j,k),Pt0(j,k)]=menunhsurprobtoteVpot...
...(L,E,dm12,dm13,fe,fu,ft,0,0,0,0,0,0,0,0,0);
Demb(j,k)=(Pemb(j,k)-Pe0mb(j,k));
Dumb(j,k)=(Pumb(j,k)-Pu0mb(j,k));
Dtmb(j,k)=(Ptmb(j,k)-Pt0(j,k));
end
end
figure(q)
contourf(LV11,LV22,Dede)
colorbar
xlabel('log_{10}(V_{11}/{eV})','FontSize',28)
ylabel('log_{10}(V_{22}/{eV})','FontSize',28)
figure(q+9)
contourf(LV11,LV22,Dude)
xlabel('log_{10}(V_{11}/{eV})','FontSize',28)
ylabel('log_{10}(V_{22}/{eV})','FontSize',28)
colorbar
figure(q+18)
contourf(LV11,LV22,Dtde)
xlabel('log_{10}(V_{11}/{eV})','FontSize',28)
ylabel('log_{10}(V_{22}/{eV})','FontSize',28)
colorbar
figure(q+27)
contourf(LV11,LV22,Deco)
```

```
colorbar
xlabel('log_{10}(V_{11}/{eV})','FontSize',28)
ylabel('log_{10}(V_{22}/{eV})','FontSize',28)
figure(q+36)
contourf(LV11,LV22,Duco)
xlabel('log_{10}(V_{11}/{eV})','FontSize',28)
ylabel('log_{10}(V_{22}/{eV})','FontSize',28)
colorbar
figure(q+45)
contourf(LV11,LV22,Dtco)
xlabel('log_{10}(V_{11}/{eV})','FontSize',28)
ylabel('log_{10}(V_{22}/{eV})','FontSize',28)
colorbar
figure(q+54)
contourf(LV11,LV22,Demb)
colorbar
xlabel('log_{10}(V_{11}/{eV})','FontSize',28)
ylabel('log_{10}(V_{22}/{eV})','FontSize',28)
figure(q+63)
contourf(LV11,LV22,Dumb)
xlabel('log_{10}(V_{11}/{eV})','FontSize',28)
ylabel('log_{10}(V_{22}/{eV})','FontSize',28)
colorbar
figure(q+72)
contourf(LV11,LV22,Dtmb)
xlabel('log_{10}(V_{11}/{eV})','FontSize',28)
ylabel('log_{10}(V_{22}/{eV})','FontSize',28)
colorbar
end
end
```

Bibliography

[1] G. Bertone and D. Hooper. History of dark matter. Reviews of Modern Physics, 90(4): 1–88, 2018.

[2] A. Y. Smirnov. The MSW Effect and Matter Effects in Neutrino Oscillations. Physica Scripta, T121:57–64, Jan 2005.

[3] Particle Data Group. Review of Particle Physics 2010. Journal of Physics G, 37(7A): 075021, July 2010.

[4] LIGO Scientific Collaboration and Virgo Collaboration. Observation of gravitational waves from a binary black hole merger. Physical Review Letters, 116: 061102, 2016.

[5] K. Zuber. Neutrino Physics. Boca Raton, FL: CRC Press, Taylor & Francis Group, 2nd ed., 2012.

[6] PTOLEMY Collaboration. Development of a Relic Neutrino Detection Experiment at PTOLEMY: Princeton Tritium Observatory for Light, Early-Universe, Massive-Neutrino Yield. Jul 2013.

[7] D. Samtleben, S. Staggs, and B. Winstein. The Cosmic Microwave Background for Pedestrians: A Review for Particle and Nuclear Physicists. Annual Review of Nuclear and Particle Science, 57(1): 1–34, Mar 2007.

[8] W. Pauli. On the earlier and more recent history of the neutrino, in Writings on physics and philosophy. Berlin: Springer-Verlag, 1958.

[9] F. Close. Neutrino. Oxford: Oxford University Press, 2012.

[10] S. M. Bilenky. Neutrino: History of a unique particle. European Physical Journal H, 38(3):345–404, 2013.

[11] B. Pontecorvo. Pages in the development of neutrino physics. Soviet Physics Uspekhi, 20(12): 1087-1108, 2020.

[12] F. Close. Half-life: The divided life of Bruno Pontecorvo, physicist or spy. New York, NY: Basic Books, 2015.

[13] S. M. Bilenky. Neutrino oscillations: brief history and present status. 1–42, Aug 2014. arXiv:1408.2864 [hep-ph]

[14] J. Bernabeu. On the history of the PMNS Matrix . . . with today's perspective. Nuovo Cimento della Societa Italiana di Fisica C 37: 145–154, Dec 2013.

[15] S. T. Petcov. The nature of massive neutrinos. Advances in High Energy Physics, 2013: 1–35, 2013.

[16] SNO Collaboration. SUDBURY NEUTRINO OBSERVATORY PROPOSAL. SUDBURY NEUTRINO OBSERVATORY, SNO-87-12, Oct 1987.

[17] IMB Collaboration. Search for Proton Decay into $e^+ + \pi^0$. Physical Review Letters, 51: 27–30, Jul 1983.

[18] Kamiokande Collaboration. KAMIOKANDE,+KAMIOKA Nucleon Decay Experiments; status and performance. AIP Conference Proceedings, 114: 54–76, 1984.

[19] IMB Collaboration. Observation of a neutrino burst in coincidence with supernova 1987A in the large magellanic cloud. Physical Review Letters, 58(14): 1494–1496, 1987.

[20] Kamiokande Collaboration. Observation in the Kamiokande-II detector of the neutrino burst from supernova SN1987A. Physical Review D, 38: 448–458, Jul 1988.

[21] Kamiokande Collaboration. Experimental study of the atmospheric neutrino flux. Physics Letters B, 205(2-3): 416–420, 1988.

[22] Super-Kamiokande Collaboration. Constraints on Neutrino Oscillation Parameters from the Measurement of Day-Night Solar Neutrino Fluxes at Super-Kamiokande. Physical Review Letters, 82: 1810–1814, Mar 1999.

[23] SNO Collaboration. Measurement of the rate of $\nu_e + d \rightarrow p + p + e^-$ interactions produced by ^8B solar neutrinos at the Sudbury Neutrino Observatory. Physical Review Letters, 87: 071301, Jun 2001.

[24] Super-Kamiokande Collaboration. The Super-Kamiokande detector. Nuclear Instruments and Methods in Physics Research Section A: Accelerators, Spectrometers, Detectors and Associated Equipment, 501: 418–462, Apr 2003.

[25] Royal Swedish Academy of Sciences. The Nobel Prize in Physics 2015, 2015.

[26] Super-Kamiokande Collaboration. Determination of Solar Neutrino Oscillation Parameters using 1496 Days of Super-Kamiokande-I Data. Physics Letters B, 539(3-4):179-187, 2002.

[27] M. Maltoni, T. Schwetz, M. A. Tòrtola and J. W.F. Valle. Constraining neutrino oscillation parameters with current solar and atmospheric data. Physical Review D, 67(1): 013011, 2003.

[28] K. Nakamura and S.T. Petrov. Neutrino Mass, Mixing and Oscillations. In: Olive, K.A., et al. (2014) Chinese Physics C, 38, Article ID: 090001, 235-258, 2014.

[29] The T2K Collaboration. Constraint on the Matter-Antimatter Symmetry-Violating Phase in Neutrino Oscillations. Nature, 580(7803): 339-344, 2020.

[30] JUNO Collaboration. Neutrino Physics with JUNO. 2015. arXiv:1507.05613 [physics.ins-det]

[31] T. Franarin, M. Fairbairn, and J. H. Davis. JUNO Sensitivity to Resonant Absorption of Galactic Supernova Neutrinos by Dark Matter. arXiv:1806.05015 [hep-ph], Jun 2018.

[32] KATRIN Collaboration. First operation of the KATRIN experiment with tritium. European Physical Journal C, 20(3), 2020.

[33] E. Giusarma, M. Gerbino, O. Mena, S. Vagnozzi, S. Ho and K. Freese. Improvement of cosmological neutrino mass bounds. Physical Review D, 94(8): 1-9, 2016.

[34] E. Di Valentino, E. Giusarma, M. Lattanzi, O. Mena, A. Melchiorri, J. Silk. Cosmological axion and neutrino mass constraints from Planck 2015 temperature and polarization data. Physics Letters B, 752(Mcmc): 182-185, 2016.

[35] L. Wolfenstein. Neutrino Oscillations in matter. Physical Review D, 61(4):937 - 979, Oct 1978.

[36] V. Barger, K. Whisnant, S. Pakvasa, and R. J. N. Phillips. Matter effects on three neutrino oscillations. Physical Review D, 22(11):2718 - 726, Dec 1980.

[37] E. K. Akhmedov and A. Y. Smirnov. Paradoxes of neutrino oscillations. Physics of Atomic Nuclei, 72(8): 1363–1381, 2009.

[38] E. K. Akhmedov, D. Hernandez, and A. Y. Smirnov. Neutrino production coherence and oscillation experiments. Journal of High Energy Physics, 2012(4), 2012.

[39] Y. Farzan and A. Y. Smirnov. Coherence and oscillations of cosmic neutrinos. Nuclear Physics B, 805(1-2): 356–376, 2008.

[40] CMSCollaboration. Precise determination of the mass of the Higgs boson and tests of compatibility of its couplings with the standard model predictions using proton collisions at 7 and 8 TeV. The European Physical Journal C, 75: 212, May 2015.

[41] J. Ellis, J. Hisano, M. Raidal, and Y. Shimizu. New parametrization of the seesaw mechanism and applications in supersymmetric models. Physical Review D, 66: 115013, Dec 2002.

[42] A. Broncano, M. B. Gavela, and E. Jenkins. Neutrino physics in the seesaw model. Nuclear Physics B, 672: 163–198, Nov 2003.

[43] F. Bazzocchi, M. Lattanzi, S. Riemer-Sorensen, and J. W. F. Valle. X-ray photons from late-decaying majoron dark matter. Journal of Cosmology and Astroparticle Physics, 2008: 13, Aug 2008.

[44] S. Kanemura and K. Yagyu. Radiative corrections to electroweak parameters in the Higgs triplet model and implication with the recent Higgs boson searches. Physical Review D, 85: 115009, Jun 2012.

[45] P. F. Pérez. Type III seesaw and left-right symmetry. Journal of High Energy Physics, 2009: 142–142, Mar 2009.

[46] G. Bandelloni, C. Becchi, A. Blasi, and R. Collina. Communications in Renormalization of Models with Radiative Mass Generation. Communications in Mathematical Physics, 67: 147–178, 1978.

[47] J. Kubo and D. Suematsu. Neutrino masses and CDM in a non-supersymmetric model. Physics Letters B, 643: 336–341, Nov 2006.

[48] H. Sugiyama. Radiative Neutrino Mass Models. arXiv:1505.01738 [hep-ph], May 2015

[49] E. Ma and D. Suematsu. Fermion triplet dark matter and radiative neutrino mass. Modern Physics Letters A, 24: 583–589, Mar 2009.

[50] S. M. Boucenna, S. Morisi, and J. W. F. Valle. Radiative neutrino mass in 3-3-1 scheme. Physical Review D, 90: 13005, Jul 2014.

[51] A. Ahriche, K. L. McDonald, and S. Nasri. The scale-invariant scotogenic model. Journal of High Energy Physics, 2016: 182, Jun 2016.

[52] A. Aranda and E. Peinado. A new radiative neutrino mass generation mechanism with higher dimensional scalar representations and custodial symmetry. Physics Letters B, 754: 11–13, Mar 2016.

[53] P. M. Ferreira, W. Grimus, D. Jurciukonis, and L. Lavoura. Scotogenic model for co-bimaximal mixing. Journal of High Energy Physics, 2016: 10, Jul 2016.

[54] S. Esch, M. Klasen, D. R. Lamprea and C. E. Yaguna. Lepton flavor violation and scalar dark matter in a radiative model of neutrino masses. The European Physical Journal C, 78(2): 88, 2018.

[55] P. Ko, T. Nomura, and H. Okada. A flavor dependent gauge symmetry, predictive radiative seesaw and LHCb anomalies. Physics Letters B, 772: 547-552, Sep 2017.

[56] W.-B. Lu and P.-H. Gu. Leptogenesis, radiative neutrino masses and inert Higgs triplet dark matter. Journal of Cosmology and Astroparticle Physics, 2016: 40, May 2016.

[57] L. Megrelidze and Z. Tavartkiladze. Soft see-saw: Radiative origin of neutrino masses in SUSY theories. Nuclear Physics B, 914: 553–576, Jan 2017.

[58] P.-H. Gu and U. Sarkar. Radiative neutrino mass, dark matter, and leptogenesis. Physical Review D, 77: 105031, May 2008.

[59] M. Aoki, S. Kanemura, and O. Seto. Neutrino mass, dark matter, and Baryon asymmetry via TeV-scale physics without fine-tuning. Physical Review Letters, 102: 051805, Feb 2009.

[60] S. Kanemura, T. Matsui, and H. Sugiyama. Loop suppression of Dirac neutrino mass in the neutrinophilic two-Higgs-doublet model. Physics Letters B, 727: 151–156, Nov 2013.

[61] M. Aoki and T. Toma. Impact of Semi-annihilation of Z3 Symmetric Dark Matter with Radiative Neutrino Masses. Journal of Cosmology and Astroparticle Physics, 2014: 16, May 2014.

[62] A. Ahriche, K. L. McDonald, S. Nasri, and T. Toma. A model of neutrino mass and dark matter with an accidental symmetry. Physics Letters B, 746: 430–435, Jun 2015.

[63] S. S. C. Law and K. L. McDonald. The simplest models of radiative neutrino mass. International Journal of Modern Physics A, 29: 1450064, Apr 2014.

[64] B. Batell, M. Pospelov, and B. Shuve. Shedding light on neutrino masses with dark forces. Journal of High Energy Physics, 2016: 52, Aug 2016.

[65] CMSCollaboration. Search for dark matter and unparticles in events with a Z boson and missing transverse momentum in proton-proton collisions at $\sqrt{s} = 13TeV$. Journal of High Energy Physics, 2017, Jan 2017.

[66] S.-Y. Ho and J. Tandean, Probing scotogenic effects in Higgs boson decays. Physical Review D, 87: 95015, May 2013.

[67] S. Y. Ho and J. Tandean. Probing scotogenic effects in $e + e-$ colliders. Physical Review D - Particles, Fields, Gravitation and Cosmology, 89: 114025, Jun 2014.

[68] F. T. Avignone, S. R. Elliott, and J. Engel. Double beta decay, Majorana neutrinos, and neutrino mass. Reviews of Modern Physics, 80(2): 481–516, 2008.

[69] R. Arnold *et al. Measurement of the double-beta decay half-life and search for the neutrinoless double-beta decay of Ca 48 with the NEMO-3 detector. Physical Review D, 93: 111101, Apr 2016.*

[70] J. W. F. Valle and C. A. Vaquera-Araujo. Dynamical seesaw mechanism for Dirac neutrinos. Physics Letters B, 755: 363–366, Apr 2016.

[71] E. Ma and O. Popov. Pathways to naturally small Dirac neutrino masses. Physics Letters B, 764: 142–144, Jan 2017.

[72] V. N. Aseev, et. al. Upper limit on the electron antineutrino mass from the Troitsk experiment. Physical Review D, 84(11), 2011.

[73] E. W. Otten and C. Weinheimer. Neutrino mass limit from tritium beta decay. Reports on Progress in Physics, 71: 86201, Sep 2009.

[74] M. Ubieto-Díaz, D. Rodríguez, S. Lukic, S. Nagy, S. Stahl, and K. Blaum. A broadband FT-ICR Penning trap system for KATRIN. International Journal of Mass Spectrometry, 288(1-3): 1–5, 2009.

[75] E. Otten. Searching the absolute neutrino mass in tritium β-decay—interplay between nuclear, atomic and molecular physics. Hyperfine Interactions, 196: 3–23, Feb 2010.

[76] F. Simkovic, R. Dvornicky, and A. Faessler. Exact relativistic tritium β-decay endpoint spectrum in a hadron model. Physical Review C, 77: 1–6, Dec 2007.

[77] S. Mertens. Direct Neutrino Mass Experiments. Journal of Physics: Conference Series, 718: 022013, May 2016.

[78] A. Ahriche, K. L. McDonald, and S. Nasri. Scalar sector phenomenology of three loop radiative neutrino mass models. Physical Review D, 92: 95020, Nov 2015.

[79] A. Merle and M. Platscher. Parity problem of the scotogenic neutrino model. Physical Review D, 92: 95002, Nov 2015.

[80] A. Merle and M. Platscher. Running of radiative neutrino masses: the scotogenic model — revisited. Journal of High Energy Physics, 2015: 148, Nov 2015.

[81] M. Lindner, M. Platscher, C. E. Yaguna, and A. Merle. Fermionic WIMPs and vacuum stability in the scotogenic model. Physical Review D, 94: 115027, Dec 2016.

[82] The MACHO Collaboration. The MACHO Project: Limits on Planetary Mass Dark Matter in the Galactic Halo from Gravitational Microlensing. The Astrophysical Journal, 471(2): 774–782, 1996.

[83] E. I. Gates, G. Gyuk, and M. S. Turner. Gravitational microlensing and the galactic halo. Physical Review D, 53(8): 4138–4176, 1996.

[84] The MACHO Collaboration. The MACHO Project Large Magellanic Cloud Microlensing Results from the First Two Years and the Nature of the Galactic Dark Halo. The Astrophysical Journal, 486(2): 697–726, 1997.

[85] EROS Collaboration. Microlensing towards the Small Magellanic Cloud. EROS 2 first year survey. Astronomy and Astrophysics, 9: 1–9, Oct 1997.

[86] J. R. Primack and M. A. K. Gross. Hot Dark Matter in Cosmology, in Current Aspects of Neutrino Physics, pp. 287–308, Berlin, Heidelberg: Springer Berlin Heidelberg, 2001.

[87] Q.-H. Cao, E. Ma, J. Wudka, and C. P. Yuan. Multipartite Dark Matter. arXiv:0711.3881 [hep-ph], Nov 2007.

[88] H. Georgi. Unparticle physics. Physical Review Letters, 98(22), 2007.

[89] H. Georgi. Another odd thing about unparticle physics. Physics Letters B, 650: 275–278, Jul 2007.

[90] H. Nikolić. Unparticle as a particle with arbitrary mass. Modern Physics Letters A, 23: 2645–2649, Oct 2008.

[91] N. V. Krasnikov. Unparticle as a field with continuously distributed mass. International Journal of Modern Physics A, 22: 5117–5120, Nov 2007.

[92] D. Majumdar. Unparticle decay of neutrinos and it's effect on ultra high energy neutrinos. arXiv:0708.3485 [hep-ph], Aug 2007.

[93] IceCube Collaboration. Flavor Ratio of Astrophysical Neutrinos above 35 TeV in IceCube. Physical Review Letters, 114: 171102, Apr 2015.

[94] A. Rajaraman. On the Decay of Unparticles. Physics Letters B, 671: 411–414, Jun 2008.

[95] T. M. Aliev, S. Bilmis, M. Solmaz, and I. Turan. Scalar Unparticle Signals at the LHC. Physical Review D, 95(9): 095005, May 2017.

[96] G. Bertone, D. Hooper, and J. Silk. Particle dark matter: evidence, candidates and constraints. Physics Reports, 405: 279–390, Jan 2005.

[97] J. A. Formaggio and G. P. Zeller. From eV to EeV: Neutrino cross sections across energy scales. Reviews of Modern Physics, 84(3): 1307–1341, 2012.

[98] R. D. Peccei. The strong CP problem and axions. Lecture Notes in Physics, 741(2): 3–17, 2008.

[99] Y. Farzan and E. Ma. Dirac neutrino mass generation from dark matter. Physical Review D, 86: 33007, Aug 2012.

[100] P. F. de Salas, R. A. Lineros, and M. Tòrtola. Neutrino propagation in the Galactic dark matter halo. Physical Review D, 94(12):123001, Dec 2016.

[101] L. Bergström and H. Snellman. Observable monochromatic photons from cosmic photino annihilation. Physical Review D, 37: 3737–3741, Jun 1988.

[102] L. Bergström and P. Ullio. Full one-loop calculation of neutralino annihilation into two photons. Nuclear Physics B, 504(1-2): 27–44, 1997.

[103] Z. Bern, P. Gondolo, and M. Perelstein. Neutralino annihilation into two photons. Physics Letters, Section B: Nuclear, Elementary Particle and High-Energy Physics, 411(1-2): 86–96, 1997.

[104] R. Laha, K. C. Y. Ng, B. Dasgupta, and S. Horiuchi. Galactic Center radio constraints on gamma-ray lines from dark matter annihilation. Physical Review D, 87(4): 1–18, 2013.

[105] A. Esmaili and P. D. Serpico. Are IceCube neutrinos unveiling PeV-scale decaying dark matter? Journal of Cosmology and Astroparticle Physics, 2013: 54, Nov 2013.

[106] C. E. Aisati, M. Gustafsson, and T. Hambye. New search for monochromatic neutrinos from dark matter decay. Physical Review D, 92(12): 1–12, 2015.

[107] K. Murase, R. Laha, S. Ando, and M. Ahlers. Testing the Dark Matter Scenario for PeV Neutrinos Observed in IceCube. Physical Review Letters, 115: 71301, Aug 2015.

[108] P. Baratella, M. Cirelli, A. Hektor, J. Pata, M. Piibeleht, and A. Strumia. PPPC 4 DMν: A Poor Particle Physicist Cookbook for Neutrinos from DM annihilations in the Sun. Journal of Cosmology and Astroparticle Physics, 2014: 53, Dec 2013.

[109] Super-Kamiokande Collaboration. Search for Neutrinos from Annihilation of Captured Low-Mass Dark Matter Particles in the Sun by Super-Kamiokande. Physical Review Letters, 114: 141301, Apr 2015.

[110] A. Challinor. Microwave background polarization in cosmological models. Physical Review D, 62(4): 43004, 2000.

[111] B. Bertoni, S. Ipek, D. McKeen, and A. E. Nelson. Constraints and consequences of reducing small scale structure via large dark matter-neutrino interactions. Journal of High Energy Physics, 2015: 170, Apr 2015.

[112] G. Mangano, A. Melchiorri, P. Serra, A. Cooray, and M. Kamionkowski. Cosmological bounds on dark-matter-neutrino interactions. Physical Review D, 74(4):043517, Aug 2006.

[113] P. Serra, F. Zalamea, A. Cooray, G. Mangano, and A. Melchiorri. Constraints on neutrino – dark matter interactions from cosmic microwave background and large scale structure data. Physical Review D, 81(4), Nov 2009.

[114] R. J. Wilkinson, C. Bœhm, and J. Lesgourgues. Constraining dark matter-neutrino interactions using the CMB and large-scale structure. Journal of Cosmology and Astroparticle Physics, 2014(05):011–011, May 2014.

[115] J. Lesgourgues and S. Pastor. Neutrino mass from cosmology. Advances in High Energy Physics, 2012(3), 2012.

[116] P. Crotty, J. Lesgourgues and S. Pastor. Measuring the cosmological background of relativistic particles with the Wilkinson Microwave Anisotropy Probe. Physical Review D, 67(12): 2-6, 2003.

[117] E. Di Valentino, A. Melchiorri, O. Mena. Dark Radiation candidates after Planck. Journal of Cosmology and Astroparticle Physics, 2013(11): 018-018, 2013.

[118] T. Weiler. Resonant Absorption of Cosmic-Ray Neutrinos by the Relic-Neutrino Background. Physical Review Letters, 49: 234–237, Jul 1982.

[119] Y. Farzan and S. Palomares-Ruiz. Dips in the diffuse supernova neutrino back ground. Journal of Cosmology and Astroparticle Physics, 2014(6), 2014.

[120] Daya Bay Collaboration. Improved measurement of electron antineutrino disappearance at Daya Bay. Chinese Physics C, 37(1): 11001, 2013.

[121] A. N. Khan, D. W. McKay, and J. P. Ralston. Optimizing the Determination of the Neutrino Mixing Angle θ_{13} from Reactor Data. International Journal of Modern Physics A, 29: 1450109, Jul 2013.

[122] Daya Bay Collaboration. Measurement of the reactor antineutrino flux and spectrum at Daya Bay. Physical Review Letters, 116(6): 1–7, 2016.

[123] Daya Bay Collaboration. New Measurement of Antineutrino Oscillation with the Full Detector Configuration at Daya Bay. Physical Review Letters, 115(11): 1–8, 2015.

[124] F. G. Cao and W. S. Marks. Extraction of neutrino mixing parameters from experiments with multiple identical detectors. International Journal of Modern Physics A, 33(22): 1–14, 2018.

[125] G. L. Fogli, E. Lisi, A. Marrone, D. Montanino and A. Palazzo. Getting the most from the statistical analysis of solar neutrino oscillations. Physical Review D, 66(5): 1-30, 2002.

[126] Daya Bay Collaboration. A Precision Measurement of the Neutrino Mixing Angle θ_{13} using Reactor Antineutrinos at Daya Bay. arXiv: hep-ex/0701029: 156, Jan 2007.

[127] T. A. Mueller, D. Lhuillier, M. Fallot, A. Letourneau, S. Cormon, M. Fechner, L. Giot, T. Lasserre, J. Martino, G. Mention, A. Porta, and F. Yermia. Improved predictions of reactor antineutrino spectra. Physical Review C, 83: 54615, May 2011.

[128] P. Vogel and J. F. Beacom. Angular distribution of neutron inverse beta decay, $\overline{\nu_e} + p \rightarrow e^+ + n$. Physical Review D, 60: 053003, Jul 1999.

[129] J. A. Nelder and R. Mead. A simplex method for function minimization. Computer Journal, 7: 148-158, 1965.

[130] M. Matsumoto and T. Nishimura. Mersenne Twister: A 623-dimensionally equidistributed uniform pseudo-random number generator. ACM Transactions on Modeling and Computer Simulation, 8(1): 3-30, 1998.

[131] RENO Collaboration. RENO: An Experiment for Neutrino Oscillation Parameter θ_{13} Using Reactor Neutrinos at Yonggwang. arXiv:1003.1391 [hep-ex], Mar 2010.

[132] RENO Collaboration. Observation of reactor electron antineutrinos disappearance in the RENO experiment. Physical Review Letters, 108(19): 1–6, 2012.

[133] W. S. Marks and F.-G. Cao. Meaningful Details: The value of adding baseline dependence to the Neutrino-Dark Matter Effect. International Journal of Theoretical Physics, 59(12): 3951–3966, 2020.

[134] J. Read. The local dark matter density. Journal of Physics G, 41(6): 63101, Jun 2014.

[135] Simona Paiano, Renato Falomo, Aldo Treves, and Riccardo Scarpa. The redshift of the bl lac object txs 0506+056. The Astrophysical Journal Letters, 854(2):L32, 2018.

[136] IceCube Collaboration. Neutrino emission from the direction of the blazar TXS 0506+056 prior to the IceCube-170922A alert. Science,151(July):2890, 2018.